Fingerprinting of Quartzitic Outcrops at Oldupai Gorge, Tanzania

María Soto [a], Julien Favreau [a], Kathryn Campeau [b, c], Tristan Carter [c, d], Matthew Abtosway [a], Pastory M. Bushozi [e], Siobhán Clarke [a], Paul R. Durkin [f], Stephen M. Hubbard [g], Jamie Inwood [a], Makarius Itambu [a, e], Samson Koromo [h], Fergus Larter [a], Patrick Lee [a, b], Aloyce Mwambwiga [a, i], Rajeev Nair [g], Lucas Olesilau [h], Robert Patalano [a], Laura Tucker [a], Julio Mercader [a]

[a] Department of Anthropology and Archaeology, University of Calgary, Calgary, AB, T2N 1N4, Canada.

[b] Department of Anthropology, University of Toronto, Toronto, ON, M5S 2S2, Canada.

[c] McMaster Archaeological XRF Lab, McMaster University, Hamilton, ON, L8S 4L9, Canada.

[d] Department of Anthropology, McMaster University, Hamilton, ON, L8S 4L9, Canada.

[e] Department of Archaeology and Heritage Studies, University of Dar es Salaam, Dar es Salaam, United Republic of Tanzania.

[f] Department of Geological Sciences, University of Manitoba, Winnipeg, MB, R3T 2N2, Canada.

[g] Department of Geoscience, University of Calgary, Calgary, AB, T2N 1N4, Canada.

[h] United Republic of Tanzania.

[i] National Natural History Museum, Arusha, United Republic of Tanzania.

Corresponding authors: María Soto (maria.sotoquesada@ucalgary.ca); Julio Mercader (mercader@ucalgary,ca)

Highlights

- Quartz-rich raw materials were extensively exploited in the African Early Stone Age.
- Few studies have characterized quartzitic outcrops as primary source areas.
- Macroscopic, petrographic, and EDXRF data used to fingerprint quartzitic outcrops at Oldupai.
- Baseline to interpret stone provenance and hominin palaeoecological behavior.

Abstract

The African Early Stone Age record, including that of Oldupai Gorge, reveals widespread evidence for hominin exploitation of quartzose lithic raw materials such as quartzite. However, few studies have sought to characterize these rock types grounded on the assumption that they are not amenable for provenance studies. Through the use of macroscopic, petrographic, and EDXRF analysis, we characterize source material from five quartzitic outcrops belonging to the Mozambique Belt adjacent to Oldupai Gorge. Our results show that certain macroscopic varieties strictly occur at some outcrops while petrographic analyses – which will be strengthened by a greater sample size – reveal that accessory minerals may be outcrop-specific. Statistical analyses of the geochemical data through linear correlations, Kruskal-Wallis tests, PCA, and DFA show that there are inter- and intra-outcrop differences, and elemental concentrations specific of certain outcrops. This multi-scalar approach provides a reproducible classificatory framework for additional characterization studies and archaeological testing at Oldupai to shed light on hominin palaeoenvironmental exploitation and palaeoecological behavior.

Keywords

Petrography; EDXRF; Quartzite; Sourcing; Oldupai Gorge.

1. Introduction

Lithic raw material studies are generally based on survey programs intended to establish geological reference collections, which are characterized using destructive and non-destructive macroscopic, mineralogical, and geochemical techniques (Andrefsky, 2005; Calogero, 1991; Carter and Shackley, 2007; Frahm, 2014; Odell, 2012; Poupeau et al., 2010; Prieto et al., 2019; Shackley, 2008; Shotton and Hendry, 1979). Established reference collections serve as a means to compare equivalent data obtained from stone tools to determine resource availability, distribution, and potentially, stone tool provenance. Such studies allow inferences to be made concerning hominin stone transport, procurement strategies, resource management, and land-use models (Bamforth, 1990; Binford, 1980; Brantingham, 2003; Braun et al., 2008a; Freeman, 1994; Hermes et al., 2001; Hovers, 2009; Jones et al., 2003; Kuhn, 1991; Laplace, 1972; Potts, 1994).

Quartz-rich rocks are among the wide variety of lithic raw materials that were exploited prehistorically by hominins. Quartzite is a hard, polycrystalline quartz-rich (~90%) rock with typically less than 10% accessory minerals, and has scarce intergranular porosity as a result of its metamorphic origin (Blatt et al., 2006; Howard, 2005; Pettijohn et al., 2012; Tucker, 2009). Throughout continental Africa, there is extensive evidence for hominin utilization of quartzose materials (e.g. quartz, quartzite, and quartzose sandstone) in the Early Stone Age (ESA), best exemplified by lithic assemblages from the Shungura Formation (Ethiopia) (Chavaillon, 1976; Howell et al., 1987; Merrick and Merrick, 1976), Kanjera South (Kenya) (Braun and Hovers, 2009; Plummer et al., 2009), Koobi Fora (Kenya) (Bunn, 1982; Isaac and Harris, 1978; Toth, 1982), Isimila (Tanzania) (Howell, 1961; Howell et al., 1962; Howell and Clark, 1963), the Lusso Beds (Democratic Republic of Congo) (Harris et al., 1987), Kamoa (Democratic Republic of Congo) (Cahen, 1975), the Chiwondo Beds (Malawi) (Kaufulu and Stern, 1987), Kalambo Falls (Zambia)

(Sheppard and Kleindienst, 1996), Sterkfontein (South Africa) (Kuman and Clarke, 2000; McNabb and Kuman, 2015), Swartkrans (South Africa) (Kuman, 1996; Kuman and Field, 2009), and Wonderwerk (South Africa) (Chazan et al., 2012). Oldupai Gorge's (Tanzania) Bed I and II sites have also yielded widespread evidence for hominin quartzite utilization (Leakey, 1971). Quartzite may have been favored for its hardness and edge durability, which suggests that hominins employed a different management strategy in terms of procurement, transport, and knapping for this rock type (Hay, 1976). However, limited efforts have been devoted towards the systematic characterization of quartz-rich source areas throughout much of Africa, including Oldupai Gorge where most prior studies have relied on macroscopic, petrographic, and geochemical approaches but have not studied large reference collections (Blumenschine et al., 2008; Hay, 1976; Jones, 1994; Kyara, 1999; Leakey, 1971; McHenry and de la Torre, 2018; Santonja et al., 2014; Stiles, 1991, 2003; Stiles et al., 1974; Tactikos, 2005). Furthermore, some of these aforementioned studies (e.g. Blumenschine et al., 2008; Kyara, 1999; Leakey, 1971; Tactikos, 2005) have strictly relied on qualitative macroscopic traits (e.g. color, mineral composition, and groundmass), that, if used in isolation, can be unreliable for classification and interpreting stone provenance (Calogero, 1992; Glascock and Neff, 2003; Goldman-Neuman and Hovers, 2012).

In this study, we use a multi-scalar approach to fingerprint five quartzitic outcrops at Oldupai Gorge as part of a wider effort to fully characterize the lithic raw materials that were prehistorically available. A geological reference collection was established by sampling local quartzite-bearing outcrops. Samples were classified into discrete Raw Material Groups (RMG), according to their macroscopic traits, and characterized using thin section petrography and Energy-Dispersive X-ray Fluorescence (EDXRF) spectroscopy. Our results suggest that some quartzitic outcrops can be differentiated from each other using a multi-proxy approach. Altogether, this study

provides a needed baseline for future studies to best interpret hominin raw material selective criteria, stone transport, as well as, on a broader scale, hominin palaeoecology and social behavior in the Oldupai palaeobasin.

2. Study Area

2.1. Geological Setting

The East African Rift System (EARS) is an active intra-continental extension zone that is characterized by an amagmatic Western Branch and a magmatic Eastern Branch that were coeval in their earliest rifting episodes (Roberts et al., 2012). Within Tanzania, the magmatic Eastern Branch flanks the centrally located Tanzania Craton, and splays into a diffuse network of rifted segments that are together known as the North Tanzania Divergence Zone (NTDZ) (Baker et al., 1972; Dawson, 1992; Foster et al., 1997). Tanzania's geology is sub-divided into five main tectono-stratigraphic units, namely Archaean cratonic rocks, Proterozoic sedimentary covers and metamorphic terranes, Neoproterozoic metamorphic rocks, Phanerozoic sedimentary basins, and Neogene volcanic rocks (Kasanzu et al., 2008).

The Archaean Tanzania Craton (Fig. 1a) is a stable continental crust and primarily consists of granitic rocks and greenstone belts. The craton is sub-divided into three units which includes the southernmost Dodoman Belt, and the central Nyanzian and northernmost Kavirondian Supergroups (Kasanzu et al., 2008; Cahen et al., 1984). These units consist of 1) high- and low-grade supracrustal metamorphic rocks; 2) six east-west trending greenstone belts, other metamorphic rocks, and banded ironstone, and 3) sedimentary and metamorphic rocks, respectively (Cahen et al., 1984; Kabete et al., 2012; Sanislav et al., 2014).

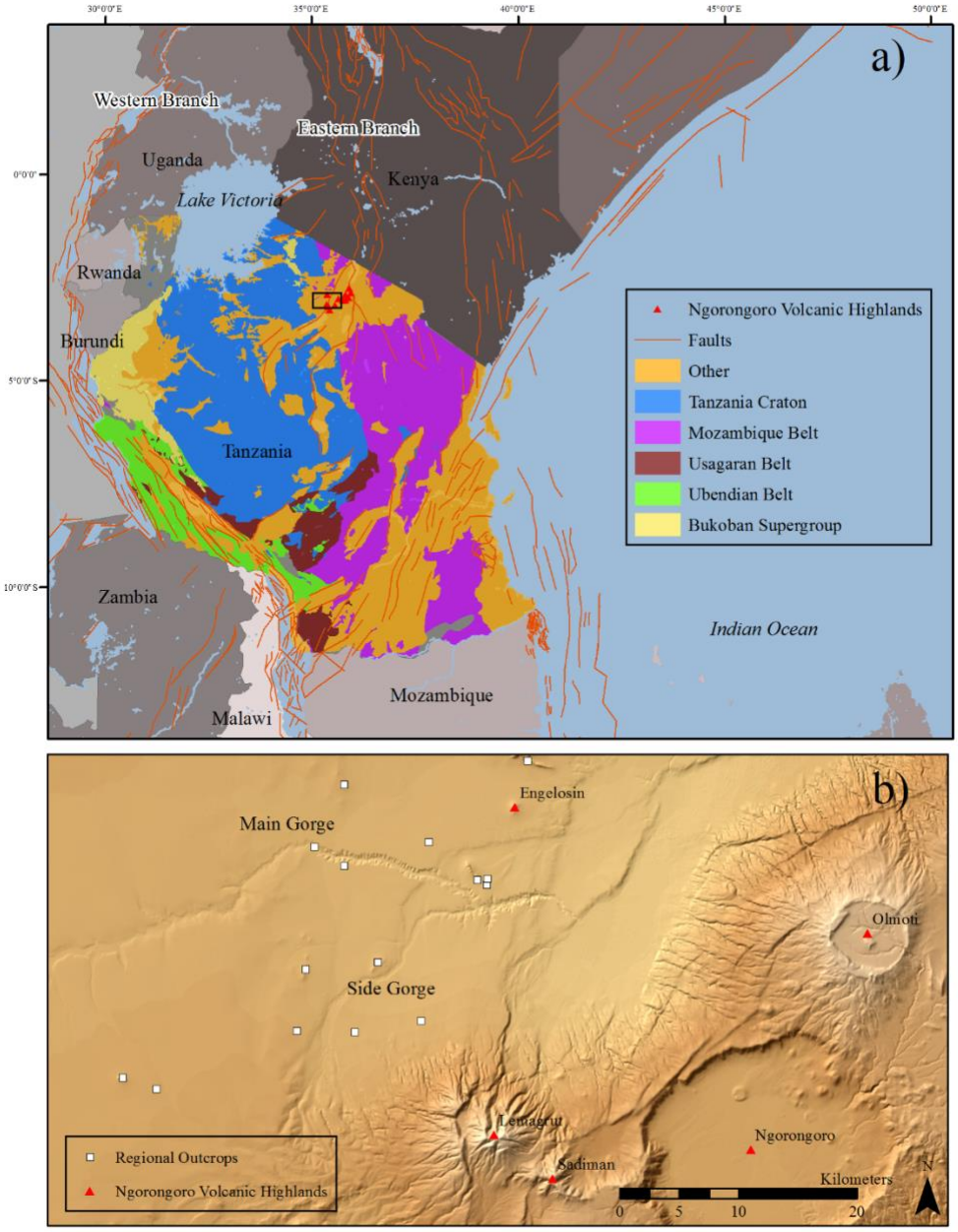

Fig. 1. a) The East African Rift System superimposed over the Tanzania Craton, the Bukoban Supergroup, orogenic belts, and other units. Black outlined polygon represents the study area in b). Geospatial data from Fritz et al. (2013) and Macgregor (2015); b) Location of the study area, regional outcrops of varied lithologies, and the volcanic centers belonging to the Ngorongoro Volcanic Highlands that directly drained into the Oldupai palaeobasin. 2-column fitting image.

The Tanzania Craton is bordered by several mobile belts, namely the Kibaran to the west, the Ubendian to the southwest, the Usagaran to the south, and the Mozambique to the east (Fig. 1a). The north-south trending Mozambique Belt was formed by the collision of East and West Gondwana as part of the Pan-African Orogeny between 850-550 Ma (Cahen et al., 1984; Fritz et al., 2013; Hepworth, 1972; Holmes, 1951; Kröner and Stern, 2005). Approximately 180 Ma, the Mozambique Belt was uplifted as a result of the breakup of the supercontinent Gondwana (Scoon, 2018). In northern Tanzania and southern Kenya, the Mozambique Belt is sub-divided into two lithological units, with the uppermost unit consisting of limestones, schists, gneisses, quartzites, and migmatites (Cahen and Snelling, 1966). The Gol Mountains in northern Tanzania belong to this upper unit (Cahen and Snelling, 1966; Cahen et al., 1984; Dawson, 2008; Scoon, 2018).

In the NTDZ, rift-associated volcanism initiated approximately 8 Ma which led to the diachronic formation of the Ngorongoro-Kilimanjaro transverse volcanic belt (Dawson, 2008). This volcanic belt is over 200 kilometers wide and its volcanic centers are aligned along four axes that show a diachronous eastward migration of magmatism (Dawson, 2008; Le Gall et al., 2008). The Ngorongoro Volcanic Highlands (NVH) are located in north-central Tanzania and represent the northeastern-most portion of Neogene volcanism in the country. This volcanic massif is centered around the Ngorongoro Caldera (2.25-2.01 Ma), and also includes the centers of Sadiman (4.63-3.5 Ma), Engelosin (3-2.7 Ma), Lemagrut (2.4-2.2 Ma), Olmoti (2.01-1.80 Ma), Oldeani (1.61-1.52 Ma), Loolmasin (1.4-1.3 Ma), Olsirwa (1.4-1.3 Ma), Embagai (1.52-0.5 Ma), Kerimasi (1.10-0.08 Ma), Oldoinyo Lengai (150 Ka-present), and Loguwinywo (?-? Ma) (Dawson, 2008; Greenwood, 2014; Mollel and Swisher III, 2012).

The strata exposed at Oldupai Gorge were deposited in an endorheic basin formed by Plio-Pleistocene uplift in the NVH (Hay, 1976). Five volcanic centers directly drained into the Oldupai

palaeobasin, namely Sadiman, Engelosin, Lemagrut, Ngorongoro, and Olmoti (McHenry and de la Torre, 2018) (Fig. 1b). These centers supplied a variety of volcanic igneous rocks ranging from nephelinitic, phonolitic, basaltic, rhyolitic, trachytic, and andesitic lithologies, all of which were available to hominins (Hay, 1976; McHenry and de la Torre, 2018; Mollel and Swisher III, 2012). In addition to these volcanic sources, the regional palaeolandscape also hosted metamorphic outcrops, occurring primarily as inselbergs of lithologies associated with the Mozambique Belt (Fig. 1b). In all probability, these mostly quartzitic inselbergs served as the primary sources of metamorphic rocks used in artifact production (Hay, 1976). Five of these quartzite-bearing outcrops were sampled for this study. The sampling locales (Fig. 2a-f) include: Naisiusiu, located over ten kilometers west of the junction between the Main and Side Gorge; Endonyo Osunyai, which is more than two kilometers north of the Main Gorge; and Oittii, Naibor Soit Kubwa, and Naibor Soit Ndogo, which are located between approximately one to two kilometers north of the junction.

Hay (1976) described and analyzed rock samples from some of the outcrops that are the subject of our study. Naisiusiu yields fine- to coarse-grained granite gneiss, as well as medium-grained white quartzite composed of quartz, muscovite, garnet, kyanite, and staurolite. Hay (1976) did not study material from Oittii, but characterized the largest of the two Naibor Soit inselbergs as a source for coarse-grained white, pale brown, and green quartzite with foliated and lineated micas, and a mineral composition of quartz and muscovite (Hay, 1976). Endonyo Osunyai yields coarse-grained quartzite that is similar to material from the largest of the two Naibor Soit inselbergs and is located four kilometers to its northwest (Hay, 1976).

Fig. 2. a) Location of the five quartzitic outcrops sampled for this study; b) Endonyo Osunyai, poorly exposed quartzitic and gneissic outcrop; c) Naibor Soit Kubwa, ~1.8 km-long northwest-southeast trending quartzitic and gneissic inselberg; d) Naibor Soit Ndogo, ~1 km-long northwest-southeast trending quartzitic inselberg; e) Naisiusiu, low-lying quartzitic, schistic, and meta-granitic outcrop; f) Oittii, low-lying quartzitic and schistic outcrop. 2-column fitting image.

123 More recently, McHenry and de la Torre (2018) studied lithic assemblages from HWK EE and
124 EF-HR in which they classified quartzites into nine RMGs (Supplementary Materials, Table 1)
125 complemented by petrographic and geochemical characterization of specimens from Naibor Soit
126 and Naisiusiu. They noted that Naibor Soit quartzite is composed of quartz and rare muscovite,
127 whereas Naisiusiu quartzite is composed of quartz, rare muscovite, and rare microcline (McHenry
128 and de la Torre, 2018).

129 **2.2. Oldupai's Raw Materials: An Overview**

130 Oldupai Gorge's sedimentary sequence (Bed I-IV, Masek, Ndutu, and Naisiusiu) has
131 yielded an exceptional quantity of Early, Middle, and Later Stone Age lithic assemblages (Hay,
132 1976; Leakey, 1971; Leakey et al., 1972; Leakey and Roe, 1994). ESA lithics were primarily
133 manufactured from igneous and metamorphic rocks, and occasionally, from local authigenic chert
134 that was intermittently exposed at lowstands in Bed II (Hay, 1976; Leakey, 1971; Stiles et al.,
135 1974). In Bed I and II, early hominins appear to have employed different technological strategies
136 depending on the raw material, as there is an abundance of igneous cores and a lack of knapping
137 products, while there is an abundance of quartzite flakes but a scarcer number of cores (Leakey,
138 1971). Altogether, this suggests that hominins may have employed a high degree of curation for
139 small quartzite lithics and large igneous cores (Hay, 1976; Leakey, 1971; Schick, 1987; Toth,
140 1985). Based on this rich archaeological record, it has been recognized that early hominins
141 transported stone in the Oldupai palaeobasin up to twelve kilometers away from their eventual
142 point of discard (Hay, 1976; Leakey, 1971).

143 Experimental studies seeking to reproduce Acheulean bifaces and determine their
144 butchering efficiencies using local raw materials (e.g. quartzite, basalt, trachyandesite, and
145 phonolite) have found the latter to varyingly influence production time, reduction strategies,

146 finished forms, and edge durability (Jones, 1979, 1980, 1981, 1994). These studies have also
147 served as an important reference into the distribution of stone sources along with their natural
148 morphometries and mechanical properties, which are key to interpret technological behavior
149 (Jones, 1979, 1980, 1981, 1994).

150 In recent years, prolific geological studies have been conducted in the NVH (Dawson, 2008;
151 Greenwood, 2014; Mana et al., 2012; McHenry et al., 2008; Mollel, 2002, 2007; Mollel et al.,
152 2008; Mollel et al., 2009; Mollel and Swisher III, 2012; Zaitsev et al., 2012). This makes it possible
153 to determine from which volcanic center the raw materials employed for artifact manufacture
154 ultimately came from, but not the location from where they were precisely sourced by early
155 hominins. However, characterization studies of the regional metamorphic inselbergs have been
156 limited. Many studies assume that the larger of the two Naibor Soit inselbergs was the primary
157 source of quartzite in the eastern palaeobasin (Blumenschine et al., 2008; Hay, 1976; McHenry
158 and de la Torre, 2018; Schick, 1987). In light of this, we sampled five of the most prominent
159 quartzite-bearing sources on the modern Oldupai landscape. These outcrops were likely frequented
160 by early hominins for raw materials since they were available in the Pleistocene and were close to
161 known sites, according to the high frequency of quartzite lithics in archaeological collections
162 (Leakey, 1971; Leakey and Roe, 1994). Therefore, the characterization of quartzite sources will
163 help to establish resource availability, and act as a referential framework for future provenance
164 studies.

165 **3. Materials and Methods**

166 Over the last two years, our research team surveyed outcrops in the greater Oldupai region.
167 Samples were collected in primary (e.g. outcrop, geologic formation) and secondary (e.g. drainage
168 sump, riverbed) positions in order to fully characterize intra- and inter-outcrop lithological

169 variation. Our reference collection currently consists of 271 rock samples curated by the Stone
170 Tools, Diet, and Sociality project in the Tropical Archaeology Lab (TAL; Earth Sciences 811,
171 University of Calgary). Sampled quartzitic outcrops include Endonyo Osunyai (n = 4), Naibor Soit
172 Kubwa (n = 104), Naibor Soit Ndogo (n = 27), Naisiusiu (n = 7), and Oittii (n = 5). The variability
173 in the number of samples from a given outcrop is a direct representation of its size, macroscopic
174 heterogeneity or lack thereof, and of our ongoing efforts to fully understand the lithological and
175 geochemical variation of the two Naibor Soit inselbergs, as these are most prominent outcrops in
176 the eastern Oldupai palaeobasin.

177 This study summarizes a multi-scalar fingerprinting approach we took to understand the
178 availability and variability of different quartzite sources in the Oldupai region. We
179 macroscopically analyzed 147 samples and classified them into twelve RMGs. Following this, a
180 representative sample from each RMG was petrographically characterized, and the geochemical
181 profiles of 30 samples were determined using EDXRF spectroscopy.

182 **3.1. Field Sampling and Reference Collection**

183 Geoarchaeological surveys were designed based on a literature review of known quartzitic
184 outcrops in combination with digital cartographic data (i.e. geological and topographic maps,
185 orthophotos, and satellite imagery), and knowledge that members of local Maasai communities
186 shared with us on the spatial distribution of regional outcrops. While sampling each outcrop, rocks
187 were selected based on diverse macroscopic characteristics in order to obtain a sample population
188 representative of intra-outcrop variability. A geological hammer was used to extract a sample, after
189 which these were labelled and photographed, and the outcrop characteristics documented. GPS
190 coordinates of sample locations were recorded using a Garmin eTrex 10.

191 **3.2. Macroscopic Classification and Petrographic Analysis**

Data collected in the field were first uploaded into a georeferenced database. Afterwards, each sample within our reference collection was measured and weighed (Table 1), and macroscopically analyzed. Macroscopic criteria included color/s by referencing the Munsell Rock Color Booklithology, morphology (tabular, angular, sub-angular, sub-tabular, subrounded or rounded blanks), grain size (Table 2), texture, gloss, transparency, mineral composition, impurities, and post-depositional alterations (Supplementary Materials Table 2) (Demars, 1982; Howard, 2005). A total of 147 quartzite samples were categorized into four quartzite types (R-Red; W-White; Gr-Gray; G-Green), and into an additional twelve RMGs (R1-R5; W1-W4; GR1-GR2; G1) based on distinct macroscopic traits, most notably color, grain size, texture, and mineral composition. The use of the term RMG was preferred over the term Raw Material Unit (RMU) as we intend to determine the availability and variability of quartzites rather than perform a temporal reconstruction of knapping sequences or identify refits (Roebroeks, 1998; Vaquero and Pasto, 2001; Vaquero, 2008).

RMG	Samples (n)	Length ($\bar{x}$; mm)	Width ($\bar{x}$; mm)	Thickness ($\bar{x}$; mm)	Total Weight (g)
R1	11	90.9	63.9	39.1	3365.46
R2	3	92.6	63.3	37	1255.24
R3	30	83.4	64.8	44	8822.90
R4	14	95	63.6	43.5	4185.67
R5	1	80	60	46	286
W1	12	92	64.4	43	3765.62
W2	9	95.4	74.8	45	2739.29
W3	29	86.4	60.5	35.7	5771.31
W4	2	80	56.5	33	107.42
GR1	14	90.9	59.9	43.8	3802.06
GR2	7	90.3	68.4	34.7	1190.95
G1	15	85.4	59.7	33.2	3868.59

Table 1. Number of samples, average size dimensions, and total weight per RMG.

Grain Size	Values (mm)
Fine-grained	<3
Medium-grained	3-5
Coarse-grained	5-10
Very coarse-grained	>10

Table 2. Grain size scale used for macroscopic analyses.

Representative samples from each RMG were thin sectioned in the TAL. A total of twelve samples were cut flat (IsoMet 4000 Linear Precision Saw), mounted (Cast N' Vac 1000 Castable Vacuum System) on frosted slides (27x46 mm) using epoxy resin (Buehler EpoThin 2), ground (PetroThin Thin Sectioning System) to ~30 μm, and polished (Metaserv 2000 Grinder Polisher). Uncovered thin sections were analyzed using a polarizing microscope (Leitz HM-POL; 2.5-40 x) to determine their mineral composition, modes, textures, and crystal habits (Folk, 1980; Melgarejo, 1997; Pettijohn et al., 1974; Perkins, 2002). Photomicrographs were taken using a Nikon ECLIPSE 50i POL microscope (2-40 x) equipped with a Moticam 2500 (Motic Images Plus 2.0).

3.3. EDXRF

A total of 30 samples (Endonyo Osunyai = 4; Naibor Soit Kubwa = 9; Naibor Soit Ndogo = 5; Naisiusiu = 7; Oittii = 5) from eight RMGs were analyzed using a Thermo Scientific *ARL Quant'X* EDXRF spectrometer in the McMaster Archaeological XRF Lab (MAX Lab). Prior to analysis, samples were cut into cubes (30 mm^2/face) using a Trim Saw (TS10, Lortone Inc.) in the TAL to obtain planar surfaces to reduce X-ray scattering. In the MAX Lab, samples were placed in individual glass beakers, immersed with distilled water, and cleaned in an ultrasonic tank for ten minutes. After completion, samples were air dried, then positioned and secured on the spectrometer's sample tray. Each sample tray run for this study included the RGM-2 reference standard (USGS) which was analyzed alongside our samples to ensure instrumentation calibration.

225 The EDXRF spectrometer is equipped with an end window Bremsstrahlung, air cooled, Rh
226 target, 50-watt, X-ray tube with a ≤7.6 μm (0.3 mil) beryllium (Be) window, an X-ray generator
227 that operates from 4-50 kV in 1 kV increments (current range, 0-1.98 mA in 0.02 mA increments),
228 and an Edwards RV8 vacuum pump for the analysis of elements below titanium (Ti). Data are
229 acquired with a pulse processor and analog to digital converter. In these preliminary stages of
230 regional quartzite characterization, an all-encompassing analytical method was run in order to
231 obtain the concentrations of eight major elements and ten trace elements under an automated series
232 of six analytical conditions (Table 3). Major elements (SiO_2, TiO_2, Al_2O_3, Fe_2O_3, MnO, MgO,
233 CaO, and K_2O) were measured as oxides in weight % and trace elements (Cu, Zn, Rb, Sr, Y, Zr,
234 Nb, Ba, Pb, and Th) were measured in ppm. X-ray intensities of elements were converted to
235 concentrations using a least-squares calibration line ratioed to the Compton scatter established for
236 each element from the analysis of international rock standards. These include AGV-2 (andesite),
237 BCR-2 (basalt), BHVO-2 (hawaiite), BIR-1a (basalt), GSP-2 (granodiorite), JR-1 (obsidian), JR-
238 2 (obsidian), QLO-1 (quartz latite), RGM-2 (rhyolite), SDC-1 (mica schist), STM-2 (syenite),
239 TLM-1 (tonalite), and W-2a (diabase).

Condition	Filter	Voltage	Atmosphere	Analytes
High Zb	Cu Thick	49 kV	Air	Ba
Mid Zb	Pd Med	20 kV	Air	Cu, Zn
Mid Zc	Pd Thick	28 kV	Air	Rb, Sr, Y, Zr, Nb, Pb, Th
Low Za	No Filter	4 kV	Vacuum	Mg, Al, Si
Low Zb	Cellulose	8 kV	Vacuum	Ca, K
Low Zc	Aluminum	14 kV	Vacuum	Mn, Ti, Fe

240 Table 3. Analytical conditions for EDXRF analyses.

241 The resulting data were imported to Microsoft Excel where these were normalized to the
242 reference standard (RGM-2) using the Min-Max scaling method (Xnorm = X−Xmin /

243 Xmax−Xmin) prior to its interrogation and plotting. This procedure ensures that results are
244 consistent in relation to the reference standard, thereby allowing for accurate comparative analyses
245 among data. Kendall's Tau, employing Monte Carlo permutation tests (N=9999) and and Kruskal-
246 Wallis tests were performed in PAST 3.22 to understand the dependence and degree of variance
247 among all elements by outcrop. With each sample classified by outcrop and RMG, Analyses
248 (PCA), , and after confirming the adequacy of our data through the Kaiser-Meyer-Olkin (KMO)
249 index, two Principal Component Analyses (PCA) were performed in R (R Core Team, 2017) using
250 Factominer (Lê et al., 2008) and Factoextra (Kassambara and Mundt, 2017) packages to explore
251 the segregation power of the geochemical data, as well as to identify factor loadings and variable
252 correlations. Discriminant Function Analyses (DFA) were also performed using the classification
253 by outcrop and RMG to confirm the discriminatory power of the geochemical and macroscopic
254 data, showing the statistical significance of the differences, and predicting a model to unknown
255 results.

256 **4. Results**

257 **4.1. Macroscopic and Petrographic Characterization**

258 Macroscopic analyses of 147 quartzite samples allowed us to identify four types (Red-R;
259 White-W; Gray-Gr; Green-G) that were further classified in twelve RMGs (R1-R5; W1-W4; GR1-
260 GR2; G1) (Table 4; Supplementary Materials Table 2). These are described below.

261 **4.1.1. Red Quartzites (R1-R5)**

262 Red quartzites are red to brown in color and occasionally oxidized, fine- to very coarse-
263 grained, and samples have tabular to sub-angular morphologies with occasional plane fractures
264 (Fig. 3). They are characterized by inequigranular and generally interlocked quartz crystals, white
265 micas, and opaque minerals. Differences in color, grain size, and texture allowed us to identify

five RMGs (Table 4). Under thin section, quartz crystals are inequigranular and anhedral, have sutured boundaries, and display undulatory extinction. Muscovite crystals have a platy or plumose habit, are either interstitial or embedded in quartz, and display a parallel to sub-parallel lineation. Hematite ranges from massive to fine, with the latter predominantly interstitial. Rare rutile and biotite are present depending on the RMG (Table 4).

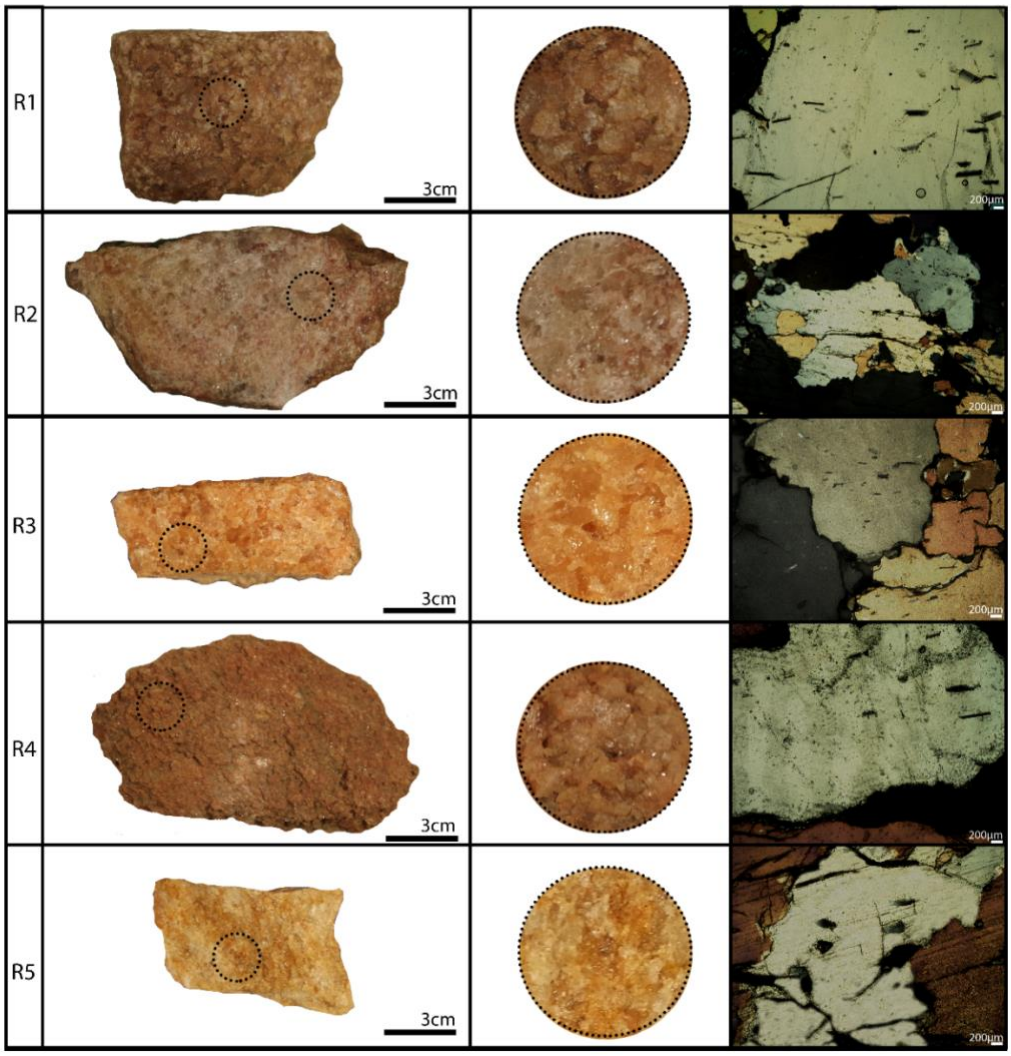

Fig. 3. Red Quartzites (RMG R1-R5): Macroscopic textures and photomicrographs under cross-polarized light. 2-column fitting image.

4.1.2. White Quartzites (W1-W4)

White quartzites are white to pinkish, medium- to very coarse-grained, and samples have tabular to sub-angular morphologies (Fig. 4). They are characterized by interlocked and anhedral quartz crystals, white micas, and opaque minerals. Differences in color, grain size, texture, and mineral composition allowed us to identify four RMGs (Table 4). Under thin section, quartz crystals are inequigranular, anhedral, have sutured boundaries, and display undulatory extinction. Muscovite crystals have platy habits, are either interstitial or embedded in quartz, and display a parallel to sub-parallel lineation. Hematite ranges from massive to fine, with the latter predominantly interstitial. Rutile is present in one RMG (Table 4).

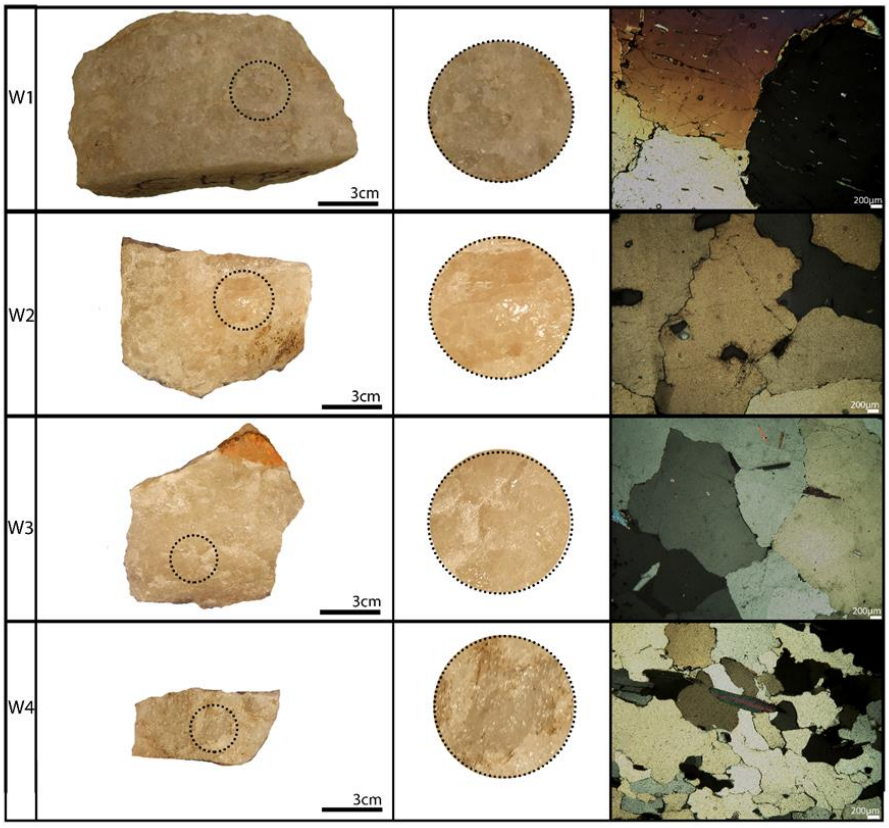

Fig. 4. White Quartzites (RMG W1-W4): Macroscopic textures and photomicrographs under cross-polarized light. 2-column fitting image.

4.1.3. Gray Quartzites (GR1-GR2)

Gray quartzites are gray to pale blue, fine- to coarse-grained, and samples have sub-angular morphologies with occasional plane fractures (Fig. 5). They are characterized by interlocked quartz crystals, white micas, and opaque minerals that are responsible for dark zonations (Table 4). Differences in color, grain size, and texture allowed us to identify two RMGs (Table 4). Under thin section, quartz crystals are inequigranular, anhedral, occasionally weakly foliated, characterized by sutured boundaries, and display undulatory extinction. Muscovite crystals have platy habits that are either interstitial or embedded in quartz, and display a parallel to random lineation. Hematite ranges from massive to fine, and rutile is rare in both RMGs (Table 4).

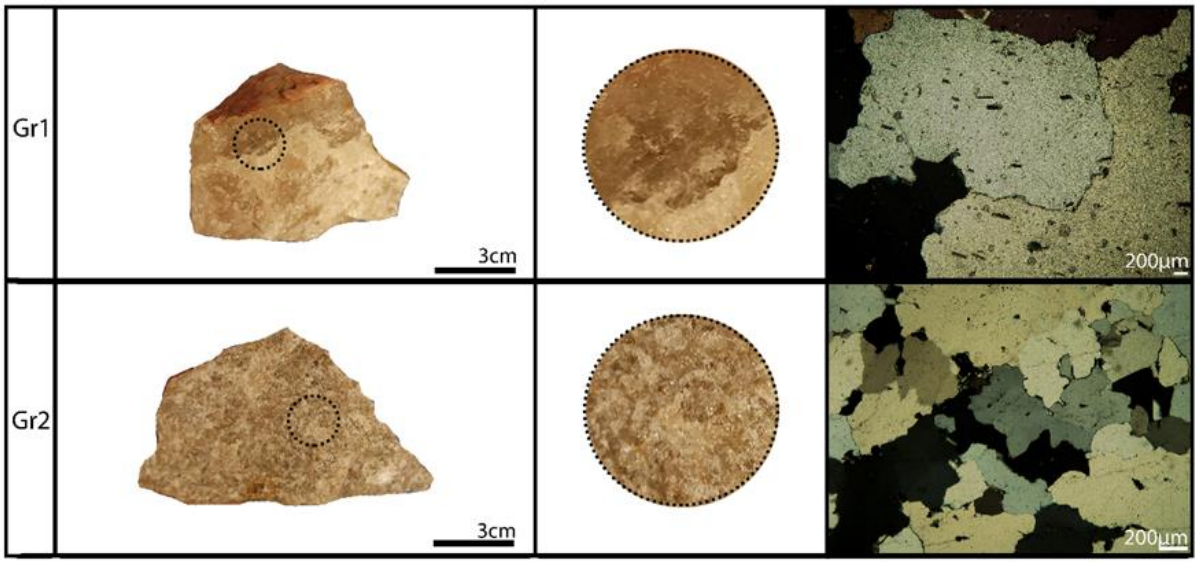

Fig. 5. Gray Quartzites (RMG GR1-GR2): Macroscopic textures and photomicrographs under cross-polarized light. 2-column fitting image.

4.1.4. Green Quartzites (G1)

Type	RMG	Macroscopic Analysis	Petrographic Analysis	Outcrop
Red Quartzites (R)	R1	5YR 7/2 Grayish Orange Pink; 5YR 6/4 Light Brown; 5YR 5/6 Light Brown Tabular blocks Very coarse-grained Interlocking quartz Mica	Quartz (90%), inequigranular, undulatory extinction Muscovite (5%), platy, inter- and intra-crystalline, parallel lineation Hematite (5%), fine, inter-crystalline **Sample ID: NSK C4A**	Naibor Soit Kubwa Naibor Soit Ndogo
	R2	5YR 6/4 Light Brown; 5R 4/2 Grayish Red Tabular blocks, plane fractures Medium- to coarse-grained Interlocking quartz Mica Opaque minerals	Quartz (90%), inequigranular, sutured boundaries Quartz (5%), anhedral, inter-crystalline between sutured boundaries Muscovite (3%), platy and plumose, sub-parallel lineation Hematite (2%), fine, inter-crystalline **Sample ID: NSK G9A**	Naibor Soit Kubwa Naibor Soit Ndogo
	R3	5YR 6/4 Light Brown; 5R 4/2 Grayish Red; 5Y 8/1 Yellowish Gray; 5YR 8/4 Grayish Brown Tabular blocks Fine- to medium- to coarse-grained Interlocking quartz Mica Opaque minerals	Quartz (93%), inequigranular Muscovite (5%), platy, inter- and intra-crystalline, parallel lineation Hematite (1%), fine, inter-crystalline Rutile (1%), prismatic, high-relief, dark red **Sample ID: Naibor Soit Kubwa 1**	Endonyo Osunyai Naibor Soit Kubwa Naibor Soit Ndogo
	R4	5YR 6/4 Light Brown; 5YR 5/6 Light Brown Sub-angular blocks, sub-parallel plane fractures and crystal disaggregation Very coarse-grained Interlocking quartz Mica	Quartz (96%), inequigranular Muscovite (3%), platy, parallel lineation Hematite (1%), fine, inter-crystalline **Sample ID: NSK K12B**	Naibor Soit Kubwa
	R5	N7 Light Gray Tabular blocks, occasional plane fractures Fine- to medium- to coarse-grained Weakly foliated quartz Mica	Quartz (90%), inequigranular, intense undulatory extinction Muscovite (2-4%), platy, inter- and intra-crystalline, sub-parallel lineation Hematite (2-4%), massive and fine Biotite (1%), massive and platy **Sample ID: Naisiusiu 1**	Naisiusiu
White Quartzites (W)	W1	N8 Very Light Gray; 5Y 8/1 Yellowish Gray Tabular blocks Coarse-grained Interlocking quartz Mica	Quartz (92%), inequigranular, undulatory extinction Muscovite (5%), platy, inter- and intra-crystalline, parallel lineation Opaque minerals and hematite (3%), massive and fine, inter- and intra-crystalline, respectively **Sample ID: NSK C4B**	Naibor Soit Kubwa Naibor Soit Ndogo
	W2	5YR 8/1 Pinkish Gray; 5G 6/1 Greenish Gray	Quartz (92%), inequigranular and anhedral	Naibor Soit Kubwa

		Tabular blocks Very coarse-grained Interlocking quartz Mica Inter-crystalline opaque minerals, some zonations	Muscovite (8%), platy, inter- and intra-crystalline, sub-parallel lineation Rutile (<1%), prismatic, high-relief, dark red **Sample ID: Naibor Soit Kubwa 13**	Naibor Soit Ndogo
	W3	N9 White; N7 Light Gray Tabular blocks Coarse-grained Interlocking quartz Mica, lustrous	Quartz (98%), inequigranular and anhedral, sutured boundaries, intense undulatory extinction Muscovite (2%), platy, inter- and intra-crystalline, sub-parallel lineation Opaque minerals and hematite (<1%), massive and fine **Sample ID: Endonyo Osunyai 2**	Endonyo Osunyai Naibor Soit Kubwa Naibor Soit Ndogo Naisiusiu
	W4	N9 White; N7 Light Gray; 5GY 8/1 Light Greenish Gray Sub-angular blocks, occasionally brittle Medium- to coarse-grained Inequigranular quartz Mica	Quartz (90%), inequigranular, weakly foliated, sutured boundaries, undulatory extinction, occasionally cemented and overgrown Quartz (5%), anhedral Muscovite (5%), platy, inter- and intra-crystalline, sub-parallel lineation **Sample ID: Naisiusiu 9**	Naisiusiu Oittii
Gray Quartzites (GR)	**GR1**	5PB 5/2 Grayish Blue; 5PB 7/2 Pale Blue Sub-angular blocks, common plane fractures Medium- to coarse-grained Interlocking quartz Mica Opaque minerals, zonations	Quartz (95%), inequigranular and anhedral, weakly foliated, sutured boundaries, undulatory extinction Muscovite (5%), platy, inter- and intra-crystalline, parallel lineation Rutile (<1%), prismatic, high-relief, dark red Opaque minerals (massive hematite?) (<1%) **Sample ID: Naibor Soit Kubwa 2**	Naibor Soit Kubwa Naibor Soit Ndogo Naisiusiu
	GR2	N8 Very Light Gray; N5 Medium Gray; 5YR 6/1 Light Brownish Gray Sub-angular blocks Fine- to medium-grained Interlocking quartz Mica Opaque minerals	Quartz (93%), inequigranular and anhedral, sutured boundaries, intense undulatory extinction Muscovite (3%), platy, fragmented, random lineation Hematite (3%), massive and fine Rutile (1%), prismatic, high-relief, dark red **Sample ID: Oittii 1A**	Endonyo Osunyai Naisiusiu Oittii
Green Quartzites (G)	**G1**	5YR 7/2 Grayish Orange Pink; 5YR 6/4 Light Brown; 5YR 8/1 Pinkish Gray; 5G 6/1 Greenish Gray; 5GY 8/1 Light Greenish Gray; 5G 6/6 Brilliant Green Tabular blocks Medium- to coarse-grained Interlocking quartz Mica Green mica	Quartz (85%), inequigranular and anhedral, weakly foliated, sutured boundaries, intense undulatory extinction Muscovite (14%), platy and plumose, inter- and intra-crystalline, sub-parallel lineation Rutile (1%), prismatic, high-relief, dark red Fuchsite (<1%), platy, intra-crystalline, sub-parallel lineation, green **Sample ID: Naibor Soit Kubwa 32**	Naibor Soit Kubwa Naibor Soit Ndogo

299 Table 4. Macroscopic and petrographic textures, grain sizes, mineral composition, and visually estimated modes for all RMGs and their source.

Green quartzites are light to bright green, medium- to coarse-grained, and samples have tabular morphologies (Fig. 6). They are characterized by interlocked quartz along with white and green micas. We identified one RMG based on color and mineral composition (Table 4). Under thin section, quartz crystals are inequigranular, anhedral, weakly foliated, characterized by sutured boundaries, and display undulatory extinction. Muscovite crystals have platy and plumose habits, are either interstitial or embedded in quartz, and display a sub-parallel lineation. Rare rutile and green fuchsite crystals are present, with the latter responsible for green zonations (Table 4).

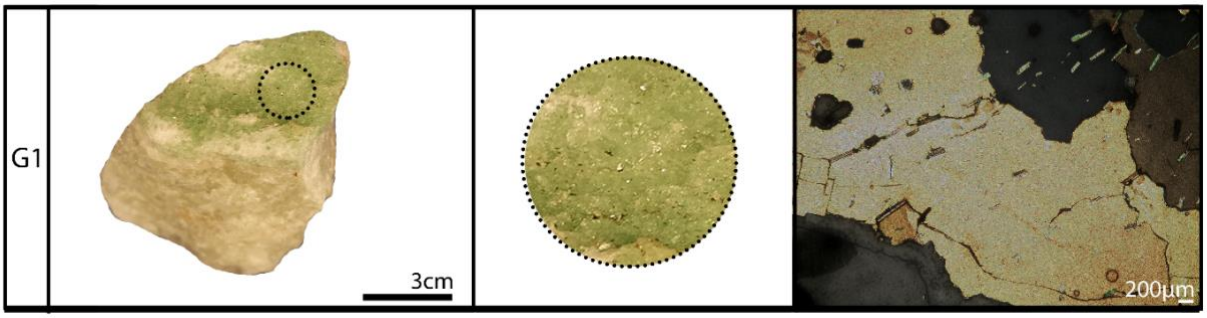

Fig. 6. Green Quartzites (RMG G1): Macroscopic textures and photomicrographs under cross-polarized light. 2-column fitting image.

4.2. Bulk Sample EDXRF Data

According to the averaged maximum and minimum concentrations for major and trace elements, the quartzites from the five sampled outcrops present different yet complex geochemical fingerprints (Supplementary Materials Fig. 1). The major and trace element concentrations per sample (Table 5; Supplementary Materials Table 4), and the relative standard deviations (RSD%) indicate that samples from Endonyo Osunyai show high variability in SiO_2, Al_2O_3, K_2O, Rb, Ba, Pb, and Th (Supplementary Materials Fig. 2). Samples from Naibor Soit Kubwa show high variability in SiO_2, MgO, Y, Ba, Cu, and Th (Supplementary Materials Fig. 3). Samples from Naibor Soit Ndogo show high variability in SiO_2, MgO, Cu, Y, and Ba (Supplementary Materials

319 Fig. 4). However, one outlier from Naibor Soit Ndogo has an unusually low SiO_2 value for
320 quartzite (Supplementary Materials Table 4) which may be explained by spectra diffracted from a
321 large non-quartz crystal, given the reanalysis of the sample proportionate higher values for the
322 SiO2 content. Samples from Naisiusiu show high variability in SiO_2, MgO, Cu, and Y
323 (Supplementary Materials Fig. 5). Samples from Oittii show a high dispersion in SiO_2, Al_2O_3,
324 K_2O, Rb, and Ba (Supplementary Materials Fig. 6).

325 The ratio between the maximum and minimum concentration of an element reflects the
326 variability among samples and outcrops. This variation indicates the complexity of the
327 geochemical profiles and the basement geology.

328 Linear correlations among the geochemical data from all samples were performed to
329 understand their relationships and identify regional patterns. The analysis indicates a slightly
330 significant negative correlation [p (uncorr.) < 0.05] among SiO_2 some trace elements as Rb (τ =
331 -0.23) , Sr (τ = -0.26), Ba (τ = -0.24) and Th (τ = -0.22) (Fig. 7a), indicating the role of these
332 elements in the composition despite the major SiO2 presence on the samles.As for other major
333 oxides, they show significant positive correlations [p (uncorr.) $\leq$ 0.001] with most of the analyzed
334 trace elements, except for Y (Fig. 7a). Trace elements show positive correlations with different
335 degrees of significance among most other elements, apart from MgO which are not significant,
336 except for Cu, Y and Zr [p (uncorr.) $\leq$ 0.001] (Supplementary Materials Tables 5 and 6).

	weight %								ppm									
	MgO	**Al_2O_3**	**SiO_2***	**K_2O**	**CaO**	**TiO_2**	**MnO**	**Fe_2O_3**	**Cu**	**Zn**	**Rb**	**Sr**	**Y**	**Zr**	**Nb**	**Ba**	**Pb**	**Th**
Endonyo Osunyai 2 (W3)	0.35	3.51	105.08	0.08	0.11	0.03	0.00	0.27	3	2	0	6	3	63	0	23	1	1
Endonyo Osunyai 3 (R3)	0.36	4.03	88.74	0.55	0.12	0.03	0.00	0.26	3	1	19	32	1	23	0	308	5	0
Endonyo Osunyai 4 (GR2)	0.63	6.81	79.47	1.80	0.12	0.11	0.00	0.84	10	6	91	89	4	100	4	637	11	11
Endonyo Osunyai 5 (GR2)	0.71	7.95	84.70	1.67	2.62	0.16	0.00	1.17	6	4	87	29	2	46	5	505	2	1
Naibor Soit Ndogo 13 (W3)	0.25	2.76	104.19	<DL	0.10	0.02	0.00	0.26	3	1	<DL	2	4	16	0	41	0	2
Naibor Soit Ndogo 13 (W3)	0.33	3.40	79.16	0.07	0.09	0.02	0.00	0.27	3	2	1	4	11	21	0	63	1	2
Naibor Soit Ndogo 14 (W3)	0.31	3.10	98.71	0.00	0.09	0.03	0.00	0.25	3	2	<DL	2	4	25	0	51	0	1
Naibor Soit Ndogo 14 (W3)	0.31	2.93	85.84	<DL	0.10	0.01	0.01	0.24	2	1	<DL	2	2	11	0	42	0	2
Naibor Soit Ndogo 15 (W3)	0.29	3.05	102.73	<DL	0.10	0.02	0.00	0.24	3	2	<DL	2	2	19	1	13	1	2
Naibor Soit Ndogo 15 (W3)	0.32	3.36	104.39	0.05	0.10	0.03	0.00	0.25	4	2	<DL	3	3	24	1	20	0	1
Naibor Soit Ndogo 6 (W3)	0.30	3.00	104.84	<DL	0.09	0.01	0.00	0.25	3	1	<DL	2	3	22	0	149	1	0
Naibor Soit Ndogo 6 (W6)	0.42	3.25	15.76	<DL	0.09	0.02	0.02	0.24	3	1	<DL	1	2	20	0	196	0	2
Naibor Soit Ndogo 8 (W3)	0.31	3.54	100.23	0.09	0.09	0.02	0.00	0.25	4	2	1	3	3	20	0	86	1	0
Naibor Soit Ndogo 8 (W3)	0.30	3.13	102.49	0.01	0.14	0.01	0.00	0.24	3	2	<DL	7	2	24	0	43	1	1
Naibor Soit Kubwa 1 (R3)	0.28	3.06	97.40	0.00	0.10	0.01	0.00	0.24	3	1	<DL	6	3	34	1	19	1	2
Naibor Soit Kubwa 11 (W3)	0.33	3.03	83.86	<DL	0.09	0.01	0.00	0.24	2	1	<DL	2	5	40	0	0	1	1
Naibor Soit Kubwa 13 (R3)	0.34	3.30	93.06	<DL	0.10	0.02	0.00	0.26	3	1	<DL	4	3	20	0	27	0	1
Naibor Soit Kubwa 14A (W2)	0.29	3.31	96.26	0.01	0.10	0.02	0.00	0.23	2	0	<DL	13	5	23	0	11	1	1
Naibor Soit Kubwa 2 (W3)	0.32	3.17	103.52	0.01	0.11	0.02	0.00	0.26	2	0	<DL	5	2	20	1	49	1	2
Naibor Soit Kubwa 24A (W2)	0.30	2.81	102.57	<DL	0.11	0.01	0.00	0.24	5	0	<DL	6	2	31	0	24	0	5
Naibor Soit Kubwa 27 (R3)	0.44	4.75	98.08	0.29	0.11	0.03	0.00	0.30	4	1	10	9	6	46	0	102	2	1
Naibor Soit Kubwa 31A (G1)	0.33	3.25	103.34	0.02	0.09	0.03	0.00	0.26	3	0	<DL	2	2	27	0	15	0	1
Naibor Soit Kubwa 33A (GR1)	0.32	2.95	85.54	<DL	0.09	0.01	0.00	0.24	3	0	<DL	1	4	15	0	32	0	1
Naisiusiu 1 (R6)	0.42	4.59	97.50	0.12	0.16	0.06	0.00	0.54	7	4	3	35	15	58	0	146	4	3
Naisiusiu 1 (R6)	0.45	5.24	94.41	0.28	0.22	0.12	0.01	0.71	7	6	8	59	20	77	1	257	6	3
Naisiusiu 13 (R5)	0.35	2.80	102.99	<DL	0.09	0.00	0.00	0.27	4	2	<DL	0	1	0	1	35	1	0
Naisiusiu 13 (R5)	0.30	2.79	104.20	<DL	0.09	0.00	0.00	0.30	3	1	<DL	1	0	0	0	0	0	0
Naisiusiu 14 (W4)	0.43	3.34	101.67	0.03	0.12	0.03	0.00	0.25	4	5	<DL	3	0	28	0	26	2	1
Naisiusiu 14 (W4)	0.45	4.55	88.37	0.39	0.35	0.05	0.00	0.28	3	4	4	9	12	93	2	21	4	3
Naisiusiu 4 (GR2)	0.37	3.51	100.17	<DL	0.17	0.01	0.00	0.37	5	3	2	31	8	38	1	0	1	2
Naisiusiu 4 (GR2)	0.35	3.39	84.72	<DL	0.21	0.02	0.00	0.34	6	6	<DL	24	6	30	0	26	1	1
Naisiusiu 6 (W3)	0.37	5.00	95.35	0.44	0.11	0.06	0.00	0.27	3	4	11	7	9	27	3	33	2	1
Naisiusiu 6 (W3)	0.37	4.56	97.17	0.32	0.10	0.04	0.00	0.27	4	4	9	5	6	23	1	27	2	3
Naisiusiu 7 (GR1)	0.41	3.44	101.46	<DL	0.26	0.03	0.01	0.56	4	5	<DL	14	5	30	1	20	2	3
Naisiusiu 7 (GR1)	0.36	3.65	89.50	<DL	0.36	0.02	0.00	0.35	4	4	<DL	19	8	38	0	34	1	3
Naisiusiu 9 (W4)	0.31	3.06	100.80	0.00	0.09	0.02	0.00	0.25	4	2	3	6	1	22	0	52	2	0
Naisiusiu 9 (W4)	0.38	3.55	102.93	0.11	0.09	0.03	0.00	0.26	4	3	3	6	0	28	1	39	2	0
Oittii 1 (GR2)	0.46	3.19	97.01	0.01	0.59	0.04	0.02	0.37	3	1	<DL	5	1	22	1	349	2	1
Oittii 2 (GR2)	0.53	3.18	101.81	<DL	0.35	0.04	0.01	0.33	12	2	<DL	6	2	32	0	629	3	1

	weight %								ppm									
	MgO	**Al_2O_3**	**SiO_2 ***	**K_2O**	**CaO**	**TiO_2**	**MnO**	**Fe_2O_3**	**Cu**	**Zn**	**Rb**	**Sr**	**Y**	**Zr**	**Nb**	**Ba**	**Pb**	**Th**
Oittii 3 (W4)	0.43	5.20	92.79	0.91	0.11	0.05	0.00	0.29	3	2	45	20	2	54	1	371	3	3
Oittii 4 (GR2)	0.39	4.27	98.73	0.66	0.10	0.04	0.00	0.33	6	2	23	24	1	39	1	227	3	1
Oittii 5 (GR2)	0.50	6.34	94.14	1.23	0.10	0.09	0.00	0.85	4	4	63	42	3	44	2	319	3	4
RGM-2 (Standard)	0.27	13.36	74.07	3.36	0.95	0.30	0.04	1.84	11	30	146	106	23	226	8	845	20	14
RGM-2 (Standard)	0.25	13.41	74.36	3.38	0.95	0.29	0.04	1.83	12	33	144	104	24	225	10	831	20	14
RGM-2 (Standard)	0.25	13.46	74.60	3.38	0.95	0.29	0.04	1.85	10	30	145	107	26	228	9	838	20	14
RGM-2 (Standard; RV)	0.28 ± 0.02	14 ± 0.02	73.4 ± 0.41	4.35 ± 0.16	1.23 ± 0.16	0.25 ± 0.02		1.86 ± 0.04	9.8 ± 0.8	33 ± 2	147 ± 5	108 ± 5	24 ± 2	222 ± 17	9.0	842 ± 35	20 ± 1	15 ± 1

Table 5. Raw EDXRF data per sample (major oxides: weight %; trace elements: ppm) (<DL: values below detection limit) (RV: Recommended Value).
* Some SiO_2 values are off the upper end of the calibration standard.

339 The grouping of samples by outcrop reduces the linear correlations compared with
340 ungrouped samples. Samples from Endonyo Osunyai (Fig. 7b) show significant negative
341 correlations among among SiO_2 and K_2O, Rb and Ba [$\tau = -1$; p (uncorr.) < 0.05), and positive ones
342 [$\tau = 1$; p (uncorr.) < 0.05] between TiO2 and MnO, among Al_2O_3 and MgO and CaO, and between
343 MgO and CaO (Supplementary Materials Table 7). These major oxides together with K2O present
344 significant positive correlations [$\tau = -1$; p (uncorr.) < 0.05], with some trace elements as Rb, Nb
345 or Ba. When existing correlations among the analyzed trace elements they are positive and
346 significants. However, must to be considered that all these correlations stop being significants [p
347 (uncorr.) > 0.05] when applying the Monte Carlo simulation (Supplementary Materials Table 8).
348 Most of the major oxides from Naibor Soit Kubwa are positively correlated (p (uncorr.) <0.05),
349 among them and with some of the trace elements as Cu, Sr, Nb, Ba and Pb, with different degrees
350 of significance (Fig. 7c) (Supplementary Materials Table 9). Only MnO and MgO present slight
351 negative correlations with Th [τ = -0.67; p (uncorr.) 0.01, and -0.59; p (uncorr.) = 0.02,
352 respectively]. Regarding the trace elements, when existing signiticant correlations they are always
353 positive (Fig. 7c). Most of these correlations are still significant [p (uncorr.) < 0.05] after applying
354 the Monte Carlo simulation (Supplementary Materials Table 10). Samples from Naibor Soit Ndogo
355 have few significant correlations. SiO_2 shows a negative correlation with MgO [τ = -0.52; p
356 (uncorr.) < 0.05], and MgO with CaO [$\tau = -0.8$; p (uncorr.)= 0.00], While K_2O presents positive
357 correlations of different degrees of significance [p (uncorr.) < 0.05] with TiO_2 ($\tau = 0.50$) and Al_2O_3
358 ($\tau = 0.8$) (Fig. 7d) (Supplementary Materials Table 11). Regarding the trace elements, only MnO
359 presents a negative correlation [p (uncorr.) < 0.05] with Cu ($\tau = -0.57$) and Sr ($\tau = -0.8$), and Nb
360 with Ba ($\tau = -0.55$). The rest of significant correlations among these are positive, and tend to

maintain its significance after performing the Monte Carlo simulation (Supplementary Materials Table 12).

Samples from Naisiusiu show significant negative correlations [p (uncorr.) < 0.05] among SiO_2 and Al_2O_3 (τ = -0.45), CaO (τ = -0.44), Rb (τ = -0.39), Sr (τ = -0.46), Y(τ = -0.53), Zr (τ = -0.44), and Th (τ = -0.41). The rest of major oxides are positively correlated among them with the exception of MnO [p (uncorr.) > 0.05] (Fig. 7e) (Supplementary Materials Table 13). Trace elements present in the Naisiusiu samples show some positive significant correlations [p (uncorr.) <0.05] with all the major elements, except for SiO_2. Most of these correlations remain significant after the Monte Carlo simulation (Supplementary Materials Table 14) Samples from Oittii show positive significant correlationsamong Al_2O_3, TiO_2 and K_2O, CaO and MnO), and TiO_2 and K_2O (Fig. 7f) (Supplementary Materials Table 15). As for trace elements, when significant linear correlations are detected,

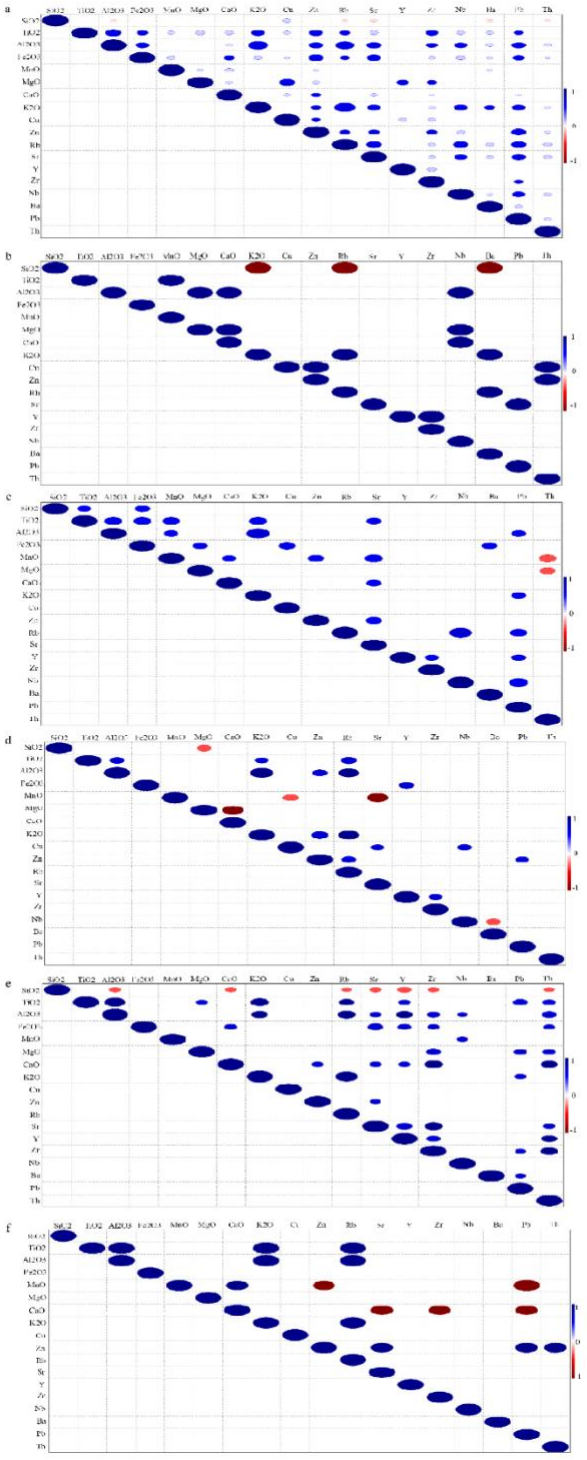

Fig. 7. Plot of significant correlations (Kendall's Tau) (positive: blue; negative: red). a) All samples; b) Endonyo Osunyai; c) Naibor Soit Kubwa; d) Naibor Soit Ndogo; e) Naisiusiu; f) Oittii. 2-column fitting image.

these are positive, apart from CaO and Sr, Zr), Pb (τ = -0.84), MnO and Zn (τ = -0.84) , and Pb (τ = -1). However, these are not significant after applying the Monte Carlo simulation (Supplementary Materials Table 16).

Variance analysis (Kruskal-Wallis test) on all samples grouped by outcrop allowed us to determine the elemental variability among samples. When comparing all samples, the Kruskal-Wallis test results in a p (same) =< 0.001.. Samples from from Naibor Soit Ndogo [p(same) = 0.99] and Oitti [p(same) = 0.37] i are the most homogeneous among the analyzed samples. Quartzites from Naibor Soit Kubwa [p (same) = < 0.0001], Naisiusiu [p (same) = 0.0001], and Oittii [p (same) < 0.0001] show variable intra-outcrop geochemical fingerprints. Further data exploration rejects the hypothesis that variance is related with differential sample size per outcrop or by RMG. Plotting the average of the Coefficient of Variation (CV= μ / σ) for each outcrop against the number of samples indicates an absence of correlation [r = 0.09; p (uncorr.) = 0.88] (r^2 =0.01). This is also the case when plotting the average CV for each RMG against the number samples [r = 0.44; p (uncorr.) = 0.32] (r^2 =0.19) (Fig. 8).

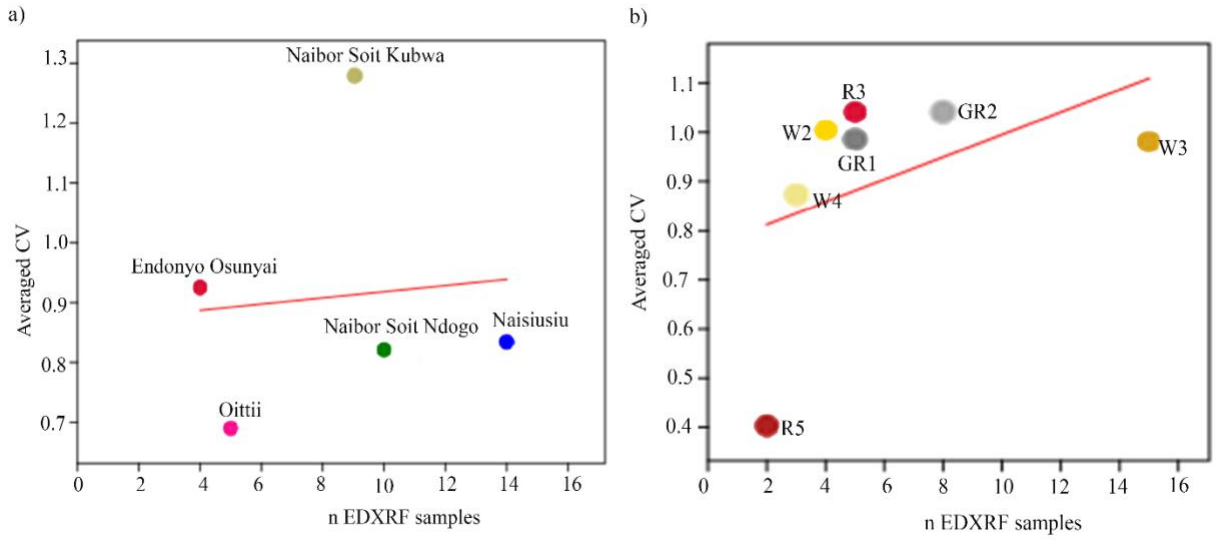

Fig. 8. a) Plot of the averaged CV against the number of EDXRF samples by outcrop; b) Plot of the averaged CV against the number of EDXRF samples by RMG. 2-column fitting image.PCA (KMO = 0.78) allowed us to explicate that the first three components retained 80.06% of the cumulative variance (Table 6), confirming the segregative power of the geochemical data according to multivariate analysis. The first component is based on Ba, SiO_2, Rb, K_2O, Th, Pb, and Al_2O_3 (eigenvector loadings range from 15-5%), the second component is mainly based on SiO_2 (eigenvector loading >60%) and MgO (eigenvector loading ~25%), and the third component is based on Y, MgO, Cu, and SiO_2 (eigenvector loadings range from 40%-~10%) (Supplementary Materials Fig. 7). According to these components, there is a high degree of correlation among the geochemical composition of Naibor Soit Ndogo and Naisiusiu, despite their different averaged geochemical profiles (Supplementary Materials Fig. 1), due to their elevated SiO_2 and MgO values. Quartzites from Endonyo Osunyai and Oittii also share similar geochemical fingerprints based on the rest of the major and trace element values. Most samples from Naibor Soit Kubwa are distinguishable from the other sampled outcrops, and have the most balanced elemental compositions (Fig. 9).

The first three components of the DFA result in a cumulative variance of 98.61% (Table 7), confirming the discriminatory power of the geochemical data. The first component is mainly determined by the presence of MgO, Y, SiO_2, and Cu. The second component is based on most of the trace elements and major oxides. The third component is determined by the presence of SiO_2 and MnO. According to these components, the geochemical profiles of the five analyzed outcrops are different enough to be distinguishable, and only Naibor Soit Ndogo and Naisiusiu present some similarities based on their SiO_2 and MgO values (Fig. 10). DFA indicate that the 97.62% samples are correctly classified according their original provenance, and only one sample from Naibor Soit

Ndogo has a geochemical profile that could be associated to Naisiusiu. 71.43% of the samples are correctly classified using the Jackknife method, confirming the high significance of the discriminant values for Naibor Soit Kubwa and Oittii (Supplementary Materials Table 17 and 18).

Principal Component	Eigenvalue	Variance Percentage	Cumulative Variance Percentage
Dim. 1	1.562	52.630	52.630
Dim. 2	0.456	15.353	67.983
Dim. 3	0.358	12.073	80.056
Dim. 4	0.209	7.037	87.093
Dim. 5	0.148	4.985	92.078
Dim. 6	0.112	3.756	95.835
Dim. 7	0.043	1.452	97.286
Dim. 8	0.035	1.187	98.474
Dim. 9	0.028	0.936	99.410
Dim. 10	0.009	0.308	99.718

Table 6. Eigenvalues and variance percentages of the PCA components.

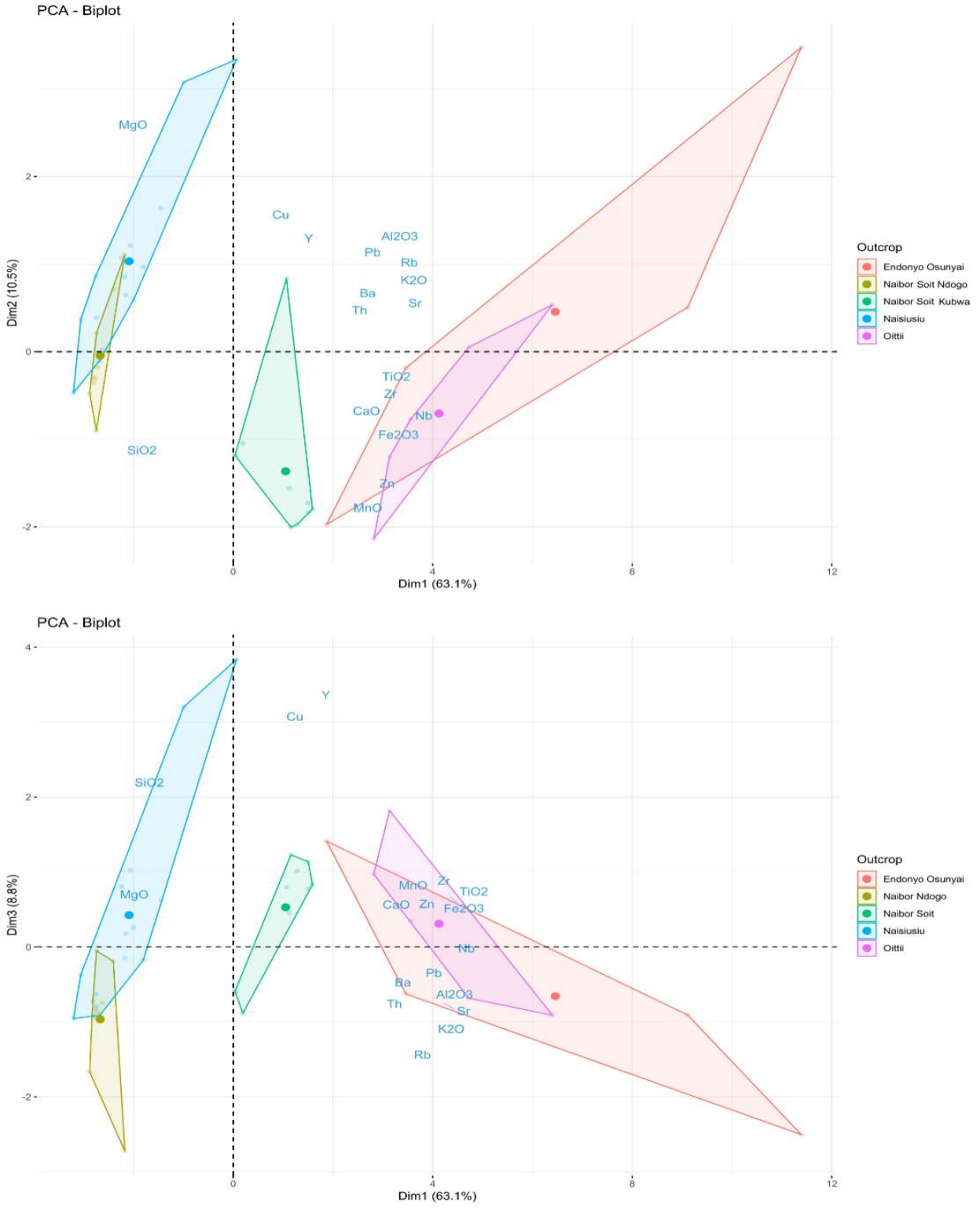

Fig. 9. PCA using EDXRF data with samples grouped by outcrop, including the variables determining the first three components. 2-column fitting image.

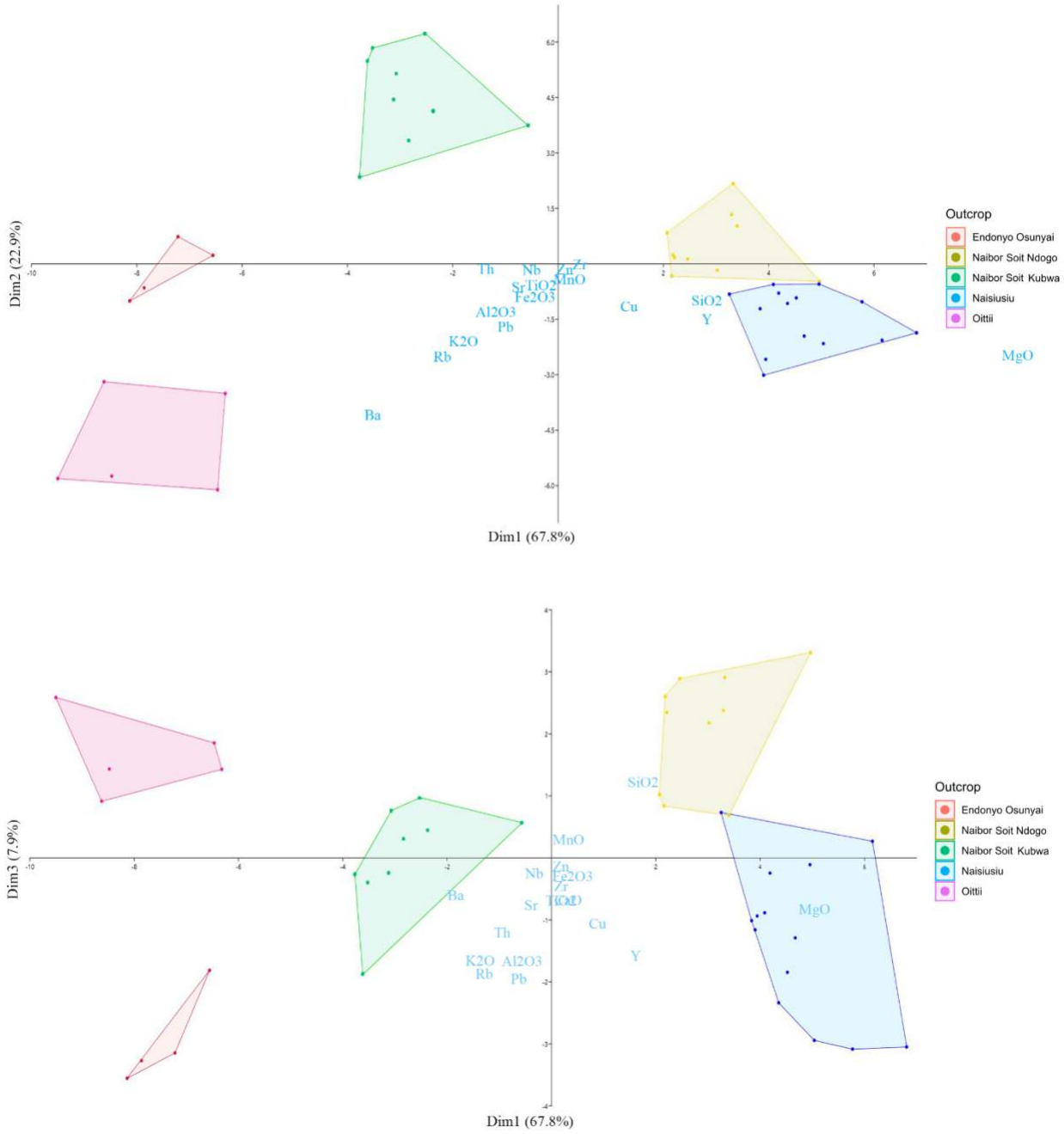

422

423 Fig.10. DFA using EDXRF data with samples grouped by outcrop, including the variables

424 determining the first three components. 2-column fitting image.

425

Principal Component	Eigenvalue	Variance Percentage	Cumulative Variance Percentage
Dim. 1	26.88	67.82	67.82
Dim. 2	9.07	22.89	90.71
Dim. 3	3.13	7.90	98.61
Dim. 4	0.55	1.38	100

Table 7. Eigenvalues and variance percentages of the DFA components

5. Discussion

5.1. Quartzite Fingerprints

The macroscopic characteristics used to classify samples into RMGs were treated as independent variables in a second PCA (Fig. 11), which relied on the same cumulative variance and components as in the first PCA (Fig. 9). This was done to determine the comparability of macroscopic, petrographic, and geochemical approaches.

Red quartzite varieties (R1-R5) can be found at Endonyo Osunyai, Naibor Soit Kubwa, Naibor Soit Ndogo, and Naisiusiu. These range in texture from fine- to very coarse-grained, and predominantly consist of quartz along with lesser amounts of muscovite, hematite, rutile, and biotite. R3 consists of fine- to coarse-grained red quartzites from Endonyo Osunyai, Naibor Soit Kubwa, and Naibor Soit Ndogo, although these have distinguishable geochemical profiles. Biotite-bearing quartzites (R5) are exclusive to Naisiusiu.

White quartzite varieties (W1-W4) can be found at all five sampled outcrops. These varieties range in texture from medium- to very coarse-grained, and predominantly consist of quartz along with minor amounts of muscovite, opaque minerals, hematite, and rutile. Very coarse-grained rutile-bearing quartzite (W2) is exclusive to Naibor Soit Kubwa and Naibor Soit Ndogo. However, differences in SiO_2 values and trace elements for Naibor Soit Kubwa, and MgO for Naibor Soit Ndogo, allow us to distinguish among the quartzites from these two outcrops. RMGs W3 and W4 can be found at Endonyo Osunyai, Oittii, Naibor Soit Kubwa, Naibor Soit Ndogo,

and Naisiusiu. However, samples classified in both varieties from Endonyo Osunyai, Oittii, and Naibor Soit Kubwa are distinguishable to those from Naibor Soit Ndogo and Naisiusiu based on MgO and SiO_2 values.

Medium- to coarse-grained gray quartzites (GR1) can be found at Naibor Soit Kubwa, Naibor Soit Ndogo, and Naisiusiu. Samples classified in GR1 from Naibor Soit Kubwa are distinguishable from those of Naibor Soit Ndogo and Naisiusiu based on major and trace elements. However, Naibor Soit Ndogo and Naisiusiu have similar geochemical profiles. Fine- to medium-grained gray quartzites (GR2) can be found at Endonyo Osunyai, Oittii, and Naisiusiu. While GR2 quartzites from the former two outcrops have similar geochemical fingerprints, they can be distinguished to those from Naisiusiu based on differences in MgO values.

Green fuchsite-bearing quartzite (G1) is exclusively found at Naibor Soit Kubwa and Naibor Soit Ndogo, affirming these inselbergs as the primary sources for this RMG.

The first three components of the DFA result in a cumulative variance of 87.28% (Table 7), confirming the discriminatory power of the geochemical data and the macroscopic classification. The first component is mainly determined by the presence of Y, Ba, Cu, Pb, Al_2O_3, and MgO The second component is based mostly on Ba, RB, K_2O, and Th. The third component is mainly determined by the presence of trace elements such as Th, Y, and Sr along with major oxides such as Fe_2O_3 or Al_2O_3. According to these components, the discrimination of samples classified in RMGs R5, and GR2 is clear according to their geochemical compositions. However, geochemical overlap exists among the RMGs W1-4, G1, and R3 due to their SiO_2 contents (Fig. 12).

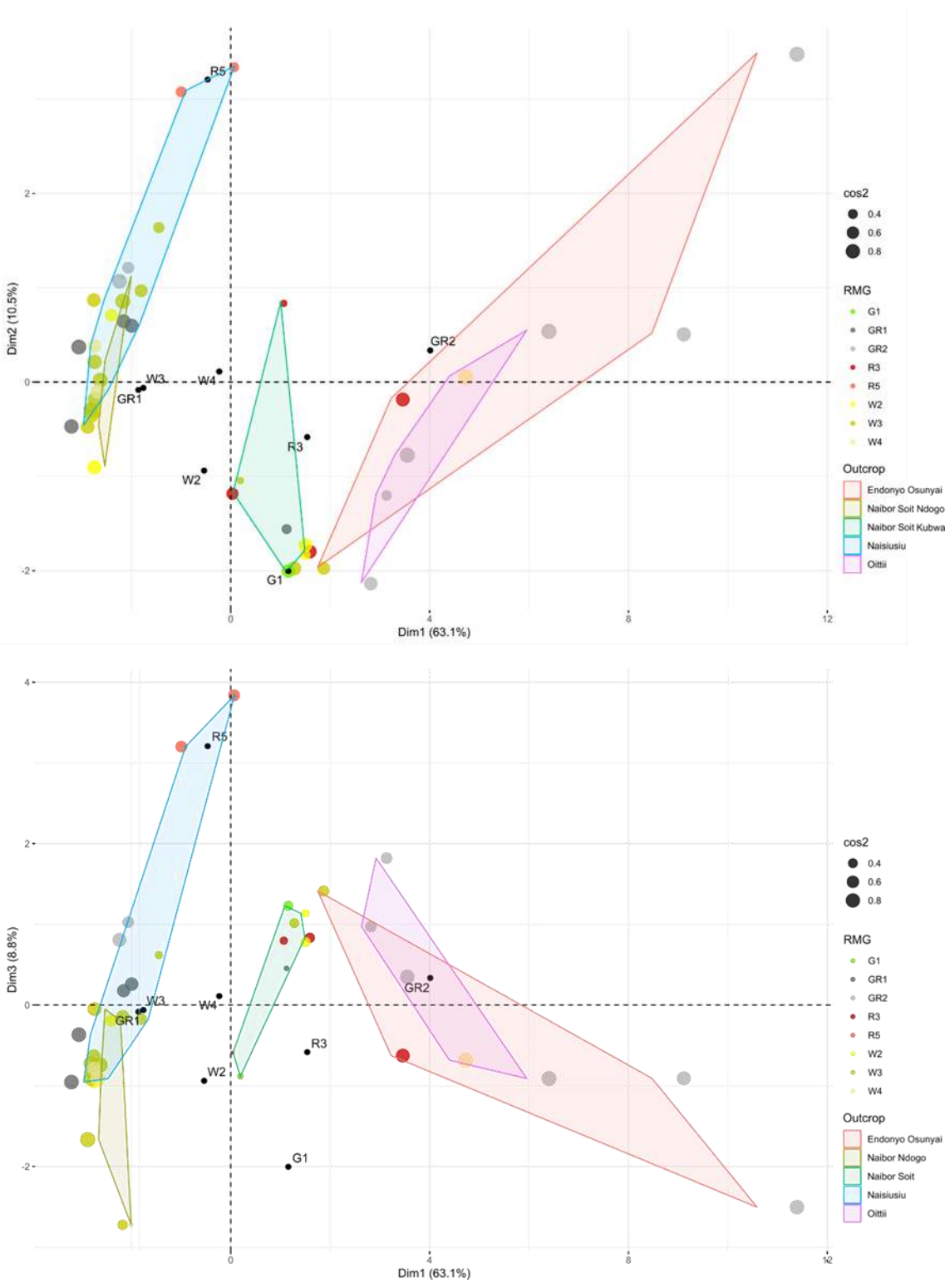

Fig. 11. PCA using EDXRF data with samples labelled by their RMG. Cumulative variance and components identical to those used in the first PCA (see Fig. 9). 2-column fitting image.

Despite this overlap, the confusion matrix of the DFA indicates that 85.71% of the samples were correctly classified, being extremely significant (100%) in the case of RMGs GR1, R5, and W4. 40.48% of the samples are correctly classified using the Jackknife method, confirming the high significance of the discriminant values for samples classified in RMG R5 (Supplementary Materials Tables 19 and 20).

Principal Component	Eigenvalue	Variance Percentage	Cumulative Variance Percentage
Dim. 1	15.227	47.53	47.53
Dim. 2	10.017	31.27	78.8
Dim. 3	2.718	8.48	87.28
Dim. 4	1.954	1.38	93.38

Table 7. Eigenvalues and variance percentages of the DFA components

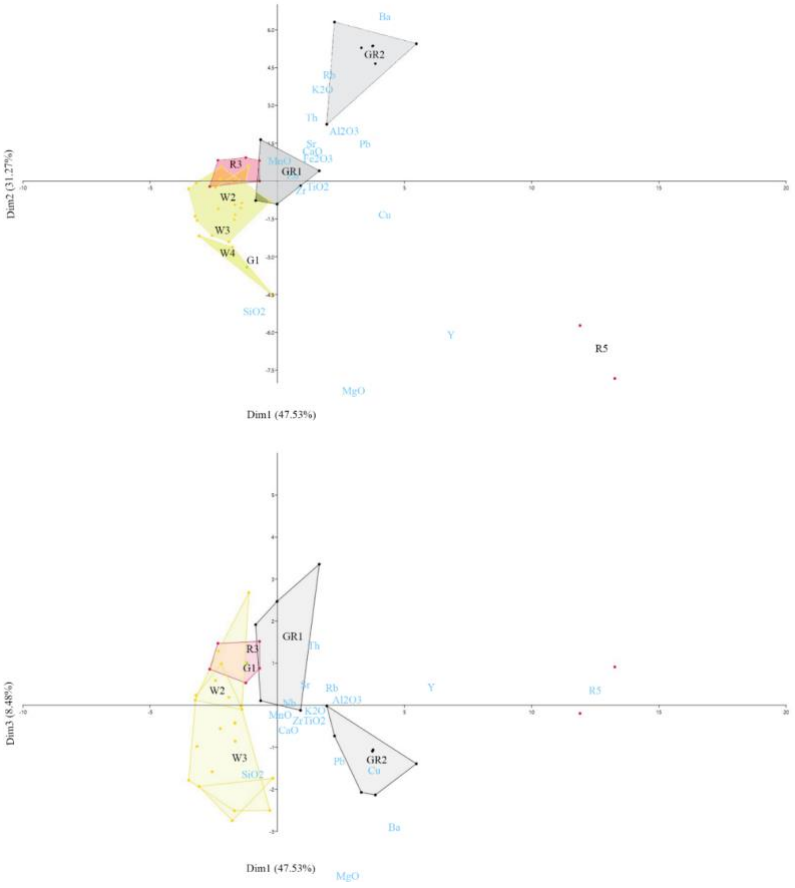

5.2. Fig. 12. DFA using EDXRF data with samples grouped by RMG, including the variables determining the first three components. 2-column fitting image. **Multi-Scalar Approach**

Considering that quartz-rich rocks were widely exploited during the ESA throughout continental Africa (Braun et al., 2009; Bunn, 1982; Chavaillon, 1976; Chazan et al., 2012; Harris et al., 1987; Howell et al., 1987; Isaac and Harris, 1978; Kaufulu and Stern, 1987; Kuman, 1996; Kuman and Field, 2009; Kuman and Clarke, 2000; McNabb and Kuman, 2015; Merrick and Merrick, 1976; Plummer, 2004; Sheppard and Kleindienst, 1996; Toth, 1982), these rock types represent an important avenue to better understand early hominin technology and ecological behavior (Ambrose, 2001; Braun and Hovers, 2009; de Heinzlein et al., 1999; Potts, 1994; Schick, 1987). However, there are only a few ESA characterization studies specifically dealing with quartzite designed to establish its sourcing prospects, and most of these studies specifically deal with material from Oldupai Gorge (Blumenschine et al. 2008; Braun et al. 2008b; Hay, 1976; Kyara, 1999; McHenry and de la Torre, 2018; Tactikos, 2005). Despite this, most of these studies have been limited by small reference collections, with the clear exception of Braun et al. (2008b). While acknowledging the inherent limitations of lithic raw material studies, such as the possibility that there are unknown and/or unexposed outcrops (Santonja et al., 2014), the characterization of known outcrops is a necessary first step to determine resource availability and lithological diversity (e.g. Dibble, 1991; Féblot-Augustins, 1990, 1997; Shackley, 1998; Wilson, 2007; Wilson et al. 2018). Therefore, this study represents an effort to build upon prior studies at Oldupai using a multi-scalar fingerprinting approach to characterize reference materials from five known quartzitic outcrops.

Macroscopic properties reveal that quartzites from different sources are relatively homogenous in terms of their morphology. However, differences in color, grain size, texture, and

mineral composition allowed us to identify twelve RMGs, some of them coincident with macroscopic varieties previously described (McHenry and de la Torre, 2018) (Supplementary Materials Table 1). Thin section petrographic analyses of twelve samples, one from each RMG, reveal that quartzites are predominantly composed of quartz (85-98%), along with varying modes of muscovite (2-14%), and other accessory minerals such as rutile (<1-1%), biotite (1%), and fuchsite (<1%). The presence of certain accessory minerals such as biotite and fuchsite occasionally coincided with our macroscopic classifications of RMGs thereby opening the possibility that stone tools may be sourced to specific outcrops based on mineralogy. Exploratory testing of the geochemical data allowed us to identify the fingerprints of eight of the twelve RMGs that may be useful for provenance studies. EDXRF results propose a high degree of heterogeneity with significant differences at the intra- and inter-outcrop levels. Major elements (except SiO_2), and particularly trace elements, are helpful to differentiate between quartzites from Endonyo Osunyai and Oittii, while high MgO values are associated with quartzites from Naibor Soit Ndogo and Naisiusiu. Besides showing the highest intra-outcrop homogeneity, Naibor Soit Kubwa quartzites have the highest SiO_2 content, which may give this raw material ideal mechanical properties for knapping stone tools. This could, at least partly, allow authors to propose that Naibor Soit Kubwa may have been the principal source of quartzite for artifact manufacture in the eastern Oldupai palaeobasin (Blumenschine et al., 2008 Santonja et al 2014; Tactikos 2005).

Historically, macroscopic and petrographic techniques have been utilized for lithic sourcing (Bond, 1948; Cogné and Giot, 1952; Keiller et al., 1941; Shotton and Hendry, 1979), although geochemical techniques have been increasingly utilized since the 1960s, particularly for obsidian (Cann and Renfrew, 1964; Heizer et al., 1965; Jack and Heizer, 1968; Parks and Tieh, 1966; Weaver and Stross, 1965). In combining these techniques, our multi-scalar analysis reveals that

most RMGs, defined based on macroscopic criteria, are ubiquitous at Oldupai Gorge, and can be found at different outcrops (see Fig. 11). The petrographic data reveal that most quartzites are mineralogically homogenous. However, certain accessory minerals are unique to some outcrops and their presence correlates with two of our RMG classifications (see Table 4). Lastly, our statistical analyses of the geochemical data show that there are elemental compositions characteristic of certain outcrops, and these coincide with most of the macroscopic classifications into RMGs. Altogether, the combination of techniques offers the strongest ability to differentiate among quartzites from different outcrops at Oldupai that no singular technique alone accomplishes on a satisfactory basis. Resource-bearing, we suggest that future provenance studies conduct detailed multi-scalar analyses to shed light on each technique's analytical power, particularly for rock types less amenable to geochemical sourcing alone (e.g. obsidian).

6. Conclusions

This study implemented a multi-scalar approach to systematically characterize the intra- and inter-outcrop lithological variability of five quartzitic outcrops adjacent to Oldupai Gorge. These outcrops were likely the primary sources for quartzitic raw materials and may have been of high importance for early hominin technological organization and palaeoecological behavior. This was accomplished by the macroscopic classification of geological samples into discrete RMGs, as well as selective petrographic and EDXRF analyses.

Using a combination of destructive and non-destructive techniques, we identified twelve RMGs that can be found at five quartzitic outcrops adjacent to Oldupai Gorge. Based on mineral assemblages and modes, we conclude that at least three RMGs are exclusively found at specific outcrops (R5: Naisiusiu; W2 and G1: Naibor Soit Kubwa and Naibor Soit Ndogo). Quartzites from Naibor Soit Kubwa have a unique geochemical composition. Quartzites from Endonyo Osunyai,

546 Oittii, Naibor Soit Ndogo, and Naisiusiu have overlapping bulk rock geochemistry but they can be
547 differentiated from each other using a combination of macroscopic, petrographic, and geochemical
548 data. Although additional research is required to establish stronger links between mineralogy and
549 geochemistry, the methodology outlined here and the promising results provide a stepping-stone
550 for future characterization studies and archaeological applications. It is hoped that our results
551 considered alongside other successful case studies (e.g. Blomme et al., 2012; Cnudde et al., 2013;
552 Dalpra and Pitblado, 2016; Pitblado et al., 2008, 2013; Veldeman et al., 2012) will spur other
553 researchers to determine the feasibility of differentiating quartzites and other quartz-rich
554 lithologies on regional scales. Such studies may come to yield surprising results and prove to be
555 of critical importance to further our understanding of hominin behavior, since quartz-rich raw
556 materials were widely exploited during the African ESA and thereafter in the archaeological
557 record.

Declarations of Interest
None.

Acknowledgements
This work was supported by the Canadian Social Sciences and Humanities Research Council under its Partnership Grant Program no. 895-2016-1017. The Tanzania Commission for Science and Technology authorized this work under permit no. 2018-112-NA-2018-36. The Tanzanian Ministry of Natural Resources and Tourism, through its Antiquities Division, granted us permission to carry out this work (14/2017/2018) and authorities at the Ngorongoro Conservation Area allowed us to enter the protected area (BE.504/620/01/53). The export license for the materials presented in this study were obtained from the Antiquities Division (EA.150/297/01: 5/2018/2019) and the Tanzanian Executive Secretary from the Mining Commission (00001258). The McMaster Archaeological XRF Lab (directed by TC) was funded by the Canada Foundation for Innovation. The SDS project acknowledges the essential contributions by the Maasai communities at Oldupai Gorge concerning the knowledge presented herein. Authors acknowledge the editor and the anonymous reviewers for their suggestions and constructive comments that contributed to the improvement of the manuscript.

Data Availability
Datasets related to this manuscript are available at the Federated Research Data Repository (doi: http://dx.doi.org/10.20383/101.0150) and a preprint is available at the Open Science Framework (https://osf.io/qmxpy/).

Funding
This work was supported by the Canadian Social Sciences and Humanities Research Council under its Partnership Grant Program no. 895-2016-1017.

References

Ambrose, S.H., 2001. Paleolithic technology and human evolution, Science 291, 1748-1753. 10.1126/science.1059487

Andrefsky, W., 2005. Lithics: Macroscopic Approaches to Analysis (Cambridge Manuals in Archaeology), Cambridge University Press Cambridge

Baker, B.H., Mohr, P.A., Williams, L.A.J., 1972. Geology of the eastern rift system of Africa, Geological Society of America.

Bamforth, D.B., 1990. Settlement, raw material, and lithic procurement in the central Mojave Desert, Journal of Anthropological Archaeology 9, 70-104. https://doi.org/10.1016/0278-4165(90)90006-Y

Binford, L.R., 1979. Organization and formation processes: looking at curated technologies, Journal of anthropological research 35, 255-273. https://doi.org/10.1086/jar.35.3.3629902

Binford, L.R., 1980. Willow smoke and dogs' tails: hunter-gatherer settlement systems and archaeological site formation, American antiquity 45, 4-20. https://doi.org/10.2307/279653

Blatt, H., Tracy, R., Owens, B., 2006. Petrology: igneous, sedimentary, and metamorphic, Macmillan.

Blomme, A., Degryse, P., Van Peer, P., Elsen, J., 2012. The characterization of sedimentary quartzite artefacts from Mesolithic sites, Belgium. Geologica Belgica 15, 193-199. https://popups.uliege.be:443/1374-8505/index.php?id=3690

Blumenschine, R.J., Masao, F.T., Tactikos, J.C., Ebert, J.I., 2008. Effects of distance from stone source on landscape-scale variation in Oldowan artifact assemblages in the Paleo-Oldupai Basin, Tanzania, Journal of Archaeological Science 35, 76-86. https://doi.org/10.1016/j.jas.2007.02.009

Bond, G., 1948. Rhodesian Stone Age Man and His Raw Materials. The South African Archaeological Bulletin 3, 55-60. https://www.jstor.org/stable/3886949

Brantingham, P.J., 2003. A neutral model of stone raw material procurement, American Antiquity 68, 487-509. https://doi.org/10.2307/3557105

Braun, D.R., Hovers, E., 2009. Introduction: Current issues in Oldowan research, Interdisciplinary approaches to the Oldowan, Springer, pp. 1-14

Braun, D.R., Rogers, M.J., Harris, J.W., Walker, S.J., 2008a. Landscape-scale variation in hominin tool use: evidence from the developed Oldowan, Journal of Human Evolution 55, 1053-1063. https://doi.org/10.1016/j.jhevol.2008.05.020

Braun, D.R., Plummer, T., Ditchfield, P., Ferraro, J.V., Maina, D., Bishop, L.C., Potts, R., 2008b. Oldowan behavior and raw material transport: perspectives from the Kanjera Formation. Journal of Archaeological Science 35, 2329-2345. https://doi.org/10.1016/j.jas.2008.03.004

Braun, D.R., Plummer, T., Ferraro, J.V., Ditchfield, P., Bishop, L.C., 2009. Raw material quality and Oldowan hominin toolstone preferences: evidence from Kanjera South, Kenya, Journal of Archaeological Science 36, 1605-1614. https://doi.org/10.1016/j.jas.2009.03.025

Bunn, H., 1982. Meat-Eating and Human Evolution: Studies on the Diet and Subsistence Patterns of Plio-Pleistocene Hominids in East Africa, University of California, Berkley

Cann, J.R., Renfrew, C., 1964. The Characterization of Obsidian and its application to the Mediterranean Region. Proceedings of the Prehistoric Society 30, 111-133. https://doi.org/10.1017/S0079497X00015097

Cahen, D., 1975. Le site archéologique de la Kamoa (région du Shaba, République du Zaïre) de l'âge de la pierre ancien à l'âge du fer. Tervuren: Musée Royal de l'Afrique Centrale.

Cahen, L., Snelling, N., 1966. The geochronology of equatorial Africa, North-Holland Publishing Company

Cahen, L., Snelling, N., Delhal, J., Vail, J., Bonhomme, M., Ledent, D., 1984. The geochronology and evolution of Africa.

Calogero, B.L., 1992. Lithic misidentification, Man in the Northeast 43, 87-90

Calogero, B.L., 1991. Macroscopic and petrographic identification of the rock types used for stone tools in central Connecticut, University of Connecticut

Carter, T., Shackley, M.S., 2007. Sourcing obsidian from Neolithic Çatalhöyük (Turkey) using energy dispersive X-ray fluorescence, Archaeometry 49, 437-454. https://doi.org/10.1111/j.1475-4754.2007.00313.x

Chavaillon, J., 1976. Evidence for the technical practices of early pleistocene hominids, Shungura Formation, Lower Omo Valley, Ethiopia

Chazan, M., Avery, D.M., Bamford, M.K., Berna, F., Brink, J., Fernandez-Jalvo, Y., Goldberg, P., Holt, S., Matmon, A., Porat, N., 2012. The Oldowan horizon in Wonderwerk Cave (South Africa): Archaeological, geological, paleontological and paleoclimatic evidence, Journal of Human Evolution 63, 859-866. http://dx.doi.org/10.1016/j.jhevol.2012.08.008

Cnudde, V., Dewanckele, J., De Kock, T., Boone, M., Baele, J.-M., Crombé, P., Robinson, E., 2013. Preliminary structural and chemical study of two quartzite varieties from the same geological formation: a first step in the sourcing of quartzites utilized during the Mesolithic in northwest Europe. Geologica Belgica 16, 27-34. https://popups.uliege.be:443/1374-8505/index.php?id=3981

Cogné, J.E., Giot, P.-R., 1952. Étude pétrographique des haches polies de Bretagne. Bulletin de la Société préhistorique française 49, 388-395. https://doi.org/10.3406/bspf.1952.5080

Dalpra, C.L., Pitblado, B.L., 2016. Discriminating Quartzite Sources Petrographically in the Upper Gunnison Basin, Colorado: Implications for Paleoamerican Lithic-Procurement Studies. PaleoAmerica 2, 22-31. https://doi.org/10.1080/20555563.2015.1137684

Dawson, J., 1992. Neogene tectonics and volcanicity in the North Tanzania sector of the Gregory Rift Valley: contrasts with the Kenya sector, Tectonophysics 204, 81-92. https://doi.org/10.1016/0040-1951(92)90271-7

Dawson, J.B., 2008. The Gregory rift valley and Neogene-recent volcanoes of northern Tanzania, Geological Society of London

De Heinzelin, J., Clark, J.D., White, T., Hart, W., Renne, P., WoldeGabriel, G., Beyene, Y., Vrba, E., 1999. Environment and behavior of 2.5-million-year-old Bouri hominids, Science 284, 625-629.10.1126/science.284.5414.625

Delagnes, A., Roche, H., 2005. Late Pliocene hominid knapping skills: the case of Lokalalei 2C, West Turkana, Kenya, Journal of Human Evolution 48, 435-472. https://doi.org/10.1016/j.jhevol.2004.12.005

Demars, P.Y., 1982. L'utilisation du silex au Paléolithique supérioir: chois, approvisionnment, circulation. L'exemple du bassin de Brive, Centre National de la Recherche Scientifique

Dibble, H.L., 1991. Local raw material exploitation and its effects on Lower and Middle Paleolithic assemblage variability, Raw material economies among prehistoric hunter-gatherers 19, 33-47

Féblot-Augustins, J., 1990. Exploitation des matières premières dans l'Acheuléen d'Afrique: perspectives comportementales, Paléo, Revue d'Archéologie Préhistorique 2, 27-42. https://doi.org/10.3406/pal.1990.987

Féblot-Augustins, J., 1997. Middle and Upper Palaeolithic raw material transfers in western and central Europe: assessing the pace of change, Journal of Middle Atlantic Archaeology 13, 57-90. 〈halshs-00436336〉

Folk, R.L., 1980. Petrology of sedimentary rocks, Hemphill Publishing Company.0914696149

Foster, A.N., Ebinger, C.J., Mbede, E., Rex, D., 1997. Tectonic development of the northern Tanzanian sector of the East Africa Rift System, Journal of the Geological Society of London

Frahm, E., 2014. Characterizing obsidian sources with portable XRF: accuracy, reproducibility, and field relationships in a case study from Armenia, Journal of Archaeological Science 49, 105-125. https://doi.org/10.1016/j.jas.2014.05.003

Freeman, L.G., 1994. Torralba and Ambrona: a review of discoveries, Integrative Paths to the Past, 597-638

Fritz, H., Abdelsalam, M., Ali, K., Bingen, B., Collins, A., Fowler, A., Ghebreab, W., Hauzenberger, C., Johnson, P., Kusky, T., 2013. Orogen styles in the East African Orogen: a review of the Neoproterozoic to Cambrian tectonic evolution, Journal of African Earth Sciences 86, 65-106

George, R., Rogers, N., Kelley, S., 1998. Earliest magmatism in Ethiopia: Evidence for two mantle plumes in one flood basalt province, Geology 26, 923-926. https://doi.org/10.1130/0091-7613(1998)026<0923:EMIEEF>2.3.CO;2

Glascock, M.D., Neff, H., 2003. Neutron activation analysis and provenance research in archaeology, Measurement Science and Technology 14, 1516.0957-0233/03/091516

Goldman-Neuman, T., Hovers, E., 2009. Methodological considerations in the study of Oldowan raw material selectivity: insights from AL 894 (Hadar, Ethiopia), Interdisciplinary approaches to the Oldowan, Springer, pp. 71-84

Goldman-Neuman, T., Hovers, E., 2012. Raw material selectivity in late Pliocene Oldowan sites in the Makaamitalu Basin, Hadar, Ethiopia, Journal of human evolution 62, 353-366. https://doi.org/10.1016/j.jhevol.2011.05.006

Goodale, N., Andrefsky, W.e., 2015. Lithic technological systems and evolutionary theory, Cambrudge University Press, New York

Greenwood, S.M., 2014. Mineralogy and Geochemistry of Pleistocene Volcanics at Embagai Caldera and Natron Basin, Tanzania: Potential Constraints on the Stratigraphy of Oldupai Gorge, p. 497

Harris, J.W., Williamson, P.G., Verniers, J., Tappen, M.J., Stewart, K., Helgren, D., de Heinzelin, J., Boaz, N.T., Bellomo, R.V., 1987. Late Pliocene hominid occupation in Central Africa: the setting, context, and character of the Senga 5A site, Zaire, Journal of Human Evolution 16, 701-728. https://doi.org/10.1016/0047-2484(87)90020-0

Hay, R.L., 1976. Geology of the Oldupai gorge, University of California Press.5885053340

Hepworth, J.V., 1972. The Mozambique orogenic belt and its foreland in northeast Tanzania: a photogeologically-based study, Journal of the Geological Society 128, 461-494

Heizer, R.F., Williams, H., Graham, J.A., 1965. Notes on Mesoamerican Obsidians and Their Significance in Archaeological Studies. Contributions of the University of California Archaeological Research Facility 1, 94-103.

Hermes, O.D., Luedtke, B.E., Ritchie, D., 2001. Melrose green rhyolite: its geologic setting and petrographic and geochemical characteristics, Journal of Archaeological Science 28, 913-928. https://doi.org/10.1006/jasc.2000.0605

Hepworth, J.V., 1972. The Mozambique orogenic belt and its foreland in northeast Tanzania: a photogeologically-based study. Journal of the Geological Society 128, 461-494.

Holmes, A., 1951. The sequence of Precambrian orogenic belts in south and central Africa, Proceed. 18th Internat. Geol. Congr. London 1948 14, 254-269

Hovers, E., 2009. Learning from mistakes: flaking accidents and knapping skills in the assemblage of AL 894 (Hadar, Ethiopia)

Howard, J.L., 2005. The quartzite problem revisited, The Journal of geology 113, 707-713. https://doi.org/10.1086/449328

Howell, F.C., 1961. Isimila: A Paleolithic site in Africa. Scientific American 205, 118-129.

Howell, F. C., Cole, G. H., Kleindienst, M. R., Haldemann, E. G., 1962. Isimila: An Acheulian Occupaton Site in the Iringa Highlands, Southern Highlands Province, Tanganyika (pp. 43-80). Tervuren: Musée royal de l'Afrique centrale.

Howell, F. C., Clark, J. D., 1963. Acheulian hunter-gatherers of sub-Saharan Africa. African ecology and human evolution, 458-533.

Howell, F.C., Haesaerts, P., de Heinzelin, J., 1987. Depositional environments, archeological occurrences and hominids from Members E and F of the Shungura Formation (Omo basin, Ethiopia), Journal of Human Evolution 16, 665-700. https://doi.org/10.1016/0047-2484(87)90019-4

Isaac, G., 1978. The food-sharing behavior of protohuman hominids, Scientific american 238, 90-109

Isaac, G.L., Harris, J., 1978. Archaeology. In (MG Leakey & REF Leakey, Eds) Koobi Fora Research Project, vol. 1, Oxford: Clarendon Press

Isaac, G.L., Harris, J.W., Marshall, F., 1981. Small is informative: the application of the study of mini-sites and least effort criteria in the interpretation of the Early Pleistocene archaeological record at Koobi Fora, Kenya, The Archaeology of Human Origins. Papers by Glynn Isaac. Cambridge University Press, Cambridge, 259-268

Jack, R.N., Heizer, R.F., 1968. “Finger-Printing” of some Mesoamerican Obsidian Artifacts. Contributions of the University of California Archaeological Research Facility 5, 81-100.

Jones, G.T., Beck, C., Jones, E.E., Hughes, R.E., 2003. Lithic source use and Paleoarchaic foraging territories in the Great Basin, American Antiquity 68, 5-38. https://doi.org/10.2307/3557031

Jones, P.R., 1979. Effects of Raw Materials on Biface Manufacture. Science 204 (4395), 835-836. 10.1126/science.204.4395.835.

Jones, P.R., 1980. Experimental butchery with modern stone tools and its relevance for Palaeolithic archaeology, World Archaeology 12, 153-165. https://doi.org/10.1080/00438243.1980.9979789

Jones, P.R., 1981. Experimental implement manufacture and use: a case study from Olduvai Gorge, Tanzania. Philosophical Transactions of the Royal Society of London 292, 189-195. https://doi.org/10.1098/rstb.1981.0027

Jones, P.R., 1994. Results of experimental work in relation to the stone industries of Oldupai Gorge, Oldupai Gorge 5, 1968-1971

Kabete, J., Groves, D., McNaughton, N., Mruma, A., 2012. A new tectonic and temporal framework for the Tanzanian Shield: implications for gold metallogeny and undiscovered endowment, Ore Geology Reviews 48, 88-124. https://doi.org/10.1016/j.oregeorev.2012.02.009

Kasanzu, C., Maboko, M.A., Manya, S., 2008. Geochemistry of fine-grained clastic sedimentary rocks of the Neoproterozoic Ikorongo Group, NE Tanzania: Implications for provenance and source rock weathering, Precambrian Research 164, 201- 213. https://doi.org/10.1016/j.precamres.2008.04.007

Kassambara, A., Mundt, F., 2017. Factoextra: Extract and Visualize the Results of Multivariate Data Analyses. R package version 1.0.5., https://CRAN.R-project.org/package=factoextra

Kaufulu, Z.M., Stern, N., 1987. The first stone artefacts to be found in situ within the Plio-Pleistocene Chiwondo Beds in northern Malawi, Journal of Human Evolution 16, 729-740. https://doi.org/10.1016/0047-2484(87)90021-2

Keiller, A., Piggott, S., Wallis, F.S., 1941. First Report of the Sub-Committee of the South-Western Group of Museums and Art Galleries on the Petrological Identification of Stone Axes. Proceedings of the Prehistoric Society 7, 50-72. https://doi.org/10.1017/S0079497X00020272

Kröner, A., Stern, R., 2005. AFRICA| Pan-African orogen

Kuhn, S.L., 1991. "Unpacking" reduction: lithic raw material economy in the Mousterian of west-central Italy, Journal of Anthropological Archaeology 10, 76-106. https://doi.org/10.1016/0278-4165(91)90022-P

Kuman, K., 1996. The Oldowan industry from Sterkfontein: raw materials and core forms.

Kuman, K., Clarke, R.J., 2000. Stratigraphy, artefact industries and hominid associations for Sterkfontein, Member 5, Journal of Human Evolution 38, 827-847. https://doi.org/10.1006/jhev.1999.0392

Kuman, K., Field, A., 2009. The Oldowan industry from Sterkfontein Caves, South Africa, Stone Age Institute Press

Kyara, O., 1999. Lithic raw materials and their implications on assemblage variation and hominid behavior during Bed II, Oldupai Gorge, PhD diss., Rutgers University

Laplace, G., 1972. La typologie analytique et structurale: base rationnelle d'étude des industries lithiques et osseuses, Colloques nationaux du CNRS Banques de données archéologiques, 92-143

Le Gall, B., Nonnotte, P., Rolet, J., Benoit, M., Guillou, H., Mousseau-Nonnotte, M., Albaric, J., Déverchère, J., 2008. Rift propagation at craton margin.: Distribution of faulting and volcanism in the North Tanzanian Divergence (East Africa) during Neogene times, Tectonophysics 448, 1-19.https://doi.org/10.1016/j.tecto.2007.11.005

Lê, S., Josse, J., Husson, F., 2008. FactoMineR: an R package for multivariate analysis, Journal of statistical software 25, 1-18

Leakey, M., Roe, D., 1994. Oldupai Gorge: Volume 5, Excavations in Beds III, IV and the Masek Beds, Cambridge University Press.0521334039

Leakey, M.D., 1971. Oldupai Gorge, Excavations in Beds I and II, 1960–1963, vol. 3.978-0-521-10518-7

Leakey, M.D., Hay, R.L., Thurber, D.L., Protsch, R., Berger, R., 1972. Stratigraphy, Archaeology, and Age of the Ndutu and Naisiusiu Beds, Oldupai Gorge, Tanzania. World Archaeology 3, 328-341.

Macgregor, D., 2015. History of the development of the East African Rift System: A series of interpreted maps through time. Journal of African Earth Sciences 101, 232-252. https://doi.org/10.1016/j.jafrearsci.2014.09.016

Mana, S., Furman, T., Carr, M., Mollel, G., Mortlock, R., Feigenson, M., Turrin, B., Swisher, C., 2012. Geochronology and geochemistry of the Essimingor volcano: melting of metasomatized lithospheric mantle beneath the North Tanzanian Divergence zone (East African Rift), Lithos 155, 310-325. https://doi.org/10.1016/j.lithos.2012.09.009

McHenry, L.J., de la Torre, I., 2018. Hominin raw material procurement in the Oldowan-Acheulean transition at Oldupai Gorge, Journal of human evolution. https://doi.org/10.1016/j.jhevol.2017.11.010

McHenry, L.J., Mollel, G.F., Swisher III, C.C., 2008. Compositional and textural correlations between Oldupai Gorge Bed I tephra and volcanic sources in the Ngorongoro Volcanic Highlands, Tanzania, Quaternary International 178, 306-319. https://doi.org/10.1016/j.quaint.2007.01.004

McNabb, J., Kuman, K., 2015. Experimental stone tool replication at the early stone age site of Sterkfontein, Gauteng, South Africa, Journal of Archaeological Science: Reports 4, 44-53. https://doi.org/10.1016/j.jasrep.2015.08.043

Melgarejo, J., 1997. Atlas de asociaciones minerales en lámina delgada.84-475-2762-X

Merrick, H.V., Merrick, J., 1976. Archaeological occurrences of earlier Pleistocene age from the Shungura Formation, Earliest man and environments in the Lake Rudolf Basin, 574-584.

Mollel, G.F., 2002. Petrology and Geochemistry of the Southeastern Ngorongoro Volcanic Highland: And Contribution to" sourcing" of Stone Tools at Oldupai Gorge, Tanzania, Rutgers University

Mollel, G.F., 2007. Petrochemistry and geochronology of Ngorongoro volcanic highland complex (NVHC) and its relationship to Laetoli and Oldupai Gorge, Tanzania, Rutgers University-Graduate School-New Brunswick, p. 233

Mollel, G.F., Swisher III, C.C., 2012. The Ngorongoro Volcanic Highland and its relationships to volcanic deposits at Oldupai Gorge and East African Rift volcanism, Journal of human evolution 63, 274-283. https://doi.org/10.1016/j.jhevol.2011.09.001

Mollel, G.F., Swisher, C.C., Feigenson, M.D., Carr, M.J., 2008. Geochemical evolution of Ngorongoro Caldera, Northern Tanzania: Implications for crust–magma interaction, Earth and Planetary Science Letters 271, 337-347. https://doi.org/10.1016/j.epsl.2008.04.014

Mollel, G.F., Swisher, C.C., McHenry, L.J., Feigenson, M.D., Carr, M.J., 2009. Petrogenesis of basalt–trachyte lavas from Olmoti Crater, Tanzania, Journal of African Earth Sciences 54, 127-143. https://doi.org/10.1016/j.jafrearsci.2009.03.008

Morales, J.I., 2016. Distribution patterns of stone-tool reduction: Establishing frames of reference to approximate occupational features and formation processes in Paleolithic societies, Journal of Anthropological Archaeology 41, 231-245. https://doi.org/10.1016/j.jaa.2016.01.004

Odell, G.H., 2012. Lithic analysis, Springer Science & Business Media.1441990097

Parks, G.A., Tieh, T.T., 1966. Identifying the geographical Source of Artefact Obsidian. Nature 211, 289-290. https://doi.org/10.1038/211289a0

Perkins, D., Henke, K. R., 2002. Minerales en lámina delgada, Prentice Hall

Pettijohn, F.J., Potter, P.E., Siever, R., 2012. Sand and sandstone, Springer Science & Business Media.1461210666

Pitblado, B.L., Dehler, C., Neff, H., Nelson, S.T., 2008. Pilot Study Experiments Sourcing Quartzite, Gunnison Basin, Colorado. Geoarchaeology 23, 742-778. https://doi.org/10.1002/gea.20240

Pitblado, B.L., Cannon, M.B., Neff, H., Dehler, C.M., Nelson, S.T., 2013. LA-ICP-MS analysis of quartzite from the Upper Gunnison Basin, Colorado. Journal of Archaeological Science 40, 2196-2216. https://doi.org/10.1016/j.jas.2012.11.016

Plummer, T., 2004. Flaked Stones and Old Bones: Biological and Cultural Evolution at the Dawn of Technology. Yearbook Of Physical Anthropology 47, 118-164. https://doi.org/10.1002/ajpa.20157

Plummer, T.W., Bishop, L.C., Ditchfield, P.W., Ferraro, J.V., Kingston, J.D., Hertel, F., Braun, D.R., 2009. The environmental context of Oldowan hominin activities at Kanjera South, Kenya, Interdisciplinary approaches to the Oldowan, Springer, pp. 149-160

Potts, R., 1994. Variables versus models of early Pleistocene hominid land use, Journal of Human Evolution 27, 7-24. https://doi.org/10.1006/jhev.1994.1033

Poupeau, G., Le Bourdonnec, F.-X., Carter, T., Delerue, S., Shackley, M.S., Barrat, J.-A., Dubernet, S., Moretto, P., Calligaro, T., Milić, M., 2010. The use of SEM-EDS, PIXE and EDXRF for obsidian provenance studies in the Near East: a case study from Neolithic Çatalhöyük (central Anatolia), Journal of Archaeological Science 37, 2705-2720. https://doi.org/10.1016/j.jas.2010.06.007

Prieto, A., Yusta, I., Arrizabalaga, A., 2019. Defining and Characterizing Archaeological Quartzite: Sedimentary and Metamorphic Processes in the Lithic Assemblages of El Habario and El Arteu (Cantabrian Mountains, Northern Spain), Archaeometry 61, 14-30. https://doi.org/10.1111/arcm.1239

Roberts, E.M., Stevens, N., O'Connor, P.M., Dirks, P., Gottfried, M.D., Clyde, W., Armstrong, R., Kemp, A., Hemming, S., 2012. Initiation of the western branch of the East African Rift coeval with the eastern branch, Nature Geoscience 5, 289.10.1038/NGEO1432

Roche, H., 1989. Technological evolution in early hominids, Ossa 14, 97-98

Sanislav, I., Wormald, R., Dirks, P., Blenkinsop, T.G., Salamba, L., Joseph, D., 2014. Zircon U–Pb ages and Lu–Hf isotope systematics from late-tectonic granites, Geita Greenstone Belt: Implications for crustal growth of the Tanzania Craton, Precambrian research 242, 187-204. https://doi.org/10.1016/j.precamres.2013.12.026

Roebroeks, W., 1988. From find scatters to early hominid behaviour: a study of Middle Palaeolithic riverside settlements at Maastricht-Belvédère (The Netherlands). Analecta Praehistorica Leidensia, vol. 21, University of Leiden: Leiden.

Santonja, M., Panera, J., Rubio-Jara, S., Pérez-González, A., Uribelarrea, D., Domínguez-Rodrigo, M., Mabulla, A.Z., Bunn, H.T., Baquedano, E., 2014. Technological strategies and the economy of raw materials in the TK (Thiongo Korongo) lower occupation, Bed II, Oldupai Gorge, Tanzania, Quaternary International 322, 181-208. https://doi.org/10.1016/j.quaint.2013.10.069

Scoon, R.N., 2018. The Gregory Rift, Geology of National Parks of Central/Southern Kenya and Northern Tanzania, Springer, pp. 39-57

Semaw, S., 2006. The oldest stone artifacts from Gona (2.6-2.5 Ma), Afar, Ethiopia: Implications for understanding the earliest stages of stone knapping, The Oldowan: Case studies into the earliest stone age, 43-75

Shackley, M.S., 1998. Geochemical differentiation and prehistoric procurement of obsidian in the Mount Taylor volcanic field, northwest New Mexico, Journal of Archaeological Science 25, 1073-1082. https://doi.org/10.1006/jasc.1998.0274

Shackley, M.S., 2008. Archaeological petrology and the archaeometry of lithic materials, Archaeometry 50, 194-215. https://doi.org/10.1111/j.1475-4754.2008.00390.x

Sheppard, P.J., Kleindienst, M.R., 1996. Technological change in the earlier and middle stone Age of Kalambo Falls (Zambia), African Archaeological Review 13, 171-196. https://doi.org/10.1007/BF01963510

Schick, K.D., 1987. Modeling the formation of Early Stone Age artifact concentrations, Journal of human evolution 16, 789-807.https://doi.org/10.1016/0047-2484(87)90024-8

Shott, M.J., Ballenger, J.A., 2007. Biface reduction and the measurement of Dalton curation: a southeastern United States case study, American Antiquity 72, 153-175. https://doi.org/10.2307/40035302

Shotton, F., Hendry, G., 1979. The developing field of petrology in archaeology, Journal of Archaeological Science 6, 75-84. https://doi.org/10.1016/0305-4403(79)90034-7

Skolnick, H., 1965. The quartzite problem, Journal of Sedimentary Research 35, 12-21. https://doi.org/10.1306/74D711E0-2B21-11D7-8648000102C1865D

Stiles, D., 1991. Early hominid behaviour and culture tradition: raw material studies in Bed II, Oldupai Gorge, African Archaeological Review 9, 1-19. https://doi.org/10.1007/BF01117214

Stiles, D., 2003. Raw material as evidence for human behaviour in the Lower Pleistocene: the Oldupai case, Early Human Behaviour in Global Context, Routledge, pp. 149-164

Stiles, D., Hay, R., O'Neil, J., 1974. The MNK chert factory site, Oldupai Gorge, Tanzania, World Archaeology 5, 285-308. https://doi.org/10.1080/00438243.1974.9979575

Tactikos, J.C., 2005. A landscape perspective on the Oldowan from Oldupai Gorge, Tanzania, Department of Anthropology, Rutgers, the State University of New Jersey

R Core Team, 2017. R: a language and environment for statistical computing. R Foundation for Statistical Computing, Vienna. http s, www. R-project. Org

Toth, N., 1985. Archaeological evidence for preferential right-handedness in the Lower and Middle Pleistocene, and its possible implications, Journal of Human Evolution 14, 607-614. https://doi.org/10.1016/S0047-2484(85)80087-7

Toth, N.P., 1982. The stone technologies of early hominids at Koobi Fora, Kenya: an experimental approach, University of California, Berkeley

Tucker, M.E., 2009. Sedimentary petrology: an introduction to the origin of sedimentary rocks, John Wiley & Sons.144431159X

Vaquero, M., Pastó, I. (2001). The definition of spatial units in Middle Palaeolithic sites: the hearth-related assemblages. Journal of Archaeological Science, 28(11), 1209-1220. https://doi.org/10.1006/jasc.2001.0656

Vaquero, M. (2008). The history of stones: behavioural inferences and temporal resolution of an archaeological assemblage from the Middle Palaeolithic. Journal of Archaeological Science, 35(12), 3178-3185. https://doi.org/10.1016/j.jas.2008.07.006

Veldeman, I., Baele, J.-M., Goemaere, E., Deceukelaire, M., Dusar, M., De Doncker, H.W.J.A., 2012. Characterizing the hypersiliceous rocks of Belgium used in (pre-)history: a case study on sourcing sedimentary quartzites. Journal of Geophysics and Engineering 9, S118-S128. https://doi.org/10.1088/1742-2132/9/4/S118

Weaver, J., Stross, F., 1965. Analysis by x-ray fluorescence of some American obsidians. Contributions of the University of California Archaeological Research Facility 1, 89-93.

Wilson, L., 2007. Understanding prehistoric lithic raw material selection: application of a gravity model, Journal of Archaeological Method and Theory 14, 388-411. https://doi.org/10.1007/s10816-007-9042-4

Wilson, L., Browne, C.L., Texier, P.-J., 2018. Provisioning on the periphery: Middle Palaeolithic raw material supply strategies on the outer edge of a territory at La Combette (France), Journal of Archaeological Science: Reports 21, 87-98. https://doi.org/10.1016/j.jasrep.2018.07.001

Zaitsev, A., Marks, M., Wenzel, T., Spratt, J., Sharygin, V., Strekopytov, S., Markl, G., 2012. Mineralogy, geochemistry and petrology of the phonolitic to nephelinitic Sadiman volcano, Crater Highlands, Tanzania, Lithos 152, 66-83. https://doi.org/10.1016/j.lithos.2012.03.001

Supplementary Materials

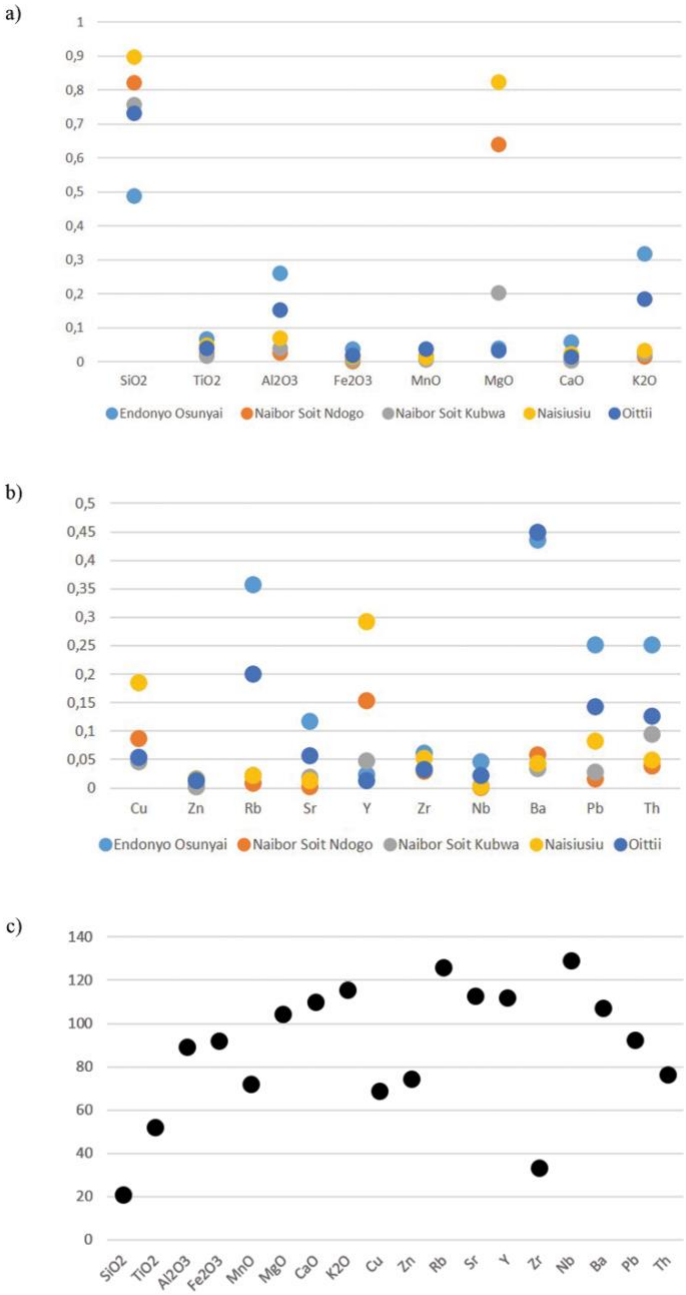

Fig. 1. a, b) Plotting of averaged concentrations for major oxide and trace element concentrations per outcrop showing the inter-outcrop variability; c) Relative Standard Deviations.

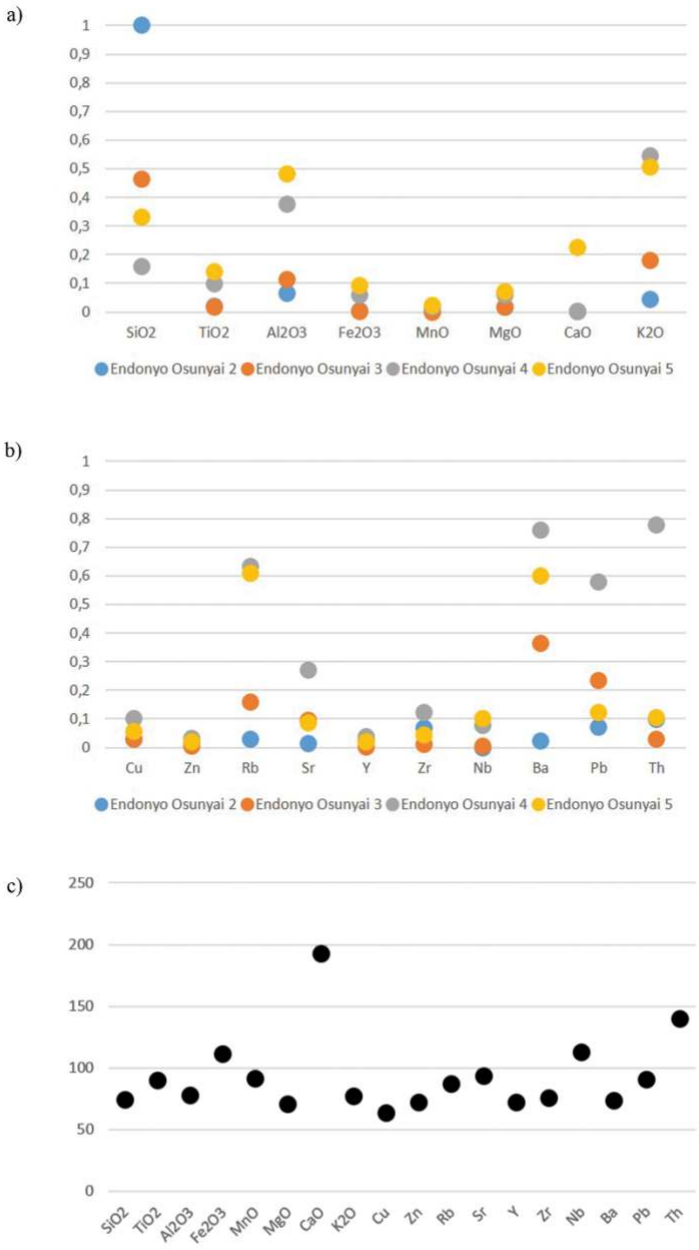

Fig. 2. a, b) Plotting of major oxide and trace element concentrations for samples from Endonyo Osunyai; c) Relative Standard Deviations for samples from Endonyo Osunyai showing the intra-outcrop variability.

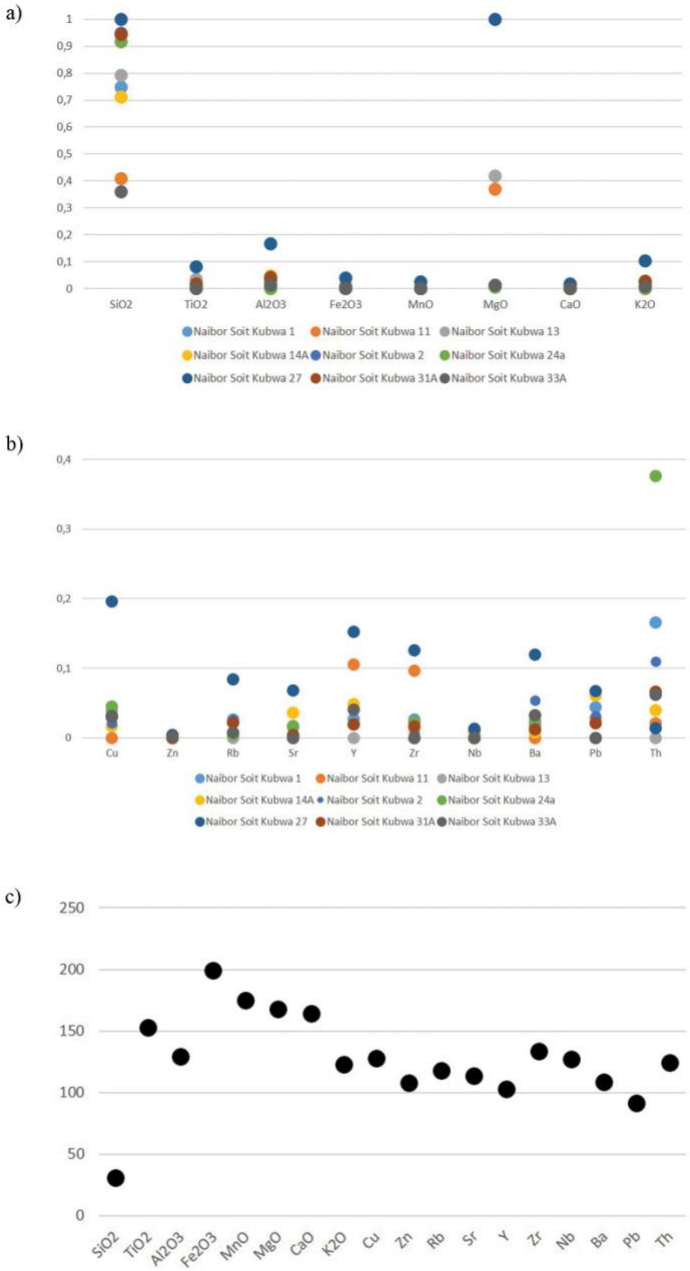

Fig. 3. a, b) Plotting of major oxide and trace element concentrations for samples from Naibor Soit Kubwa; c) Relative Standard Deviations for samples from Naibor Soit Kubwa showing the intra-outcrop variability.

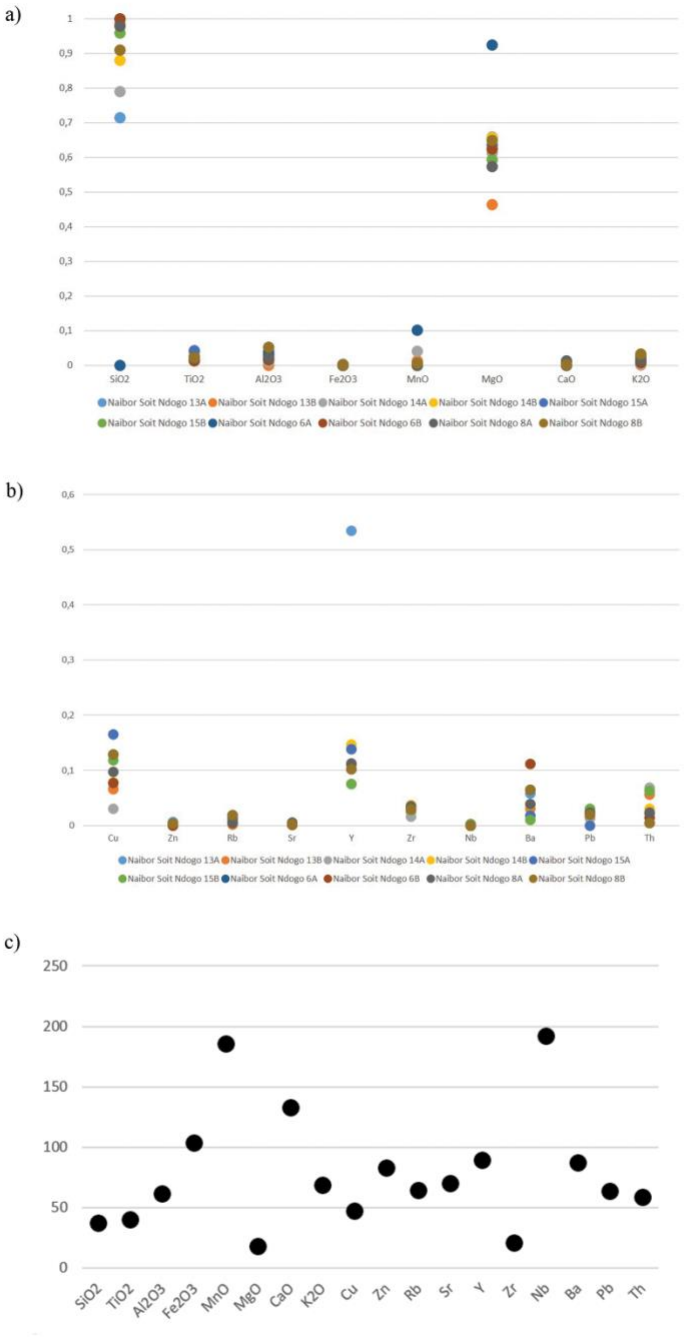

Fig. 4. a, b) Plotting of major oxide and trace element concentrations for samples from Naibor Soit Ndogo; c) Relative Standard Deviations for samples from Naibor Soit Ndogo showing the intra-outcrop variability.

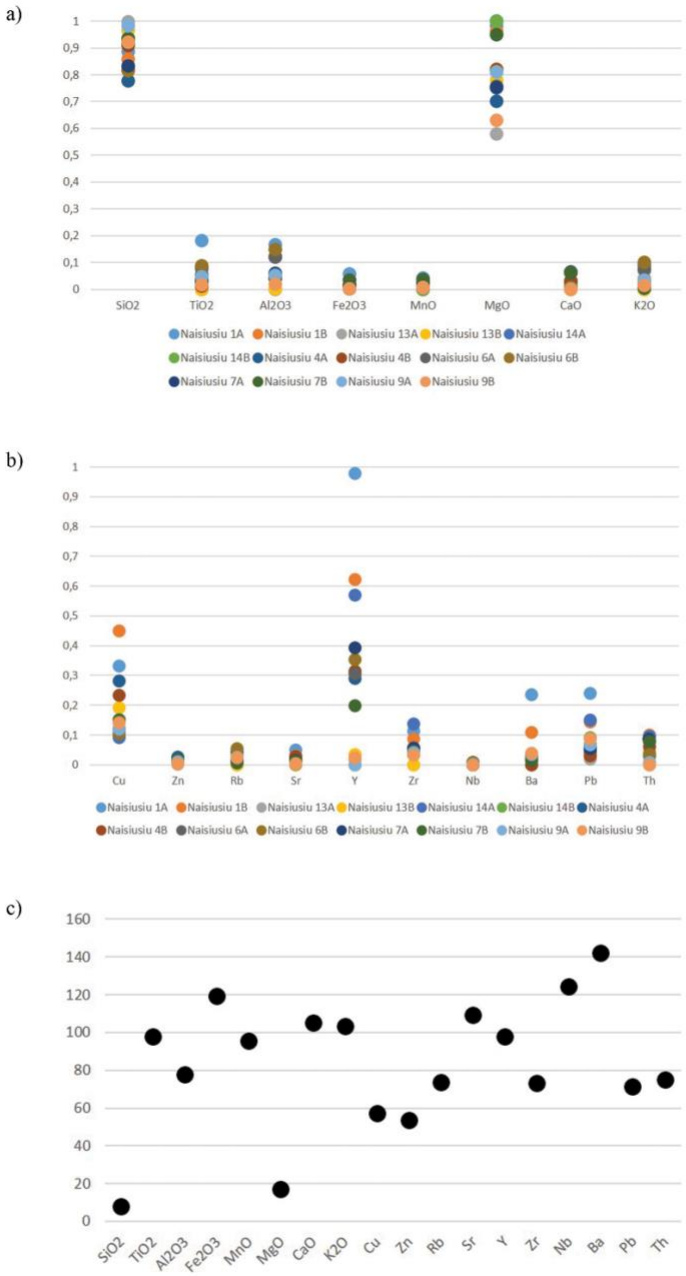

Fig. 5. a, b) Plotting of major oxide and trace element concentrations for samples from Naisiusiu; c) Relative Standard Deviations for samples from Naisiusiu showing the intra-outcrop variability.

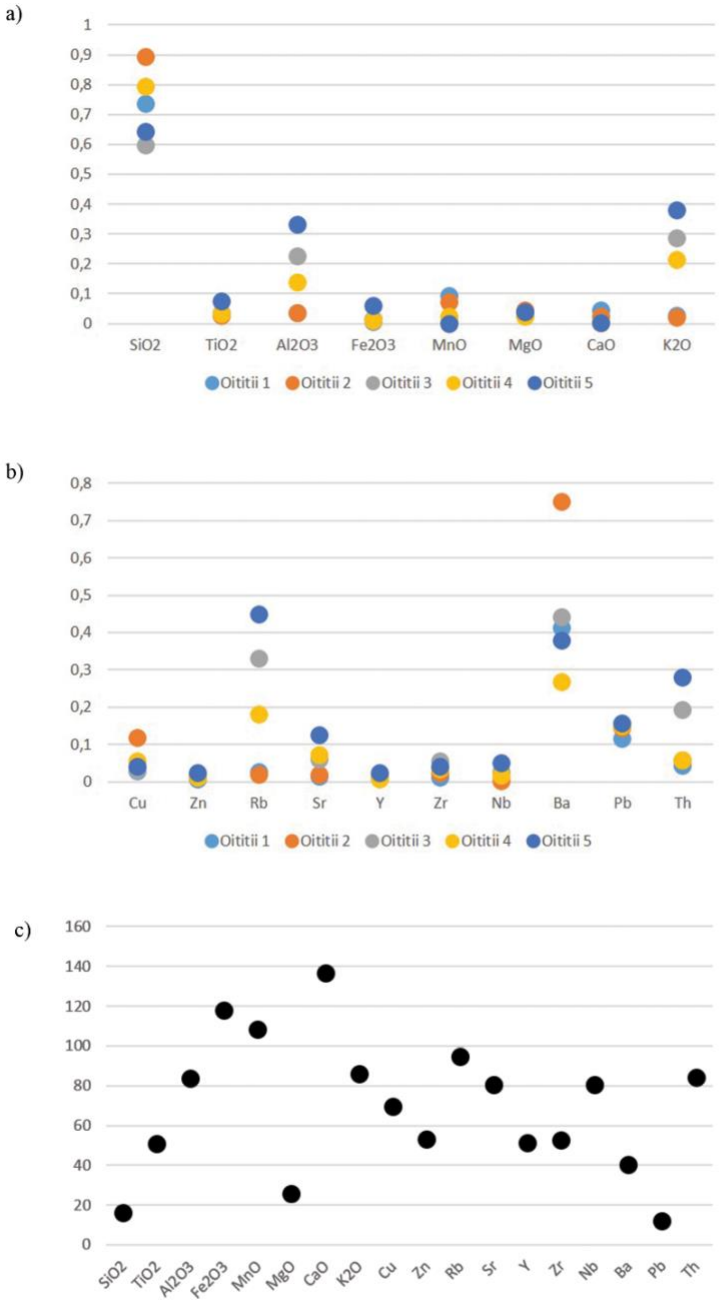

Fig. 6. a, b) Plotting of major oxide and trace element concentrations for samples from Oittii; c) Relative Standard Deviations for samples from Oittii showing the intra-outcrop variability.

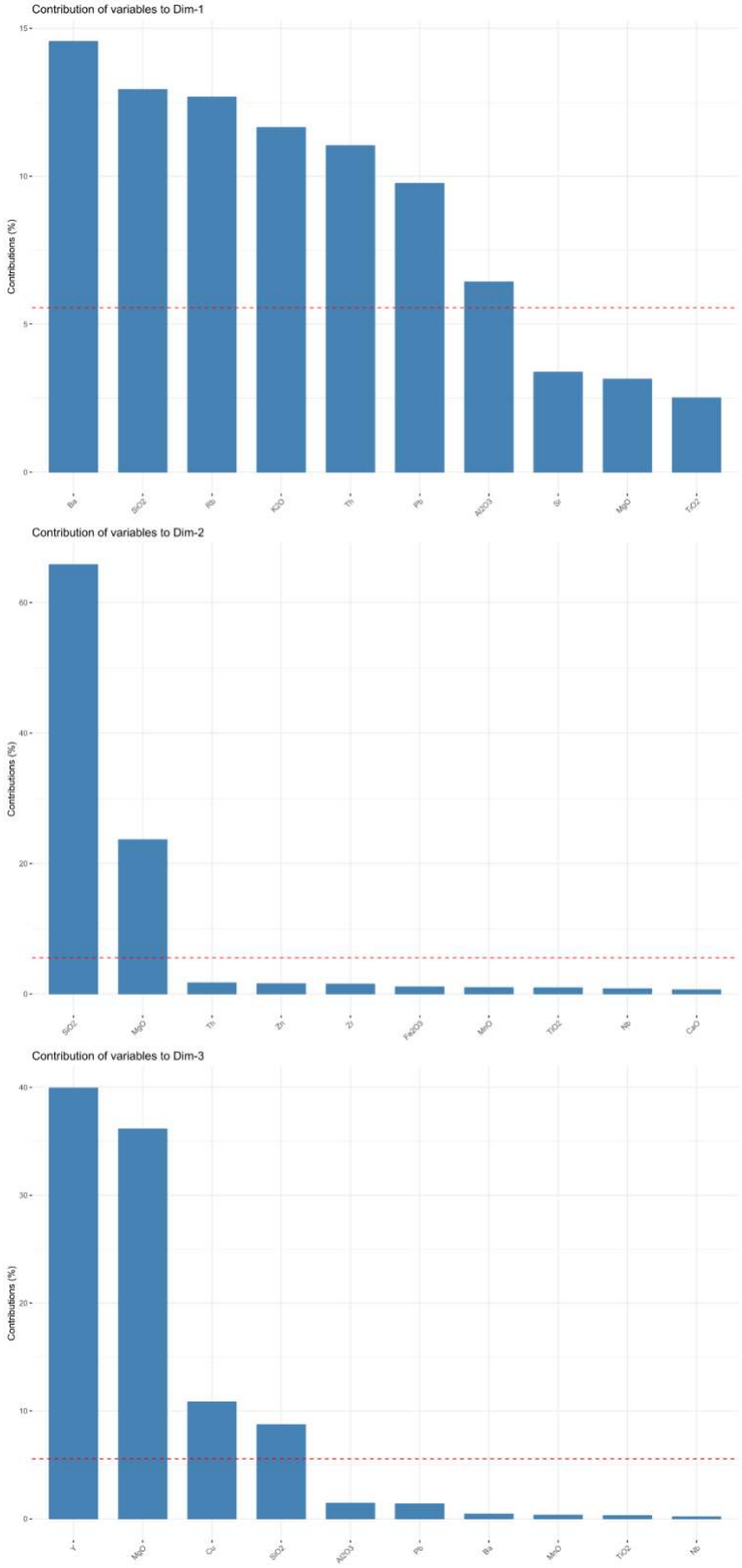

Fig. 7. PCA contribution percentages of the three components based on EDXRF data.

RMGs (McHenry and de la Torre, 2018)	RMGs (this study)
7.1	W*
7.1.1	W*
7.1.2	W*
7.1.3	W*
7.1.4	W*
7.2	R5
7.3	W3/W4
7.4	G1
7.5	Gr*
7.5.1	Gr1
7.6	W1/W2/ Gr2
7.6.1	Gr1
7.6.2	R2
7.7	W*
7.8	nd
7.9	nd

Table 1. Correlation between quartzite RMGs identified in McHenry and de la Torre (2018) and those in this study.

* Specific RMGs were only correlated where possible, and to avoid misclassification, some were only correlated at a general level.

Outcrop	Sample ID	Rock	RMG	EDXRF	Petrography	Long.	Lat.	Alt.	Mass (g)	Size (mm; LxWxT)	Munsell Code	Striping Zonation	Patina	Patina Color	Cortex Type	Cortex Proportion	Gloss	Transparency	Grain Size	Foliation
Endonyo Osunyai	Endonyo Osunyai 2	Qtz	W3	Y	Y	35.31601 8	-2.941903	1537.7944	nd	105*82*10	N9	Homogenous	N-P		Primary	Cortex Non-Dominant	Dull-Milky	Opaque	Coarse	Non-Foliated
	Endonyo Osunyai 3	Qtz	R3	Y	N	35.31616 3	-2.941388	1541.7842	262.39	100*63*20	N8	Homogenous	N-P		Primary	Cortex Dominant	Dull	Opaque	Coarse	Non-Foliated
	Endonyo Osunyai 4	Qtz	GR2	Y	N	35.31591 9	-2.94128	1539.9926	113.04	110*60*20	N8-N5	Zoned	N-P		Primary	Cortex Non-Dominant	Dull	Edge-Transparent	Medium	Non-Foliated
	Endonyo Osunyai 5	Qtz	GR2	Y	N	35.31621 6	-2.941525	1538.4061	142.44	105*55*18	5YR 8/1-5Y 6/1	Striped	N-P		Primary	Cortex Non-Dominant		Opaque	Coarse	Foliated
Naibor Soit Kubwa	Naibor Soit Kubwa C4A	Qtz	R1	N	Y	35.34430 4	-2.957241	1510.62	272.47	79*54*41	5YR 6/4-5YR 5/6	Homogeneous	N-P		Primary	Fully Cortical	Dull	Opaque	Very Coarse	Non-Foliated
	Naibor Soit Kubwa C4B	Qtz	W1	N	Y	35.34426 8	-2.957389	1510.37	>500.00	88*61*53	N8	Homogeneous	N-P		Primary	Fully Cortical	Dull-Milky	Opaque	Coarse	Non-Foliated
	Naibor Soit Kubwa C4C	Qtz	G1	N	N	35.34427 1	-2.957393	1511.47	208.77	89*51*29	5GY 8/1	Homogeneous	N-P		Primary	Fully Cortical	Dull-Milky	Opaque	Medium	Non-Foliated
	Naibor Soit Kubwa C4D	Qtz	G1	N	N	35.34427 4	-2.957378	1510.82	145.47	78*37*25	5GY 8/1	Homogeneous	N-P		Primary	Fully Cortical	Dull-Milky	Opaque	Medium	Non-Foliated
	Naibor Soit Kubwa C5A	Qtz	R1	N	N	35.34448 1	-2.958702	1520.4	378.29	104*82*33	5YR 7/2-5YR 5/6	Homogeneous	N-P		Primary	Fully Cortical	Dull	Opaque	Very Coarse	Non-Foliated
	Naibor Soit Kubwa C5B	Qtz	W2	N	N	35.34449 3	-2.958721	1519.4	>500.00	133*84*61	5YR 8/1	Zoned	N-P		Primary	Fully Cortical	Dull-Milky	Opaque	Coarse	Non-Foliated
	Naibor Soit Kubwa D4A	Qtz	W1	N	N	35.34426 4	-2.956652	1514.39	329.82	67*67*40	N8	Homogeneous	N-P		Primary	Fully Cortical	Dull-Milky	Opaque	Coarse	Non-Foliated
	Naibor Soit Kubwa D4B	Qtz	R3	N	N	35.3454	-2.956736	1516.88	334.98	62*61*42	5YR 6/4-5R 4/2	Homogeneous	N-P		Primary	Fully Cortical	Dull-Milky	Opaque	Coarse	Non-Foliated
	Naibor Soit Kubwa D4C	Qtz	G1	N	N	35.34539 5	-2.956724	1517.02	289.07	96*57*34	5GY 8/1	Zoned	N-P		Primary	Fully Cortical	Dull-Milky	Opaque	Coarse	Non-Foliated
	Naibor Soit Kubwa D4D	Qtz	R2	N	N	35.34539 4	-2.956725	1517.06	>500.00	82*72*50	5YR 6/4-5R 4/2	Homogeneous	N-P		Primary	Fully Cortical	Dull-Milky	Opaque	Very Coarse	Foliated
	Naibor Soit Kubwa D5A	Qtz	R4	N	N	35.34551 9	-2.958493	1591.47	255.66	82*66*40	5YR 6/4-5YR 5/6	Homogeneous	N-P		Primary	Fully Cortical	Dull-Milky	Opaque	Very Coarse (Uncons.)	Non-Foliated
	Naibor Soit Kubwa D6A	Qtz	R4	N	N	35.34522 4	-2.959073	1565.7	368.27	93*57*52	5YR 6/4-5YR 5/6	Homogeneous	N-P		Primary	Fully Cortical	Dull-Milky	Opaque	Very Coarse (Uncons.)	Foliated
	Naibor Soit Kubwa D7A	Qtz	R4	N	N	35.34535 7	-2.959616	1571.84	380.42	105*51*48	5YR 6/4-5YR 5/6	Homogeneous	N-P		Primary	Fully Cortical	Dull-Milky	Opaque	Very Coarse (Uncons.)	Foliated
	Naibor Soit Kubwa D7B	Qtz	R3	N	N	35.34509 7	-2.960264	1539.44	221.91	82*47*42	5YR 6/4-5R 4/2	Homogeneous	N-P		Primary	Cortex Dominant	Dull-Milky	Opaque	Coarse	Non-Foliated
	Naibor Soit Kubwa E4A	Qtz	W1	N	N	35.34579 9	-2.957101	1521.37	293.67	101*76*31	N8-5Y 8/1	Homogeneous	N-P		Primary	Fully Cortical	Dull-Milky	Opaque	Coarse	Non-Foliated

Outcrop	Sample ID	Rock	RMG	EDXRF	Petrography	Long.	Lat.	Alt.	Mass (g)	Size (mm; LxWxT)	Munsell Code	Striping Zonation	Patina	Patina Color	Cortex Type	Cortex Proportion	Gloss	Transparency	Grain Size	Foliation
	Naibor Soit Kubwa E4B	Qtz	G1	N	N	35.34579	-2.957093	1520.87	350.56	121*68*26	5GY 8/1	Homogeneous	N-P		Primary	Fully Cortical	Dull-Milky	Opaque	Coarse	Foliated
	Naibor Soit Kubwa E5A	Qtz	W1	N	N	35.34633	-2.957749	1529.25	234.62	77*58*25	N8-5Y 8/1	Homogeneous	N-P		Primary	Fully Cortical	Dull-Milky	Opaque	Coarse	Non-Foliated
	Naibor Soit Kubwa E5B	Qtz	R2	N	N	35.34633	-2.95775	1529.21	373.92	82*64*53	5YR 6/4-5R 4/2	Homogeneous	N-P		Primary	Fully Cortical	Dull	Opaque	Coarse	Foliated
	Naibor Soit Kubwa E5C	Qtz	G1	N	N	35.34634	-2.957739	1531.17	321.41	102*59*32	5GY 8/1	Homogeneous	N-P		Primary	Fully Cortical	Dull	Opaque	Coarse-Medium	Foliated
	Naibor Soit Kubwa E5D	Qtz	R3	N	N	35.34634	-2.957738	1531.87	>500.00	81*67*43	5YR 6/4-5R 4/2	Homogeneous	N-P		Primary	Fully Cortical	Dull	Opaque	Coarse	Non-Foliated
	Naibor Soit Kubwa E5E	Qtz	R4	N	N	35.34634	-2.957747	1532.03	214.83	86*67*36	5YR 6/4-5YR 5/6	Homogeneous	N-P		Primary	Fully Cortical	Dull	Opaque	Very Coarse (Uncons.)	Foliated
	Naibor Soit Kubwa E6A	Qtz	R1	N	N	35.34570	-2.958902	1600.4	288.67	96*54*37	5YR 6/4-5YR 5/6	Homogeneous	N-P		Primary	Cortex Dominant	Dull	Opaque	Coarse	Non-Foliated
	Naibor Soit Kubwa E7A	Qtz	R1	N	N	35.34535	-2.959585	1571.84	256.81	92*73*28	5YR 6/4-5YR 5/6	Homogeneous	N-P		Primary	Cortex Dominant	Dull	Opaque	Very Coarse-Coarse	Non-Foliated
	Naibor Soit Kubwa E8A	Qtz	R4	N	N	35.34702	-2.96235	1566.7	361.10	113*61*42	5YR 5/6	Homogeneous	N-P		Primary	Cortex Dominant	Dull-Milky	Opaque	Coarse-Medium	Foliated
	Naibor Soit Kubwa F11A	Qtz	W1	N	N	35.34588	-2.962445	1531.74	384.32	105*65*47	N8-5Y 8/1	Homogeneous	N-P		Primary	Cortex Dominant	Milky	Opaque	Coarse	Foliated
	Naibor Soit Kubwa F11C	Qtz	GR1	N	N	35.34589	-2.962448	1531.64	339.14	94*91*55	5PB 5/2-5PB 7/2	Homogeneous	N-P		Primary	Cortex Dominant	Milky	Opaque	Coarse-Medium	Foliated
	Naibor Soit Kubwa F5A	Qtz	W3	N	N	35.34743	-2.958407	1536.4	390.49	105*101*37	N9	Homogeneous	N-P		Primary	Cortex Dominant	Dull-Milky	Opaque	Coarse	Foliated
	Naibor Soit Kubwa F5B	Qtz	GR1	N	N	35.34743	-2.958418	1535.19	288.41	72*48*42	5PB 5/2-5PB 7/2	Homogeneous	N-P		Primary	Fully Cortical	Milky	Opaque	Coarse-Medium	Foliated
	Naibor Soit Kubwa F5C	Qtz	R3	N	N	35.34743	-2.958418	1535.05	165.20	73*50*30	5YR 6/4-5R 4/2	Homogeneous	N-P		Primary	Fully Cortical	Dull	Opaque	Very Coarse	Non-Foliated
	Naibor Soit Kubwa F6A	Qtz	GR1	N	N	35.34807	-2.961217	1572.7	288.92	123*58*32	5PB 5/2-5PB 7/2	Homogeneous	N-P		Primary	Fully Cortical	Milky	Opaque	Coarse-Medium	Foliated
	Naibor Soit Kubwa F6B	Qtz	G1	N	N	35.34807	-2.961215	1573.37	192.70	71*42*38	5GY 8/1	Homogeneous	N-P		Primary	Fully Cortical	Dull	Opaque	Coarse-Medium	Foliated
	Naibor Soit Kubwa F6C	Qtz	G1	N	N	35.34806	-2.96121	1573.56	223.88	79*73*21	5GY 8/1	Homogeneous	N-P		Primary	Fully Cortical	Dull	Opaque	Coarse-Medium	Foliated
	Naibor Soit Kubwa F6D	Qtz	R4	N	N	35.34806	-2.961211	1574.49	234.03	93*64*54	5YR 6/4-5YR 5/6	Homogeneous	N-P		Primary	Fully Cortical	Dull	Opaque	Very Coarse (Uncons.)	Non-Foliated
	Naibor Soit Kubwa F7A	Qtz	R1	N	N	35.34567	-2.95934	1593.17	397.54	109*58*51	5YR 6/4-5YR 5/6	Homogeneous	N-P		Primary	Fully Cortical	Dull	Opaque	Coarse	Non-Foliated

Outcrop	Sample ID	Rock	RMG	EDXRF	Petrography	Long.	Lat.	Alt.	Mass (g)	Size (mm; LxWxT)	Munsell Code	Striping Zonation	Patina	Patina Color	Cortex Type	Cortex Proportion	Gloss	Transparency	Grain Size	Foliation
	Naibor Soit Kubwa F7B	Qtz	R3	N	N	35.3457	-2.959321	1595.17	349.34	94*92*31	5YR 6/4-5R 4/2	Homogeneous	N-P		Primary	Cortex Dominant	Milky	Opaque	Very Coarse	Non-Foliated
	Naibor Soit Kubwa F8A	Qtz	R4	N	N	35.34731	-2.961912	1608.05	193.89	102*57*28	5YR 6/4-5YR 5/6	Homogeneous	N-P		Primary	Cortex Dominant	Dull	Opaque	Very Coarse	Non-Foliated
	Naibor Soit Kubwa F9A	Qtz	R1	N	N	35.34735	-2.963064	1557.12	255.47	76*70*46	5YR 6/4-5YR 5/6	Homogeneous	N-P		Primary	Fully Cortical	Dull	Opaque	Coarse	Non-Foliated
	Naibor Soit Kubwa F9B	Qtz	W1	N	N	35.34736	-2.963075	1557.75	339.14	105*65*47	N8-5Y 8/1	Homogeneous	N-P		Primary	Cortex Dominant	Dull-Milky	Opaque	Coarse	Foliated
	Naibor Soit Kubwa G10A	Qtz	R4	N	N	35.34747 2	-2.963825	1558.18	291.05	79*69*49	5YR 6/4-5YR 5/6	Homogeneous	Patina Dominant	10YR 8/2 (Very Pale Orange)	Primary	Fully Cortical	Dull	Opaque	Very Coarse	Non-Foliated
	Naibor Soit Kubwa G10B	Qtz	W3	N	N	35.34746 3	-2.963851	1560.16	310.30	121*73*35	N9	Homogeneous	N-P		Primary	Cortex Dominant	Dull-Milky	Opaque	Very Coarse	Non-Foliated
	Naibor Soit Kubwa G10C	Qtz	R3	N	N	35.34748 1	-2.963832	1562.27	284.07	83*82*49	5YR 6/4-5R 4/2	Homogeneous	N-P		Primary	Cortex Dominant	Milky	Opaque	Very Coarse	Non-Foliated
	Naibor Soit Kubwa G6A	Qtz	GR1	N	N	35.34804 3	-2.96077	1563.64	197.25	78*52*50	5PB 5/2-5PB 7/2	Homogeneous	N-P		Primary	Fully Cortical	Milky	Opaque	Coarse-Medium	Foliated
	Naibor Soit Kubwa G6D	Qtz	W2	N	N	35.34806	-2.960773	1564.1	>500.00	96*95*38	5YR 8/1	Zoned	N-P		Primary	Fully Cortical	Dull-Milky	Opaque	Coarse	Non-Foliated
	Naibor Soit Kubwa G9A	Qtz	R2	N	Y	35.34837	-2.963464	1607.63	381.32	121*71*38	5YR 6/4-5R 4/2	Homogeneous	N-P		Primary	Cortex Dominant	Milky	Opaque	Coarse	Foliated
	Naibor Soit Kubwa H10A	Qtz	GR1	N	N	35.34891	-2.963749	1582.36	429.22	95*62*37	5PB 5/2-5PB 7/2	Homogeneous	N-P		Primary	Cortex Dominant	Milky	Opaque	Coarse-Medium	Foliated
	Naibor Soit Kubwa H10B	Qtz	R3	N	N	35.34893	-2.963754	1583.75	>500.00	85*66*64	5YR 6/4-5R 4/2	Homogeneous	N-P		Primary	Cortex Dominant	Milky	Opaque	Very Coarse	Foliated
	Naibor Soit Kubwa H12A	Qtz	R3	N	N	35.34943 3	-2.966538	1545.45	>500.00	90*89*44	5YR 6/4-5R 4/2	Homogeneous	N-P		Primary	Fully Cortical	Milky	Opaque	Very Coarse (partially uncons.)	Non-Foliated
	Naibor Soit Kubwa H12B	Qtz	R3	N	N	35.34942 9	-2.966535	1547.15	>500.00	75*68*55	5YR 6/4-5R 4/2	Homogeneous	N-P		Primary	Cortex Dominant	Milky	Opaque	Very Coarse	Non-Foliated
	Naibor Soit Kubwa I10B	Qtz	W3	N	N	35.34920 3	-2.963771	1571.74	245.91	73*51*40	N9	Homogeneous	N-P		Primary	Cortex Dominant	Milky	Opaque	Coarse	Non-Foliated
	Naibor Soit Kubwa I10C	Qtz	W2	N	N	35.34919 5	-2.963768	1570.58	>500.00	127*114*57	5G 6/1	Homogeneous	N-P		Primary	Cortex Dominant	Milky	Opaque	Coarse	Non-Foliated
	Naibor Soit Kubwa I10D	Qtz	GR1	N	N	35.34916 5	-2.963752	1570.4	>500.00	104*75*49	5PB 5/2-5PB 7/2	Homogeneous	N-P		Primary	Cortex Dominant	Milky	Opaque	Coarse-Medium	Foliated
	Naibor Soit Kubwa I11B	Qtz	R1	N	N	35.34940 9	-2.964755	1569.26	380.11	86*73*29	5YR 6/4-5YR 5/6	Homogeneous	N-P		Primary	Fully Cortical	Milky	Opaque	Very Coarse	Foliated
	Naibor Soit Kubwa I11C	Qtz	GR1	N	N	35.34939 1	-2.964757	1569.62	>500.00	117*54*50	5PB 5/2-5PB 7/2	Homogeneous	N-P		Primary	Cortex Dominant	Milky	Opaque	Very Coarse	Non-Foliated

Outcrop	Sample ID	Rock	RMG	EDXRF	Petrography	Long.	Lat.	Alt.	Mass (g)	Size (mm; LxWxT)	Munsell Code	Striping Zonation	Patina	Patina Color	Cortex Type	Cortex Proportion	Gloss	Transparency	Grain Size	Foliation
	Naibor Soit Kubwa I12A	Qtz	R4	N	N	35.34993	-2.966197	1547.41	>500.00	129*79*51	5YR 6/4-5YR 5/6	Homogeneous	N-P		Primary	Cortex Dominant	Dull	Opaque	Very Coarse (Uncons.)	Non-Foliated
	Naibor Soit Kubwa I12B	Qtz	R3	N	N	35.34993	-2.966197	1547.41	209.90	91*54*34	5YR 6/4-5R 4/2	Homogeneous	N-P		Primary	Cortex Dominant	Milky	Opaque	Very Coarse	Non-Foliated
	Naibor Soit Kubwa I9A	Qtz	R1	N	N	35.34861	-2.963073	1582.81	276.89	100*64*35	5YR 6/4-5YR 5/6	Homogeneous	N-P		Primary	Fully Cortical	Milky	Opaque	Very Coarse	Non-Foliated
	Naibor Soit Kubwa I9B	Qtz	W1	N	N	35.34861	-2.963073	1582.81	>500.00	115*100*85	N8-5Y 8/1	Homogeneous	N-P		Primary	Cortex Dominant	Milky	Opaque	Coarse	Non-Foliated
	Naibor Soit Kubwa J12A	Qtz	R4	N	N	35.35084	-2.966152	1548.54	335.73	83*79*41	5YR 6/4-5YR 5/6	Homogeneous	Patina Dominant	10YR 8/2 (Very Pale Orange)	Primary	Cortex Dominant	Dull	Opaque	Very Coarse	Non-Foliated
	Naibor Soit Kubwa K12A	Qtz	R3	N	N	35.351598	-2.966689	1556	292.56	82*65*51	5YR 6/4-5R 4/2	Zoned	N-P		Primary	Cortex Dominant	Milky	Opaque	Coarse	Non-Foliated
	Naibor Soit Kubwa K12B	Qtz	R4	N	Y	35.35158	-2.966692	1556.98	371.27	83*57*56	5YR 6/4-5YR 5/6	Homogeneous	N-P		Primary	Fully Cortical	Dull	Opaque	Very Coarse (Uncons.)	Foliated
	Naibor Soit Kubwa K13A	Qtz	R4	N	N	35.347113	-2.964314	1540.42	186.11	86*67*36	5YR 6/4-5YR 5/6	Homogeneous	N-P		Primary	Fully Cortical	Dull	Opaque	Very Coarse (Uncons.)	Non-Foliated
	Naibor Soit Kubwa K13B	Qtz	W3	N	N	35.347107	-2.964326	1539.1	357.96	85*75*49	N9	Homogeneous	N-P		Primary	Fully Cortical	Dull-Milky	Opaque	Coarse	Foliated
	Naibor Soit Kubwa K13C	Qtz	W1	N	N	35.347107	-2.964329	1539.93	206.67	102*58*26	N8-5Y 8/1	Homogeneous	N-P		Primary	Fully Cortical	Dull-Milky	Opaque	Coarse	Foliated
	Naibor Soit Kubwa K13D	Qtz	R3	N	N	35.347107	-2.964325	1539.53	401.38	88*84*48	5Y 8/1	Homogeneous	N-P		Primary	Cortex Dominant	Milky	Opaque	Very Coarse	Non-Foliated
	Naibor Soit Kubwa K15A	Qtz	R3	N	N	35.351909	-2.969783	1524.89	401.38	88*84*48	5Y 8/1	Homogeneous	N-P		Primary	Fully Cortical	Milky	Opaque	Very Coarse	Non-Foliated
	Naibor Soit Kubwa K15B	Qtz	R4	N	N	35.351924	-2.969796	1523.85	224.05	92*66*30	5YR 6/4-5YR 5/6	Homogeneous	N-P		Primary	Cortex Dominant	Dull	Opaque	Very Coarse (Uncons.)	Non-Foliated
	Naibor Soit Kubwa K16A	Qtz	W1	N	N	35.352136	-2.970256	1517.62	293.55	94*70*40	N8-5Y 8/1	Homogeneous	N-P		Primary	Fully Cortical	Dull-Milky	Opaque	Coarse	Foliated
	Naibor Soit Kubwa K16B	Qtz	R3	N	N	35.351994	-2.970327	1516.98	332.61	106*61*42	5YR 6/4-5R 4/2	Homogeneous	N-P		Primary	Fully Cortical	Milky	Opaque	Very Coarse	Non-Foliated
	Naibor Soit Kubwa K16C	Qtz	R1	N	N	35.352067	-2.97031	1516.66	205.66	101*55*28	5YR 6/4-5YR 5/6	Homogeneous	N-P		Primary	Cortex Dominant	Dull	Opaque	Coarse	Non-Foliated
	Naibor Soit Kubwa M14A	Qtz	R4	N	N	35.352817	-2.968238	1552.86	269.26	104*50*46	5YR 6/4-5YR 5/6	Homogeneous	N-P		Primary	Cortex Dominant	Dull	Opaque	Very Coarse (Uncons.)	Non-Foliated
	Naibor Soit Kubwa 1	Qtz	R3	Y	Y	35.352662	-2.970767	1500.8934	293.17	100*60*41	5YR 8/4	Homogenous	N-P		Primary	Cortex Dominant	Dull	Opaque	Coarse	Non-Foliated
	Naibor Soit Kubwa 10	Qtz	W3	N	N	35.35291	-2.970448	1511.5214	172.86	80*45*38	N9	Homogenous	N-P		Primary	Cortex Dominant	Dull	Edge-Transparent	Coarse	Non-Foliated

Outcrop	Sample ID	Rock	RMG	EDXRF	Petrography	Long.	Lat.	Alt.	Mass (g)	Size (mm; LxWxT)	Munsell Code	Striping Zonation	Patina	Patina Color	Cortex Type	Cortex Proportion	Gloss	Transparency	Grain Size	Foliation
	Naibor Soit Kubwa 11	Qtz	W3	Y	N	35.3529	-2.970252	1518.2634	157.11	110*48*25	N9	Homogenous	N-P		Primary	Cortex Non-Dominant	Dull-Milky	Edge-Transparent	Coarse	Non-Foliated
	Naibor Soit Kubwa 12	Qtz	R3	N	N	35.35275	-2.969684	1533.119	332.98	73*72*70	5YR 8/4	Homogenous	N-P		Primary	Cortex Dominant	Dull	Opaque	Coarse	Non-Foliated
	Naibor Soit Kubwa 13	Qtz	R3	Y	Y	35.352535	-2.96955	1543.7609	234.13	92*70*30	5YR 8/1	Homogenous	N-P		Primary	Cortex Non-Dominant	Dull	Edge-Transparent	Coarse	Non-Foliated
	Naibor Soit Kubwa 14	Qtz	W2	Y	N	35.352403	-2.969346	1546.0233	nd	86*53*40	5YR 8/1	Homogenous	N-P		Primary	Cortex Non-Dominant	Dull	Edge-Transparent	Coarse	Non-Foliated
	Naibor Soit Kubwa 15	Qtz	R3	N	N	35.352419	-2.968874	1545.2975	131.19	68*51*28	5YR 8/4	Homogenous	N-P		Primary	Cortex Non-Dominant	Dull	Edge-Transparent	Coarse	Non-Foliated
	Naibor Soit Kubwa 16	Qtz	W3	N	N	35.352485	-2.968661	1548.3639	106.11	113*45*21	N9	Homogenous	N-P		Primary	Cortex Non-Dominant	Dull	Transparent	Coarse	Non-Foliated
	Naibor Soit Kubwa 18	Qtz	W3	N	N	35.351899	-2.967022	1565.4736	167.51	67*67*45	N8	Homogenous	N-P		Primary	Cortex Non-Dominant	Dull	Edge-Transparent	Coarse	Non-Foliated
	Naibor Soit Kubwa 19	Qtz	R3	N	N	35.352118	-2.966782	1549.9695	87.16	74*50*25	10R 7/4	Homogenous	N-P		Primary	Cortex Non-Dominant	Dull	Edge-Transparent	Coarse	Non-Foliated
	Naibor Soit Kubwa 2	Qtz	W3	Y	Y	35.352446	-2.970747	1499.9459	255.12	78*68*49	10R 8/2	Homogenous	N-P		Primary	Cortex Non-Dominant	Dull	Opaque	Coarse	Non-Foliated
	Naibor Soit Kubwa 20	Qtz	W3	N	N	35.352537	-2.96687	1543.9885	72.77	53*40*25	N8	Homogenous	N-P		Secondary	Cortex Non-Dominant	Dull	Edge-Transparent	Coarse	Non-Foliated
	Naibor Soit Kubwa 21	Qtz	R3	N	N	35.352719	-2.966844	1536.4908	73.87	66*43*30	5YR 7/2-5YR 8/4	Zoned	N-P		Primary	Cortex Non-Dominant	Dull	Edge-Transparent	Coarse	Non-Foliated
	Naibor Soit Kubwa 22	Qtz	W3	N	N	35.353075	-2.967735	1539.7751	146.50	60*40*40	N8	Homogenous	N-P		Primary	Cortex Non-Dominant	Dull	Edge-Transparent	Coarse	Non-Foliated
	Naibor Soit Kubwa 23	Qtz	R3	N	N	35.351312	-2.967576	1534.3789	361.75	70*67*47	5YR 8/4	Homogenous	N-P		Primary	Cortex Dominant	Dull	Opaque	Coarse	Non-Foliated
	Naibor Soit Kubwa 24	Qtz	W2	Y	N	35.351325	-2.966961	1546.6187	240.18	75*72*60	N9-5YR 8/4	Zoned	N-P		Primary	Cortex Non-Dominant	Dull	Opaque	Coarse	Non-Foliated
	Naibor Soit Kubwa 25	Qtz	W3	N	N	35.350917	-2.966682	1541.7576	71.68	64*50*15	N8	Homogenous	N-P		Primary	Cortex Non-Dominant	Dull	Transparent	Coarse	Non-Foliated
	Naibor Soit Kubwa 26	Qtz	R3	N	N	35.349203	-2.966415	1546.5098	325.33	105*65*53	5YR 8/4	Homogenous	N-P		Primary	Cortex Dominant	Dull	Edge-Transparent	Coarse	Non-Foliated
	Naibor Soit Kubwa 27	Qtz	R3	Y	N	35.347411	-2.964801	1544.8213	353.85	100*70*40	5YR 7/2	Homogenous	N-P		Primary	Cortex Dominant	Dull	Opaque	Coarse	Foliated
	Naibor Soit Kubwa 3	Qtz	W3	N	N	35.352141	-2.970678	1498.0298	84.36	72*50*37	5YR 8/1	Homogenous	N-P		Secondary	Cortex Non-Dominant	Dull	Edge-Transparent	Coarse	Non-Foliated
	Naibor Soit Kubwa 30	Qtz	G1	N	N	35.347655	-2.960745	1586.8807	350.64	77*67*45	5G 8/1	Homogenous	N-P		Primary	Cortex Non-Dominant	Dull	Edge-Transparent	Coarse	Non-Foliated

Outcrop	Sample ID	Rock	RMG	EDXRF	Petrography	Long.	Lat.	Alt.	Mass (g)	Size (mm; LxWxT)	Munsell Code	Striping Zonation	Patina	Patina Color	Cortex Type	Cortex Proportion	Gloss	Transparency	Grain Size	Foliation
	Naibor Soit Kubwa 31	Qtz	G1	Y	N	35.34789	-2.96111	1582.8259	599.00	80*75*72	10GY 6/4-5G 7/4	Zoned	N-P		Primary	Cortex Non-Dominant	Dull	Opaque	Coarse	Foliated
	Naibor Soit Kubwa 32	Qtz	GR1	N	Y	35.34810	-2.96 1593	1575.5309	272.41	70*60*55	10R 3/4	Homogenous	N-P		Primary	Cortex Dominant	Dull	Opaque	Medium	Non-Foliated
	Naibor Soit Kubwa 33	Qtz	GR1	Y	N	35.34821	-2.96 1993	1573.3862	402.85	115*55*50	N8-N3	Striped	Patina Non-Dominant	10YR 8/2 (Very Pale Orange)	Primary	Cortex Dominant	Dull	Opaque	Coarse	Non-Foliated
	Naibor Soit Kubwa 4	Qtz	R3	N	N	35.35190	-2.97 0537	1494.8928	263.98	80*63*62	10R 7/4	Homogenous	N-P		Secondary	Cortex Dominant	Dull	Opaque	Coarse	Non-Foliated
	Naibor Soit Kubwa 5	Qtz	R3	N	N	35.35192	-2.97 0368	1502.7794	311.44	90*75*56	5YR 8/4	Homogenous	N-P		Secondary	Cortex Dominant	Dull	Opaque	Coarse	Non-Foliated
	Naibor Soit Kubwa 6	Qtz	GR1	N	N	35.35199	-2.97 0451	1508.7437	184.54	110*60*55	N6	Zoned	N-P		Primary	Cortex Dominant	Dull	Edge-Transparent	Coarse	Non-Foliated
	Naibor Soit Kubwa 7	Qtz	W3	N	N	35.35221	-2.97 0569	1507.1538	91.72	73*55*28	N8	Homogenous	N-P		Primary	Cortex Non-Dominant	Dull	Edge-Transparent	Medium	Non-Foliated
	Naibor Soit Kubwa 8	Qtz	R3	N	N	35.35238	-2.97 058	1510.9121	145.61	80*43*21	5YR 8/1-5YR 6/1	Zoned	N-P		Primary	Cortex Non-Dominant	Dull	Edge-Transparent	Coarse	Non-Foliated
	Naibor Soit Kubwa 9	Qtz	R3	N	N	35.35289	-2.97 0443	1511.2061	156.82	75*53*40	5YR 8/4	Homogenous	N-P		Secondary	Cortex Non-Dominant	Dull	Edge-Transparent	Coarse	Non-Foliated
Naibor Soit Ndogo	Naibor Soit Ndogo 1	Qtz	W3	N	N	35.36002	-2.97 4166	1486.8446	203.96	95*63*51	N7	Homogenous	N-P		Primary	Cortex Non-Dominant	Dull	Transparent	Coarse	Non-Foliated
	Naibor Soit Ndogo 10	Qtz	G1	N	N	35.35950	-2.97 3738	1490.55	280.20	70*65*50	N8-5G 6/6	Zoned	N-P		Secondary	Cortex Non-Dominant	Dull	Edge-Transparent	Coarse	Non-Foliated
	Naibor Soit Ndogo 11	Qtz	G1	N	N	35.35958	-2.97 3786	1495.7919	54.25	97*34*20	N8-5G 6/6	Zoned	N-P		Primary	Cortex Dominant	Dull	Edge-Transparent	Coarse	Non-Foliated
	Naibor Soit Ndogo 12	Qtz	W3	N	N	35.35973	-2.97 3783	1498.2604	159.01	85*40*28	N8	Homogenous	N-P		Primary	Cortex Non-Dominant	Dull	Edge-Transparent	Coarse	Non-Foliated
	Naibor Soit Ndogo 13	Qtz	W2	Y	N	35.36024	-2.97 4388	1488.5499	133.68	85*72*30	N8-5G 5/6	Zoned	N-P		Primary	Cortex Non-Dominant	Dull-Milky	Transparent	Coarse	Non-Foliated
	Naibor Soit Ndogo 14	Qtz	W3	Y	N	35.36024	-2.97 4429	1487.3405	261.27	115*70*35	5GY 6/1	Homogenous	N-P		Primary	Cortex Non-Dominant	Dull	Edge-Transparent	Coarse	Non-Foliated
	Naibor Soit Ndogo 15	Qtz	W3	Y	N	35.36085	-2.97 5039	1474.8833	95.96	65*50*38	5YR 8/1	Homogenous	N-P		Primary	Non-Cortical	Dull	Edge-Transparent	Coarse	Non-Foliated
	Naibor Soit Ndogo 2	Qtz	W3	N	N	35.35990	-2.97 4048	1490.822	274.35	110*62*43	N7	Homogenous	N-P		Primary	Cortex Non-Dominant	Dull	Edge-Transparent	Coarse	Non-Foliated
	Naibor Soit Ndogo 3	Qtz	W3	N	N	35.35963	-2.97 3971	1489.6641	128.57	76*63*35	N7	Homogenous	N-P		Primary	Cortex Non-Dominant	Dull	Edge-Transparent	Coarse	Non-Foliated
	Naibor Soit Ndogo 4	Qtz	W3	N	N	35.35930	-2.97 3612	1486.9193	238.35	105*63*35	5GY 8/1	Homogenous	N-P		Primary	Cortex Non-Dominant	Dull	Edge-Transparent	Coarse	Non-Foliated

Outcrop	Sample ID	Rock	RMG	EDXRF	Petrography	Long.	Lat.	Alt.	Mass (g)	Size (mm; LxWxT)	Munsell Code	Striping Zonation	Patina	Patina Color	Cortex Type	Cortex Proportion	Gloss	Transparency	Grain Size	Foliation
	Naibor Soit Ndogo 5	Qtz	W3	N	N	35.35956	-2.973586	1487.4619	311.07	100*80*28	N7	Homogenous	N-P		Primary	Cortex Non-Dominant	Dull	Edge-Transparent	Coarse	Non-Foliated
	Naibor Soit Ndogo 6	Qtz	W3	Y	N	35.35990 5	-2.973845	1490.3723	162.00	75*65*33	5Y 8/1	Homogenous	N-P		Primary	Cortex Non-Dominant	Dull	Edge-Transparent	Coarse	Non-Foliated
	Naibor Soit Ndogo 7	Qtz	W3	N	N	35.36010 7	-2.974133	1489.7449	285.80	85*75*55	N8	Homogenous	N-P		Primary	Cortex Non-Dominant	Dull	Edge-Transparent	Coarse	Non-Foliated
	Naibor Soit Ndogo 8	Qtz	W3	Y	N	35.35974 6	-2.973955	1491.949	130.27	94*65*35	N8	Homogenous	N-P		Primary	Non-Cortical	Dull	Edge-Transparent	Coarse	Non-Foliated
	Naibor Soit Ndogo 9	Qtz	W3	N	N	35.35955 2	-2.973714	1495.2074	206.00	81*50*45	N9	Homogenous	N-P		Primary	Cortex Non-Dominant	Dull	Edge-Transparent	Coarse	Non-Foliated
	Naibor Soit Ndogo S18A	Qtz	G1	N	N	35.35859 7	-2.973413	1475.71	308.18	77*70*35	5GY 8/1	Zoned	N-P		Primary	Fully Cortical	Milky	Opaque	Coarse-Medium	Non-Foliated
	Naibor Soit Ndogo S18B	Qtz	W2	N	N	35.35858 3	-2.973375	1476.78	>500.00	120*69*49	5YR 8/1	Homogeneous	N-P		Primary	Cortex Dominant	Milky	Opaque	Coarse	Non-Foliated
	Naibor Soit Ndogo S18C	Qtz	W1	N	N	35.35858 4	-2.97338	1477.48	271.39	71*54*39	N8-5Y 8/1	Homogeneous	N-P		Primary	Cortex Dominant	Milky	Opaque	Coarse	Non-Foliated
	Naibor Soit Ndogo S19A	Qtz	W1	N	N	35.35905 6	-2.974098	1471.82	200.07	81*56*46	N8-5Y 8/1	Homogeneous	N-P		Primary	Cortex Dominant	Milky	Opaque	Coarse	Non-Foliated
	Naibor Soit Ndogo S19B	Qtz	R1	N	N	35.35904 7	-2.974093	1473.01	153.55	72*38*38	5YR 6/4-5YR 5/6	Homogeneous	N-P		Primary	Fully Cortical	Milky	Opaque	Coarse	Non-Foliated
	Naibor Soit Ndogo S19C	Qtz	G1	N	N	35.35904 6	-2.974096	1473.57	195.95	84*79*31	5GY 8/1	Zoned	N-P		Primary	Cortex Dominant	Milky	Opaque	Coarse	Non-Foliated
	Naibor Soit Ndogo S19D	Qtz	W2	N	N	35.35904	-2.974102	1473.49	254.88	66*65*41	5YR 8/1	Homogeneous	N-P		Primary	Fully Cortical	Dull-Milky	Opaque	Coarse	Non-Foliated
	Naibor Soit Ndogo T19A	Qtz	W1	N	N	35.35989 9	-2.974605	1478.65	212.37	98*43*37	N8-5Y 8/1	Homogeneous	N-P		Primary	Cortex Dominant	Milky	Opaque	Coarse	Non-Foliated
	Naibor Soit Ndogo T19B	Qtz	R1	N	N	35.35989 7	-2.974606	1480.23	>500.00	85*82*64	5YR 6/4-5YR 5/6	Homogeneous	N-P		Primary	Fully Cortical	Dull	Opaque	Coarse	Non-Foliated
	Naibor Soit Ndogo T19C	Qtz	R3	N	N	35.35989 8	-2.974604	1479.95	206.86	73*72*24	5YR 6/4-5R 4/2	Homogeneous	N-P		Primary	Cortex Dominant	Milky	Opaque	Very Coarse	Foliated
	Naibor Soit Ndogo T19D	Qtz	G1	N	N	35.35990 3	-2.974602	1480.06	246.15	86*82*21	5GY 8/1	Homogeneous	N-P		Primary	Fully Cortical	Milky	Opaque	Coarse-Medium	Non-Foliated
	Naibor Soit Ndogo U18A	Qtz	GR1	N	N	35.35977 2	-2.973137	1482.04	141.59	70*52*26	5PB 5/2-5PB 7/2	Homogeneous	N-P		Primary	Fully Cortical	Milky	Opaque	Coarse-Medium	Foliated
	Naibor Soit Ndogo U18B	Qtz	W2	N	N	35.35977 3	-2.973146	1483.6	110.55	71*49*30	5YR 8/1	Homogeneous	N-P		Primary	Fully Cortical	Milky	Opaque	Coarse	Non-Foliated
	Naibor Soit Ndogo U18C	Qtz	GR1	N	N	35.35977 6	-2.973148	1483.66	127.76	58*47*32	5PB 5/2-5PB 7/2	Homogeneous	N-P		Primary	Cortex Dominant	Milky	Opaque	Coarse-Medium	Non-Foliated

Outcrop	Sample ID	Rock	RMG	EDXRF	Petrography	Long.	Lat.	Alt.	Mass (g)	Size (mm; LxWxT)	Munsell Code	Striping Zonation	Patina	Patina Color	Cortex Type	Cortex Proportion	Gloss	Transparency	Grain Size	Foliation
	Naibor Soit Ndogo U18D	Qtz	G1	N	N	35.35977 9	-2.973146	1484.26	102.36	74*36*20	5GY 8/1	Homogeneous	N-P		Primary	Fully Cortical	Milky	Opaque	Coarse-Medium	Foliated
	Naibor Soit Ndogo U18E	Qtz	R3	N	N	35.35977 2	-2.973144	1484.35	289.04	77*56*50	5YR 6/4-5R 4/2	Homogeneous	N-P		Primary	Fully Cortical	Milky	Opaque	Very Coarse	Non-Foliated
Naisiusiu	Naisiusiu 1	Qtz	R5	Y	Y	35.25122 7	-2.959617	1555.4606	286.00	100*65*50	N7	Homogenous	Patina Non-Dominant	5YR 5/6 (Light Brown)	Primary	Cortex Dominant	Dull	Opaque	Medium	Non-Foliated
	Naisiusiu 13	Qtz	GR1	Y	N	35.25114 5	-2.959435	1557.5073	129.97	92*70*35	5YR 8/1-5R 3/4	Zoned	N-P		Primary	Cortex Non-Dominant	Dull	Transparent	Medium	Non-Foliated
	Naisiusiu 14	Qtz	W3	Y	N	35.25113 6	-2.959515	1553.1958	265.08	70*65*40	N7	Homogenous	N-P		Primary	Cortex Non-Dominant	Dull	Edge-Transparent	Coarse	Non-Foliated
	Naisiusiu 4	Qtz	GR2	Y	N	35.25186 7	-2.959682	1562.4293	nd	75*72*50	N6	Homogenous	N-P		Primary	Cortex Non-Dominant	Dull	Opaque	Medium	Non-Foliated
	Naisiusiu 6	Qtz	W3	Y	N	35.25211 2	-2.9596	1556.1541	419.22	92*54*40	N8	Homogenous	N-P		Primary	Cortex Dominant	Dull	Opaque	Coarse	Non-Foliated
	Naisiusiu 7	Qtz	GR1	Y	N	35.25196	-2.959362	1560.9147	nd	75*55*45	5PB 5/2-5PB 7/2	Homogenous	N-P		Primary	Cortex Non-Dominant	Dull	Opaque	Medium	Non-Foliated
	Naisiusiu 9	Qtz	W4	Y	Y	35.25182 3	-2.958939	1557.0894	nd	70*65*40	N8	Homogenous	N-P		Primary	Cortex Non-Dominant	Dull-Milky	Opaque	Medium	Non-Foliated
Oittii	Oittii 1	Qtz	GR2	Y	Y	35.3595	-2.969553	1480.819	343.57	94*75*60	N6	Homogenous	N-P		Primary	Cortex Non-Dominant	Dull	Opaque	Coarse	Non-Foliated
	Oittii 2	Qtz	GR2	Y	N	35.35953 5	-2.969442	1483.8256	235.79	80*72*38	5Y 6/1	Homogenous	N-P		Primary	Cortex Non-Dominant	Dull	Edge-Transparent	Coarse	Non-Foliated
	Oittii 3	Qtz	W4	Y	N	35.36028 2	-2.969093	1482.4216	107.42	90*48*26	N8	Dotted	N-P		Primary	Cortex Non-Dominant	Dull	Edge-Transparent	Medium	Non-Foliated
	Oittii 4	Qtz	GR2	Y	N	35.36051 7	-2.969093	1475.3026	105.80	78*67*25	5YR 6/1	Homogenous	N-P		Primary	Cortex Dominant	Dull	Edge-Transparent	Coarse	Non-Foliated
	Oittii 5	Qtz	GR2	Y	N	35.35991 9	-2.968886	1482.4751	250.31	90*78*32	N6	Flecked	N-P		Primary	Cortex Non-Dominant		Opaque	Coarse	Foliated

Table 2. Sample metadata and macroscopic characteristics (Qtz: Quartzite) (Y: Yes; N: No) (Long.: Longitude; Lat.: Latitude; Alt.: Altitude) (N-P: Non-Patinated) (Uncons.: Unconsolidated).

	STD *	weight (%)								ppm									
		MgO	Al_2O_3	SiO_2 **	K_2O	CaO	TiO_2	MnO	Fe_2O_3	Cu	Zn	Rb	Sr	Y	Zr	Nb	Ba	Pb	Th
Endonyo Osunyai 2 (W3)	STD-3	0.35	3.51	105.08	0.08	0.11	0.03	0.00	0.27	3.10	1.89	0.12	5.63	3.42	62.94	0.00	22.47	1.39	1.37
Endonyo Osunyai 3 (R3)	STD-3	0.36	4.03	88.74	0.55	0.12	0.03	0.00	0.26	2.87	0.93	19.40	32.12	0.64	22.89	0.18	308.16	4.59	0.40
Endonyo Osunyai 4 (GR2)	STD-3	0.63	6.81	79.47	1.80	0.12	0.11	0.00	0.84	10.42	5.60	90.57	89.03	3.98	99.49	3.72	636.92	11.29	10.80
Endonyo Osunyai 5 (GR2)	STD-3	0.71	7.95	84.70	1.67	2.62	0.16	0.00	1.17	5.80	3.68	86.60	28.70	2.30	46.00	4.82	504.81	2.40	1.44
Naibor Soit Ndogo 13 (W3)	STD-2	0.25	2.76	104.19	-0.07	0.10	0.02	0.00	0.26	2.71	1.12	-3.55	1.62	3.51	16.33	0.13	40.66	0.34	1.80
Naibor Soit Ndogo 13 (W3)	STD-1	0.33	3.40	79.16	0.07	0.09	0.02	0.00	0.27	2.92	2.21	0.62	3.49	11.11	20.92	0.00	62.80	0.69	1.76
Naibor Soit Ndogo 14 (W3)	STD-2	0.31	3.10	98.71	0.00	0.09	0.03	0.00	0.25	2.86	1.50	-0.94	1.47	3.71	24.49	0.00	51.06	0.00	0.96
Naibor Soit Ndogo 14 (W3)	STD-1	0.31	2.93	85.84	-0.05	0.10	0.01	0.01	0.24	2.40	1.05	-2.68	1.74	1.56	10.53	0.00	41.51	0.31	2.14
Naibor Soit Ndogo 15 (W3)	STD-2	0.29	3.05	102.73	-0.02	0.10	0.02	0.00	0.24	3.35	1.64	-2.25	1.99	2.02	18.77	0.57	13.27	0.74	2.03
Naibor Soit Ndogo 15 (W3)	STD-1	0.32	3.36	104.39	0.05	0.10	0.03	0.00	0.25	4.32	1.48	-0.65	2.99	2.87	23.48	0.75	19.63	0.00	0.67
Naibor Soit Ndogo 6 (W3)	STD-2	0.30	3.00	104.84	-0.04	0.09	0.01	0.00	0.25	2.84	1.04	-2.88	1.77	2.87	21.81	0.00	148.50	0.55	0.43
Naibor Soit Ndogo 6 (W3)	STD-1	0.42	3.25	15.76	-0.02	0.09	0.02	0.02	0.24	2.58	1.39	-2.36	0.72	2.06	20.09	0.00	196.42	0.36	1.67
Naibor Soit Ndogo 8 (W3)	STD-2	0.31	3.54	100.23	0.09	0.09	0.02	0.00	0.25	3.47	1.72	1.15	2.85	2.67	19.45	0.00	86.41	0.49	0.15
Naibor Soit Ndogo 8 (W3)	STD-1	0.30	3.13	102.49	0.01	0.14	0.01	0.00	0.24	3.35	1.61	-2.55	6.63	2.35	23.78	0.00	42.80	0.57	0.73
Naibor Soit Kubwa 1 (R3)	STD-3	0.28	3.06	97.40	0.00	0.10	0.01	0.00	0.24	2.99	0.73	-0.13	6.16	3.00	33.48	0.47	19.41	0.86	2.30
Naibor Soit Kubwa 11 (W3)	STD-1	0.33	3.03	83.86	-0.06	0.09	0.01	0.00	0.24	2.28	0.65	-2.41	1.78	4.78	39.62	0.00	0.41	0.69	1.30
Naibor Soit Kubwa 13 (R3)	STD-1	0.34	3.30	93.06	-0.01	0.10	0.02	0.00	0.26	2.63	0.74	-2.66	3.56	2.61	19.86	0.00	27.29	0.14	1.02
Naibor Soit Kubwa 14A (W2)	STD-3	0.29	3.31	96.26	0.01	0.10	0.02	0.00	0.23	1.72	0.38	-0.66	12.69	4.89	23.25	0.25	10.58	1.18	0.56
Naibor Soit Kubwa 2 (W3)	STD-3	0.32	3.17	103.52	0.01	0.11	0.02	0.00	0.26	2.20	0.16	-0.18	5.30	2.25	19.48	0.46	49.35	0.62	1.53
Naibor Soit Kubwa 24A (W2)	STD-3	0.30	2.81	102.57	-0.08	0.11	0.01	0.00	0.24	4.72	0.26	-3.29	5.97	2.26	30.84	0.00	23.89	0.00	5.23
Naibor Soit Kubwa 27 (R3)	STD-1	0.44	4.75	98.08	0.29	0.11	0.03	0.00	0.30	4.01	0.78	9.78	8.87	5.74	45.70	0.10	101.52	1.46	1.20
Naibor Soit Kubwa 31A (G1)	STD-3	0.33	3.25	103.34	0.02	0.09	0.03	0.00	0.26	3.18	0.17	-0.74	2.04	2.27	26.85	0.00	14.62	0.41	0.92
Naibor Soit Kubwa 33A (GR1)	STD-3	0.32	2.95	85.54	-0.05	0.09	0.01	0.00	0.24	3.27	0.37	-2.93	0.80	4.15	15.12	0.00	31.78	0.00	0.86
Naisiusiu 1 (R6)	STD-2	0.42	4.59	97.50	0.12	0.16	0.06	0.00	0.54	7.37	3.98	3.09	34.78	14.91	58.39	0.00	146.27	3.55	3.18
Naisiusiu 1 (R6)	STD-1	0.45	5.24	94.41	0.28	0.22	0.12	0.01	0.71	6.70	5.52	7.79	59.35	20.32	76.91	0.52	257.12	5.79	2.50

	STD *	weight (%)								ppm									
		MgO	Al_2O_3	SiO_2 **	K_2O	CaO	TiO_2	MnO	Fe_2O_3	Cu	Zn	Rb	Sr	Y	Zr	Nb	Ba	Pb	Th
Naisiusiu 13 (R5)	STD-2	0.35	2.80	102.99	-0.08	0.09	0.00	0.00	0.27	4.25	1.84	-4.07	0.00	1.07	0.00	0.53	35.40	0.96	0.10
Naisiusiu 13 (R5)	STD-1	0.30	2.79	104.20	-0.07	0.09	0.00	0.00	0.30	3.40	1.20	-4.07	0.70	0.34	0.00	0.00	0.00	0.44	0.00
Naisiusiu 14 (W4)	STD-2	0.43	3.34	101.67	0.03	0.12	0.03	0.00	0.25	3.76	5.18	-1.14	2.68	0.25	28.09	0.00	25.70	2.27	1.31
Naisiusiu 14 (W4)	STD-1	0.45	4.55	88.37	0.39	0.35	0.05	0.00	0.28	3.26	3.63	3.80	8.83	11.83	92.90	2.04	20.55	3.66	2.99
Naisiusiu 4 (GR2)	STD-2	0.37	3.51	100.17	-0.02	0.17	0.01	0.00	0.37	4.74	3.15	2.10	30.81	7.67	37.89	0.45	0.10	0.77	1.94
Naisiusiu 4 (GR2)	STD-1	0.35	3.39	84.72	-0.04	0.21	0.02	0.00	0.34	6.00	6.01	-0.17	23.77	6.01	29.85	0.00	25.81	1.10	0.96
Naisiusiu 6 (W3)	STD-2	0.37	5.00	95.35	0.44	0.11	0.06	0.00	0.27	3.17	3.76	10.75	6.46	8.56	27.16	2.17	32.84	1.51	1.12
Naisiusiu 6 (W3)	STD-1	0.37	4.56	97.17	0.32	0.10	0.04	0.00	0.27	3.67	3.92	8.47	5.15	6.34	23.01	0.61	26.74	1.51	2.50
Naisiusiu 7 (GR1)	STD-2	0.41	3.44	101.46	-0.06	0.26	0.03	0.01	0.56	3.73	4.44	-2.23	13.65	4.93	29.97	0.60	20.10	1.68	2.49
Naisiusiu 7 (GR1)	STD-1	0.36	3.65	89.50	-0.02	0.36	0.02	0.00	0.35	3.68	4.27	-0.40	19.35	8.17	37.76	0.37	34.22	1.33	2.69
Naisiusiu 9 (W4)	STD-2	0.31	3.06	100.80	0.00	0.09	0.02	0.00	0.25	3.62	1.75	2.58	5.58	0.79	21.45	0.00	52.25	2.13	0.00
Naisiusiu 9 (W4)	STD-1	0.38	3.55	102.93	0.11	0.09	0.03	0.00	0.26	3.69	3.19	3.32	6.40	0.00	27.99	0.63	38.63	1.62	0.27
Oittii 1 (GR2)	STD-3	0.46	3.19	97.01	0.01	0.59	0.04	0.02	0.37	2.93	1.13	-0.38	5.03	1.33	22.09	0.89	348.72	2.22	0.59
Oittii 2 (GR2)	STD-3	0.53	3.18	101.81	-0.01	0.35	0.04	0.01	0.33	12.31	2.07	-1.33	6.36	1.53	31.61	0.05	629.33	2.82	0.80
Oittii 3 (W4)	STD-3	0.43	5.20	92.79	0.91	0.11	0.05	0.00	0.29	3.06	2.11	45.01	19.95	1.81	53.87	1.26	371.14	2.99	2.67
Oittii 4 (GR2)	STD-3	0.39	4.27	98.73	0.66	0.10	0.04	0.00	0.33	5.60	2.06	22.69	24.32	1.11	38.54	0.76	226.44	2.89	0.79
Oittii 5 (GR2)	STD-3	0.50	6.34	94.14	1.23	0.10	0.09	0.00	0.85	4.15	4.21	62.80	41.83	2.62	43.48	2.38	319.30	3.04	3.89
RGM-2 (STD-1)		0.27	13.36	74.07	3.36	0.95	0.30	0.04	1.84	11.11	30.19	145.99	106.20	23.20	225.48	7.59	845.13	19.95	14.40
RGM-2 (STD-2)		0.25	13.41	74.36	3.38	0.95	0.29	0.04	1.83	11.66	32.60	144.37	103.70	23.82	224.91	9.65	830.69	20.42	13.93
RGM-2 (STD-3)		0.25	13.46	74.60	3.38	0.95	0.29	0.04	1.85	10.09	29.44	145.21	107.01	25.53	227.65	8.46	837.81	19.50	13.91
RGM-2 (STD RV)		0.28 ± 0.02	14 ± 0.02	73.4 ± 0.41	4.35 ± 0.16	1.23 ± 0.16	0.25 ± 0.02		1.86 ± 0.04	9.8 ± 0.8	33 ± 2	147 ± 5	108 ± 5	24 ± 2	222 ± 17	9.0	842 ± 35	20 ± 1	15 ± 1

Table 3. Raw EDXRF data per sample (major oxides: weight %; trace elements: ppm) (RV: Recommended Value) (STD-1-2-3: Standard 1-2-3).

* Sample data normalized according to which RGM-2 STD values.

** Some SiO_2 values are off the upper end of the calibration standard.

Negative values are below detection limits.

	SiO_2	TiO_2	Al_2O_3	Fe_2O_3	MnO	MgO	CaO	K_2O	Cu	Zn	Rb	Sr	Y	Zr	Nb	Ba	Pb	Th
Endonyo Osunyai 2 (W3)	1.000	0.019	0.066	0.003	0.005	0.016	0.001	0.044	0.030	0.010	0.028	0.015	0.032	0.069	0.000	0.022	0.071	0.099
Endonyo Osunyai 3 (R3)	0.464	0.015	0.115	0.003	0.000	0.017	0.002	0.181	0.028	0.004	0.157	0.096	0.001	0.011	0.004	0.365	0.235	0.029
Endonyo Osunyai 4 (GR2)	0.160	0.099	0.376	0.058	0.016	0.060	0.003	0.544	0.100	0.031	0.634	0.270	0.038	0.121	0.078	0.759	0.579	0.776
Endonyo Osunyai 5 (GR2)	0.331	0.140	0.483	0.091	0.021	0.072	0.225	0.507	0.056	0.020	0.607	0.085	0.020	0.044	0.102	0.600	0.123	0.104
Naibor Soit Ndogo 13 (W2)	0.715	0.027	0.042	0.003	0.000	0.658	0.000	0.027	0.066	0.006	0.016	0.002	0.535	0.031	0.000	0.058	0.028	0.056
Naibor Soit Ndogo 13 (W2)	0.987	0.018	0.000	0.002	0.012	0.464	0.005	0.001	0.066	0.000	0.002	0.001	0.138	0.024	0.000	0.030	0.014	0.056
Naibor Soit Ndogo 14 (W3)	0.791	0.014	0.010	0.000	0.041	0.613	0.003	0.004	0.030	0.000	0.005	0.001	0.075	0.015	0.000	0.038	0.013	0.068
Naibor Soit Ndogo 14 (W3)	0.881	0.036	0.023	0.000	0.006	0.658	0.000	0.015	0.078	0.000	0.011	0.001	0.147	0.036	0.000	0.038	0.000	0.030
Naibor Soit Ndogo 15 (W3)	1.000	0.043	0.039	0.001	0.000	0.636	0.002	0.024	0.165	0.002	0.012	0.002	0.138	0.034	0.003	0.018	0.000	0.021
Naibor Soit Ndogo 15 (W3)	0.959	0.019	0.019	0.000	0.000	0.594	0.002	0.011	0.119	0.003	0.007	0.002	0.075	0.028	0.002	0.010	0.030	0.063
Naibor Soit Ndogo 6 (W3)	0.000	0.022	0.031	0.000	0.102	0.924	0.000	0.011	0.043	0.002	0.006	0.000	0.099	0.029	0.000	0.180	0.015	0.053
Naibor Soit Ndogo 6 (W3)	1.000	0.013	0.016	0.001	0.006	0.624	0.002	0.008	0.077	0.000	0.004	0.002	0.111	0.032	0.000	0.111	0.022	0.014
Naibor Soit Ndogo 8 (W3)	0.979	0.019	0.023	0.001	0.000	0.573	0.013	0.016	0.097	0.003	0.005	0.005	0.113	0.035	0.000	0.039	0.023	0.023
Naibor Soit Ndogo 8 (W3)	0.910	0.022	0.052	0.001	0.006	0.648	0.002	0.033	0.128	0.004	0.019	0.002	0.102	0.029	0.000	0.065	0.020	0.005
Naibor Soit Kubwa 1 (R3)	0.748	0.005	0.024	0.001	0.000	0.005	0.001	0.023	0.029	0.003	0.026	0.016	0.027	0.026	0.010	0.018	0.044	0.165
Naibor Soit Kubwa 1 (R3)	0.408	0.000	0.000	0.000	0.000	0.369	0.000	0.000	0.000	0.000	0.002	0.000	0.105	0.096	0.000	0.000	0.028	0.021
Naibor Soit Kubwa 13 (R3)	0.791	0.035	0.027	0.011	0.023	0.417	0.013	0.014	0.039	0.003	0.000	0.017	0.000	0.000	0.000	0.032	0.000	0.000
Naibor Soit Kubwa 14 (W2)	0.710	0.009	0.047	0.000	0.005	0.007	0.001	0.026	0.017	0.001	0.023	0.036	0.048	0.012	0.005	0.008	0.061	0.040
Naibor Soit Kubwa 2 (W3)	0.949	0.006	0.034	0.002	0.000	0.011	0.002	0.025	0.021	0.000	0.026	0.014	0.019	0.006	0.010	0.054	0.032	0.110
Naibor Soit Kubwa 24 (W2)	0.917	0.003	0.000	0.001	0.000	0.008	0.002	0.000	0.045	0.001	0.005	0.016	0.019	0.023	0.000	0.023	0.000	0.376
Naibor Soit Kubwa 27 (R3)	1.000	0.080	0.167	0.040	0.023	1.000	0.002	0.102	0.196	0.004	0.084	0.068	0.152	0.126	0.013	0.120	0.067	0.014
Naibor Soit Kubwa 31 (G1)	0.943	0.016	0.041	0.003	0.000	0.012	0.000	0.027	0.031	0.000	0.022	0.004	0.019	0.017	0.000	0.012	0.021	0.066
Naibor Soit Kubwa 33 (GR1)	0.359	0.000	0.013	0.001	0.000	0.011	0.000	0.008	0.031	0.001	0.008	0.000	0.040	0.000	0.000	0.033	0.000	0.062
Naisiusiu 1 (R5)	0.887	0.182	0.167	0.057	0.041	0.983	0.031	0.069	0.332	0.023	0.040	0.049	0.977	0.113	0.002	0.236	0.239	0.079

	SiO_2	TiO_2	Al_2O_3	Fe_2O_3	MnO	MgO	CaO	K_2O	Cu	Zn	Rb	Sr	Y	Zr	Nb	Ba	Pb	Th
Naisiusiu 1 (R5)	0.857	0.077	0.122	0.033	0.000	0.964	0.025	0.039	0.449	0.015	0.026	0.030	0.622	0.087	0.000	0.110	0.144	0.099
Naisiusiu 13 (GR1)	0.998	0.000	0.000	0.007	0.007	0.579	0.001	0.000	0.100	0.001	0.000	0.000	0.016	0.000	0.000	0.000	0.018	0.000
Naisiusiu 13 (GR1)	0.964	0.000	0.002	0.003	0.006	0.779	0.001	0.000	0.193	0.004	0.000	0.000	0.034	0.000	0.002	0.026	0.039	0.003
Naisiusiu 14 (W3)	0.819	0.076	0.120	0.006	0.014	1.000	0.063	0.090	0.091	0.013	0.027	0.007	0.569	0.136	0.008	0.019	0.151	0.095
Naisiusiu 14 (W3)	0.938	0.034	0.039	0.001	0.000	1.000	0.011	0.021	0.152	0.021	0.011	0.002	0.000	0.042	0.000	0.019	0.092	0.041
Naisiusiu 4 (GR2)	0.778	0.025	0.041	0.013	0.007	0.701	0.029	0.007	0.282	0.026	0.013	0.019	0.289	0.044	0.000	0.024	0.045	0.031
Naisiusiu 4 (GR2)	0.909	0.012	0.050	0.014	0.006	0.821	0.029	0.012	0.233	0.011	0.023	0.027	0.315	0.056	0.002	0.000	0.031	0.060
Naisiusiu 6 (W3)	0.919	0.056	0.121	0.004	0.014	0.757	0.003	0.076	0.119	0.015	0.042	0.004	0.305	0.034	0.002	0.025	0.062	0.079
Naisiusiu 6 (W3)	0.816	0.088	0.149	0.003	0.019	0.812	0.006	0.100	0.103	0.014	0.054	0.006	0.352	0.040	0.008	0.025	0.061	0.035
Naisiusiu 7 (GR1)	0.832	0.029	0.059	0.014	0.027	0.751	0.065	0.009	0.120	0.017	0.012	0.016	0.393	0.055	0.001	0.031	0.055	0.085
Naisiusiu 7 (GR1)	0.934	0.036	0.045	0.035	0.037	0.948	0.062	0.004	0.150	0.018	0.007	0.012	0.198	0.045	0.002	0.015	0.068	0.078
Naisiusiu 9 (W4)	0.984	0.046	0.052	0.003	0.007	0.811	0.001	0.035	0.120	0.011	0.025	0.005	0.000	0.041	0.002	0.035	0.067	0.008
Naisiusiu 9 (W4)	0.921	0.018	0.020	0.001	0.006	0.630	0.000	0.015	0.141	0.004	0.024	0.005	0.023	0.032	0.000	0.039	0.086	0.000
Oittii 1 (GR2)	0.735	0.029	0.036	0.013	0.091	0.033	0.044	0.026	0.028	0.006	0.025	0.013	0.009	0.010	0.019	0.413	0.114	0.042
Oittii 2 (GR2)	0.893	0.027	0.034	0.009	0.070	0.043	0.023	0.021	0.118	0.011	0.018	0.017	0.011	0.024	0.001	0.750	0.144	0.058
Oittii 3 (W4)	0.597	0.036	0.224	0.005	0.005	0.029	0.001	0.284	0.029	0.011	0.329	0.059	0.014	0.056	0.026	0.440	0.153	0.192
Oittii 4 (GR2)	0.791	0.031	0.138	0.009	0.021	0.022	0.001	0.214	0.054	0.011	0.179	0.072	0.006	0.034	0.016	0.266	0.148	0.057
Oittii 5 (GR2)	0.641	0.075	0.331	0.060	0.000	0.039	0.001	0.378	0.040	0.023	0.448	0.125	0.023	0.041	0.050	0.378	0.156	0.280

Table 4. Normalized EDXRF data per sample and RMG.

All Outcrops																		
τ / p (uncorr.)	**SiO2**	**TiO2**	**Al2O3**	**Fe2O3**	**MnO**	**MgO**	**CaO**	**K2O**	**Cu**	**Zn**	**Rb**	**Sr**	**Y**	**Zr**	**Nb**	**Ba**	**Pb**	**Th**
SiO2		0.482	0.044	0.486	0.468	0.113	0.917	0.060	0.005	0.146	0.029	0.017	0.734	0.767	0.055	0.026	0.079	0.045
TiO2	-0.075		0.000	0.000	0.008	0.001	0.002	0.000	0.009	0.000	0.000	0.002	0.082	0.000	0.003	0.004	0.001	0.184
Al2O3	-0.216	0.597		0.000	0.156	0.101	0.035	0.000	0.278	0.000	0.000	0.000	0.273	0.000	0.000	0.003	0.000	0.008
Fe2O3	-0.075	0.426	0.514		0.002	0.092	0.000	0.001	0.025	0.000	0.000	0.000	0.758	0.008	0.001	0.018	0.000	0.049
MnO	-0.078	0.286	0.152	0.336		0.017	0.001	0.805	0.223	0.039	0.638	0.432	0.393	0.378	0.208	0.039	0.200	0.543
MgO	0.170	0.357	0.176	0.181	0.257		0.021	0.904	0.000	0.008	0.921	0.386	0.000	0.000	0.656	0.654	0.381	0.149
CaO	0.011	0.326	0.226	0.413	0.340	0.247		0.620	0.011	0.000	0.453	0.008	0.052	0.035	0.115	0.512	0.038	0.102
K2O	-0.201	0.507	0.760	0.349	0.026	0.013	0.053		0.742	0.000	0.000	0.000	0.767	0.006	0.000	0.000	0.000	0.032
Cu	0.303	0.282	0.116	0.241	0.130	0.585	0.273	-0.035		0.001	0.930	0.903	0.002	0.002	0.603	0.670	0.410	0.182
Zn	-0.156	0.522	0.554	0.580	0.221	0.283	0.384	0.388	0.355		0.000	0.000	0.404	0.000	0.003	0.051	0.000	0.027
Rb	-0.234	0.415	0.719	0.374	0.050	-0.011	0.080	0.798	-0.009	0.417		0.000	0.991	0.003	0.000	0.001	0.000	0.002
Sr	-0.256	0.329	0.570	0.533	0.084	-0.093	0.285	0.503	0.013	0.425	0.593		0.624	0.007	0.000	0.005	0.000	0.002
Y	0.036	0.186	0.118	0.033	0.092	0.437	0.209	-0.032	0.326	0.089	0.001	-0.052		0.000	0.407	0.314	0.583	0.381
Zr	-0.032	0.487	0.453	0.286	0.094	0.380	0.225	0.293	0.325	0.426	0.314	0.288	0.373		0.142	0.660	0.001	0.057
Nb	-0.206	0.323	0.503	0.372	0.135	-0.048	0.169	0.523	-0.056	0.323	0.588	0.496	-0.089	0.157		0.028	0.000	0.006
Ba	-0.239	0.306	0.315	0.254	0.221	-0.048	0.070	0.408	-0.046	0.209	0.351	0.300	-0.108	0.047	0.235		0.005	0.260
Pb	-0.188	0.363	0.541	0.439	0.137	0.094	0.223	0.498	0.088	0.554	0.572	0.528	-0.059	0.365	0.481	0.302		0.013
Th	-0.215	0.143	0.286	0.211	-0.065	-0.154	0.175	0.230	-0.143	0.237	0.340	0.330	0.094	0.204	0.297	0.121	0.267	

Table 5. Correlations [τ / p (uncorr.] for EDXRF data for all samples based on Kendall's Tau coefficient.

All Outcrops																		
p Permutations	**SiO2**	**TiO2**	**Al2O3**	**Fe2O3**	**MnO**	**MgO**	**CaO**	**K2O**	**Cu**	**Zn**	**Rb**	**Sr**	**Y**	**Zr**	**Nb**	**Ba**	**Pb**	**Th**
SiO2		0.494	0.046	0.508	0.494	0.121	0.928	0.063	0.005	0.162	0.028	0.019	0.738	0.775	0.082	0.026	0.085	0.044
TiO2	0.494		0.000	0.000	0.011	0.001	0.004	0.000	0.009	0.000	0.000	0.002	0.090	0.000	0.007	0.004	0.001	0.195
Al2O3	0.046	0.000		0.000	0.184	0.107	0.044	0.000	0.290	0.000	0.000	0.000	0.292	0.000	0.000	0.003	0.000	0.008
Fe2O3	0.508	0.000	0.000		0.004	0.111	0.000	0.003	0.027	0.000	0.001	0.000	0.776	0.008	0.002	0.023	0.000	0.057
MnO	0.494	0.011	0.184	0.004		0.024	0.002	0.819	0.257	0.057	0.662	0.472	0.423	0.407	0.277	0.051	0.228	0.565
MgO	0.121	0.001	0.107	0.111	0.024		0.027	0.914	0.000	0.010	0.931	0.406	0.000	0.001	0.691	0.660	0.394	0.153
CaO	0.928	0.004	0.044	0.000	0.002	0.027		0.641	0.014	0.001	0.489	0.012	0.062	0.045	0.158	0.540	0.051	0.123
K2O	0.063	0.000	0.000	0.003	0.819	0.914	0.641		0.757	0.001	0.000	0.000	0.780	0.007	0.000	0.000	0.000	0.034
Cu	0.005	0.009	0.290	0.027	0.257	0.000	0.014	0.757		0.001	0.940	0.909	0.002	0.002	0.649	0.680	0.426	0.186
Zn	0.162	0.000	0.000	0.000	0.057	0.010	0.001	0.001	0.001		0.000	0.000	0.418	0.000	0.006	0.058	0.000	0.033
Rb	0.028	0.000	0.000	0.001	0.662	0.931	0.489	0.000	0.940	0.000		0.000	0.999	0.003	0.000	0.001	0.000	0.001
Sr	0.019	0.002	0.000	0.000	0.472	0.406	0.012	0.000	0.909	0.000	0.000		0.642	0.008	0.000	0.006	0.000	0.002
Y	0.738	0.090	0.292	0.776	0.423	0.000	0.062	0.780	0.002	0.418	0.999	0.642		0.000	0.452	0.333	0.597	0.397
Zr	0.775	0.000	0.000	0.008	0.407	0.001	0.045	0.007	0.002	0.000	0.003	0.008	0.000		0.181	0.663	0.001	0.062
Nb	0.082	0.007	0.000	0.002	0.277	0.691	0.158	0.000	0.649	0.006	0.000	0.000	0.452	0.181		0.046	0.000	0.011
Ba	0.026	0.004	0.003	0.023	0.051	0.660	0.540	0.000	0.680	0.058	0.001	0.006	0.333	0.663	0.046		0.005	0.276
Pb	0.085	0.001	0.000	0.000	0.228	0.394	0.051	0.000	0.426	0.000	0.000	0.000	0.597	0.001	0.000	0.005		0.013
Th	0.044	0.195	0.008	0.057	0.565	0.153	0.123	0.034	0.186	0.033	0.001	0.002	0.397	0.062	0.011	0.276	0.013	

Table 6. Correlations [p (uncorr.] for EDXRF data for all samples based on Kendall's Tau Monte Carlo simulations.

Endonyo Osunyai																		
τ / p (uncorr.)	**SiO2**	**TiO2**	**Al2O3**	**Fe2O3**	**MnO**	**MgO**	**CaO**	**K2O**	**Cu**	**Zn**	**Rb**	**Sr**	**Y**	**Zr**	**Nb**	**Ba**	**Pb**	**Th**
SiO2		0.497	0.174	0.264	0.497	0.174	0.174	0.042	0.174	0.174	0.042	0.174	0.497	0.497	0.174	0.042	0.174	0.174
TiO2	-0.333		0.174	0.063	0.042	0.174	0.174	0.497	0.174	0.174	0.497	1.000	0.497	0.497	0.174	0.497	1.000	0.174
Al2O3	-0.667	0.667		0.063	0.174	0.042	0.042	0.174	0.497	0.497	0.174	0.497	1.000	1.000	0.042	0.174	0.497	0.497
Fe2O3	-0.548	0.913	0.913		0.063	0.063	0.063	0.264	0.264	0.264	0.264	0.710	0.710	0.710	0.063	0.264	0.710	0.264
MnO	-0.333	1.000	0.667	0.913		0.174	0.174	0.497	0.174	0.174	0.497	1.000	0.497	0.497	0.174	0.497	1.000	0.174
MgO	-0.667	0.667	1.000	0.913	0.667		0.042	0.174	0.497	0.497	0.174	0.497	1.000	1.000	0.042	0.174	0.497	0.497
CaO	-0.667	0.667	1.000	0.913	0.667	1.000		0.174	0.497	0.497	0.174	0.497	1.000	1.000	0.042	0.174	0.497	0.497
K2O	-1.000	0.333	0.667	0.548	0.333	0.667	0.667		0.174	0.174	0.042	0.174	0.497	0.497	0.174	0.042	0.174	0.174
Cu	-0.667	0.667	0.333	0.548	0.667	0.333	0.333	0.667		0.042	0.174	0.497	0.174	0.174	0.497	0.174	0.497	0.042
Zn	-0.667	0.667	0.333	0.548	0.667	0.333	0.333	0.667	1.000		0.174	0.497	0.174	0.174	0.497	0.174	0.497	0.042
Rb	-1.000	0.333	0.667	0.548	0.333	0.667	0.667	1.000	0.667	0.667		0.174	0.497	0.497	0.174	0.042	0.174	0.174
Sr	-0.667	0.000	0.333	0.183	0.000	0.333	0.333	0.667	0.333	0.333	0.667		1.000	1.000	0.497	0.174	0.042	0.497
Y	-0.333	0.333	0.000	0.183	0.333	0.000	0.000	0.333	0.667	0.667	0.333	0.000		0.042	1.000	0.497	1.000	0.174
Zr	-0.333	0.333	0.000	0.183	0.333	0.000	0.000	0.333	0.667	0.667	0.333	0.000	1.000		1.000	0.497	1.000	0.174
Nb	-0.667	0.667	1.000	0.913	0.667	1.000	1.000	0.667	0.333	0.333	0.667	0.333	0.000	0.000		0.174	0.497	0.497
Ba	-1.000	0.333	0.667	0.548	0.333	0.667	0.667	1.000	0.667	0.667	1.000	0.667	0.333	0.333	0.667		0.174	0.174
Pb	-0.667	0.000	0.333	0.183	0.000	0.333	0.333	0.667	0.333	0.333	0.667	1.000	0.000	0.000	0.333	0.667		0.497
Th	-0.667	0.667	0.333	0.548	0.667	0.333	0.333	0.667	1.000	1.000	0.667	0.333	0.667	0.667	0.333	0.667	0.333	

Table 7. Correlations [τ / p (uncorr.] for EDXRF data for Endonyo Osunyai based on Kendall's Tau coefficient.

Endonyo Osunyai																		
p Permutations	**SiO2**	**TiO2**	**Al2O3**	**Fe2O3**	**MnO**	**MgO**	**CaO**	**K2O**	**Cu**	**Zn**	**Rb**	**Sr**	**Y**	**Zr**	**Nb**	**Ba**	**Pb**	**Th**
SiO2		0.747	0.332	0.494	0.739	0.326	0.329	0.087	0.338	0.338	0.083	0.338	0.751	0.749	0.333	0.086	0.334	0.336
TiO2	0.747		0.344	0.170	0.077	0.332	0.324	0.752	0.330	0.338	0.747	1.000	0.753	0.750	0.335	0.747	1.000	0.331
Al2O3	0.332	0.344		0.166	0.331	0.081	0.081	0.332	0.747	0.756	0.334	0.759	1.000	1.000	0.085	0.338	0.745	0.747
Fe2O3	0.494	0.170	0.166		0.170	0.160	0.168	0.501	0.502	0.499	0.507	1.000	1.000	1.000	0.172	0.509	1.000	0.486
MnO	0.739	0.077	0.331	0.170		0.329	0.336	0.750	0.340	0.342	0.750	1.000	0.752	0.747	0.341	0.750	1.000	0.336
MgO	0.326	0.332	0.081	0.160	0.329		0.085	0.335	0.748	0.743	0.337	0.757	1.000	1.000	0.083	0.336	0.740	0.752
CaO	0.329	0.324	0.081	0.168	0.336	0.085		0.331	0.747	0.751	0.326	0.753	1.000	1.000	0.084	0.330	0.754	0.751
K2O	0.087	0.752	0.332	0.501	0.750	0.335	0.331		0.332	0.326	0.085	0.332	0.749	0.753	0.334	0.084	0.345	0.338
Cu	0.338	0.330	0.747	0.502	0.340	0.748	0.747	0.332		0.083	0.338	0.744	0.336	0.335	0.736	0.325	0.754	0.081
Zn	0.338	0.338	0.756	0.499	0.342	0.743	0.751	0.326	0.083		0.328	0.758	0.323	0.334	0.744	0.337	0.741	0.081
Rb	0.083	0.747	0.334	0.507	0.750	0.337	0.326	0.085	0.338	0.328		0.338	0.751	0.749	0.340	0.086	0.332	0.323
Sr	0.338	1.000	0.759	1.000	1.000	0.757	0.753	0.332	0.744	0.758	0.338		1.000	1.000	0.754	0.330	0.084	0.753
Y	0.751	0.753	1.000	1.000	0.752	1.000	1.000	0.749	0.336	0.323	0.751	1.000		0.085	1.000	0.748	1.000	0.336
Zr	0.749	0.750	1.000	1.000	0.747	1.000	1.000	0.753	0.335	0.334	0.749	1.000	0.085		1.000	0.754	1.000	0.346
Nb	0.333	0.335	0.085	0.172	0.341	0.083	0.084	0.334	0.736	0.744	0.340	0.754	1.000	1.000		0.325	0.752	0.753
Ba	0.086	0.747	0.338	0.509	0.750	0.336	0.330	0.084	0.325	0.337	0.086	0.330	0.748	0.754	0.325		0.326	0.332
Pb	0.334	1.000	0.745	1.000	1.000	0.740	0.754	0.345	0.754	0.741	0.332	0.084	1.000	1.000	0.752	0.326		0.749
Th	0.336	0.331	0.747	0.486	0.336	0.752	0.751	0.338	0.081	0.081	0.323	0.753	0.336	0.346	0.753	0.332	0.749	

Table 8. Correlations [p (uncorr.)] for EDXRF data for samples from Endonyo Osunyai based on Kendall's Tau Monte Carlo simulations.

Naibor Soit Kubwa																		
τ / p (uncorr.)	**SiO2**	**TiO2**	**Al2O3**	**Fe2O3**	**MnO**	**MgO**	**CaO**	**K2O**	**Cu**	**Zn**	**Rb**	**Sr**	**Y**	**Zr**	**Nb**	**Ba**	**Pb**	**Th**
SiO2		0.045	0.113	0.027	0.401	0.341	0.081	0.113	0.113	0.727	0.113	0.283	0.446	0.597	0.104	0.095	0.327	0.835
TiO2	0.535		0.010	0.010	0.011	0.198	0.126	0.010	0.198	0.157	0.391	0.030	0.508	1.000	0.253	0.341	0.269	0.169
Al2O3	0.423	0.686		0.093	0.047	0.520	0.480	0.001	0.830	0.346	0.054	0.064	0.659	0.830	0.057	0.459	0.047	0.245
Fe2O3	0.589	0.687	0.448		0.182	0.033	0.109	0.093	0.019	0.218	0.432	0.306	0.133	0.737	0.426	0.027	0.817	0.507
MnO	0.224	0.680	0.529	0.356		0.156	0.043	0.156	0.256	0.019	0.777	0.010	0.559	0.887	0.314	0.401	0.243	0.012
MgO	0.254	0.343	0.171	0.568	0.378		0.637	0.520	0.284	1.000	0.391	0.913	0.825	0.830	0.612	0.341	0.825	0.026
CaO	0.464	0.408	0.188	0.427	0.540	0.126		0.814	0.195	0.092	0.637	0.031	0.182	0.637	0.210	0.081	0.808	0.727
K2O	0.423	0.686	0.886	0.448	0.378	0.171	0.063		0.830	0.480	0.054	0.157	0.659	0.520	0.057	0.459	0.047	0.459
Cu	0.423	0.343	0.057	0.628	0.302	0.286	0.345	0.057		0.059	1.000	0.231	0.377	1.000	0.899	0.072	0.377	0.916
Zn	0.093	0.377	0.251	0.328	0.623	0.000	0.448	0.188	0.502		0.480	0.023	0.716	0.637	0.163	0.201	0.544	0.416
Rb	0.423	0.229	0.514	0.209	0.076	-0.229	0.126	0.514	0.000	0.188		0.231	0.269	0.391	0.002	0.245	0.015	0.459
Sr	0.286	0.580	0.493	0.273	0.690	-0.029	0.573	0.377	0.319	0.605	0.319		0.911	0.586	0.071	0.391	0.093	0.830
Y	-0.203	-0.177	0.118	-0.400	0.156	0.059	-0.356	0.118	-0.235	0.097	0.294	0.030		0.047	0.240	0.586	0.041	0.157
Zr	0.141	0.000	0.057	-0.090	-0.038	0.057	-0.126	0.171	0.000	0.126	0.229	0.145	0.530		0.253	0.597	0.098	0.916
Nb	0.433	0.304	0.507	0.212	0.268	-0.135	0.334	0.507	0.034	0.371	0.845	0.480	0.313	0.304		0.169	0.006	0.900
Ba	0.444	0.254	0.197	0.589	0.224	0.254	0.464	0.197	0.479	0.340	0.310	0.229	-0.145	-0.141	0.367		0.913	0.835
Pb	0.261	0.294	0.530	-0.062	0.311	-0.059	0.065	0.530	-0.235	0.162	0.647	0.448	0.545	0.441	0.731	-0.029		0.744
Th	0.056	-0.366	-0.310	-0.177	-0.671	-0.592	-0.093	-0.197	0.028	-0.217	0.197	-0.057	-0.377	0.028	0.033	0.056	-0.087	

Table 9 . Correlations [τ / p (uncorr.] for EDXRF data for Naibor Soit Kubwa based on Kendall's Tau coefficient.

Naibor Soit Kubwa																		
p Permutations	**SiO2**	**TiO2**	**Al2O3**	**Fe2O3**	**MnO**	**MgO**	**CaO**	**K2O**	**Cu**	**Zn**	**Rb**	**Sr**	**Y**	**Zr**	**Nb**	**Ba**	**Pb**	**Th**
SiO2		0.055	0.152	0.040	0.538	0.411	0.130	0.149	0.148	0.835	0.143	0.352	0.533	0.688	0.168	0.120	0.418	0.919
TiO2	0.055		0.012	0.013	0.020	0.252	0.154	0.013	0.255	0.229	0.472	0.030	0.602	1.000	0.332	0.408	0.339	0.217
Al2O3	0.152	0.012		0.137	0.084	0.601	0.581	0.000	0.916	0.451	0.068	0.087	0.756	0.912	0.093	0.533	0.065	0.300
Fe2O3	0.040	0.013	0.137		0.291	0.051	0.165	0.133	0.024	0.297	0.518	0.352	0.186	0.825	0.535	0.041	0.860	0.602
MnO	0.538	0.020	0.084	0.291		0.237	0.099	0.238	0.364	0.049	0.839	0.015	0.704	0.967	0.378	0.545	0.367	0.025
MgO	0.411	0.252	0.601	0.051	0.237		0.735	0.601	0.357	1.000	0.473	0.995	0.910	0.914	0.717	0.406	0.913	0.031
CaO	0.130	0.154	0.581	0.165	0.099	0.735		0.904	0.244	0.166	0.739	0.051	0.259	0.734	0.321	0.130	0.883	0.836
K2O	0.149	0.013	0.000	0.133	0.238	0.601	0.904		0.918	0.578	0.071	0.206	0.756	0.613	0.091	0.543	0.067	0.539
Cu	0.148	0.255	0.916	0.024	0.364	0.357	0.244	0.918		0.099	1.000	0.296	0.460	1.000	0.940	0.089	0.463	1.000
Zn	0.835	0.229	0.451	0.297	0.049	1.000	0.166	0.578	0.099		0.578	0.040	0.796	0.745	0.255	0.287	0.622	0.528
Rb	0.143	0.472	0.068	0.518	0.839	0.473	0.739	0.071	1.000	0.578		0.292	0.341	0.470	0.001	0.305	0.021	0.539
Sr	0.352	0.030	0.087	0.352	0.015	0.995	0.051	0.206	0.296	0.040	0.292		0.989	0.679	0.114	0.468	0.125	0.920
Y	0.533	0.602	0.756	0.186	0.704	0.910	0.259	0.756	0.460	0.796	0.341	0.989		0.065	0.346	0.680	0.057	0.207
Zr	0.688	1.000	0.912	0.825	0.967	0.914	0.734	0.613	1.000	0.745	0.470	0.679	0.065		0.318	0.680	0.113	1.000
Nb	0.168	0.332	0.093	0.535	0.378	0.717	0.321	0.091	0.940	0.255	0.001	0.114	0.346	0.318		0.251	0.010	1.000
Ba	0.120	0.408	0.533	0.041	0.545	0.406	0.130	0.543	0.089	0.287	0.305	0.468	0.680	0.680	0.251		1.000	0.918
Pb	0.418	0.339	0.065	0.860	0.367	0.913	0.883	0.067	0.463	0.622	0.021	0.125	0.057	0.113	0.010	1.000		0.838
Th	0.919	0.217	0.300	0.602	0.025	0.031	0.836	0.539	1.000	0.528	0.539	0.920	0.207	1.000	1.000	0.918	0.838	

Table 10. Correlations [p (uncorr.)] for EDXRF data for samples from Naibor Soit Kubwa based on Kendall's Tau Monte Carlo simulations.

Naibor Soit Ndogo																		
τ / p (uncorr.)	**SiO2**	**TiO2**	**Al2O3**	**Fe2O3**	**MnO**	**MgO**	**CaO**	**K2O**	**Cu**	**Zn**	**Rb**	**Sr**	**Y**	**Zr**	**Nb**	**Ba**	**Pb**	**Th**
SiO2		0.355	0.410	0.245	0.189	0.035	0.106	0.784	0.120	0.319	0.314	0.086	0.711	0.647	0.141	0.234	0.784	0.170
TiO2	-0.230		0.026	0.915	0.260	0.139	0.102	0.042	0.139	0.158	0.016	1.000	0.160	0.052	0.234	0.579	0.459	0.355
Al2O3	-0.205	0.552		0.526	0.266	0.055	0.086	0.000	0.170	0.017	0.001	0.334	0.355	0.314	0.659	0.234	0.784	0.170
Fe2O3	0.289	0.027	0.157		0.243	0.526	0.484	0.342	0.833	0.249	1.000	0.137	0.019	0.833	0.610	0.751	0.398	0.398
MnO	-0.327	-0.280	-0.276	-0.290		0.613	0.911	0.086	0.020	0.078	0.266	0.001	0.220	0.129	0.051	0.189	0.129	0.613
MgO	-0.523	0.368	0.477	-0.157	0.126		0.001	0.170	0.784	0.425	0.082	0.238	0.579	0.410	0.659	0.120	0.522	0.647
CaO	0.402	-0.407	-0.427	0.174	-0.028	-0.804		0.189	0.762	0.508	0.086	0.286	0.413	0.363	1.000	0.363	0.762	0.919
K2O	-0.068	0.506	0.886	0.236	-0.427	0.341	-0.327		0.055	0.009	0.001	0.108	0.267	0.234	0.556	0.410	0.647	0.082
Cu	0.386	0.368	0.341	0.052	-0.578	-0.068	0.075	0.477		0.231	0.120	0.042	0.711	0.120	0.027	0.314	0.784	0.067
Zn	-0.248	0.351	0.595	0.286	-0.438	0.198	-0.164	0.644	0.297		0.028	0.079	0.920	0.690	0.630	0.765	0.046	0.690
Rb	-0.250	0.598	0.795	0.000	-0.276	0.432	-0.427	0.795	0.386	0.545		0.453	0.579	0.522	0.303	0.784	0.927	0.410
Sr	0.426	0.000	0.240	0.369	-0.796	-0.293	0.265	0.400	0.506	0.436	0.187		0.664	0.163	0.300	0.668	0.108	0.238
Y	0.092	0.349	0.230	0.584	-0.305	0.138	-0.203	0.276	0.092	0.025	0.138	0.108		0.042	0.655	0.853	0.711	0.711
Zr	0.114	0.483	0.250	0.052	-0.377	0.205	-0.226	0.295	0.386	0.099	0.159	0.346	0.506		0.883	0.927	0.927	0.120
Nb	0.366	0.296	0.110	-0.127	-0.485	-0.110	0.000	0.146	0.548	0.120	0.256	0.257	-0.111	0.037		0.027	1.000	0.883
Ba	-0.295	-0.138	0.295	0.079	0.327	0.386	-0.226	0.205	-0.250	0.074	0.068	-0.107	-0.046	0.023	-0.548		0.647	0.234
Pb	-0.068	-0.184	0.068	0.210	-0.377	-0.159	0.075	0.114	0.068	0.496	0.023	0.400	-0.092	-0.023	0.000	0.114		0.647
Th	-0.341	-0.230	-0.341	-0.210	0.126	-0.114	0.025	-0.432	-0.455	-0.099	-0.205	-0.293	-0.092	-0.386	0.037	-0.295	0.114	

Table 11 . Correlations [τ / p (uncorr.] for EDXRF data for Naibor Soit Ndogo based on Kendall's Tau coefficient.

Naibor Soit Ndogo p Permutations	SiO2	TiO2	Al2O3	Fe2O3	MnO	MgO	CaO	K2O	Cu	Zn	Rb	Sr	Y	Zr	Nb	Ba	Pb	Th
SiO2		0.430	0.468	0.317	0.262	0.044	0.138	0.854	0.154	0.403	0.368	0.126	0.788	0.730	0.250	0.289	0.862	0.216
TiO2	0.430		0.036	0.974	0.320	0.175	0.151	0.059	0.184	0.209	0.020	1.000	0.204	0.058	0.405	0.662	0.534	0.418
Al2O3	0.468	0.036		0.626	0.347	0.073	0.130	0.000	0.218	0.025	0.002	0.432	0.429	0.382	0.779	0.287	0.863	0.218
Fe2O3	0.317	0.974	0.626		0.350	0.629	0.595	0.415	0.906	0.350	1.000	0.234	0.034	0.906	0.869	0.798	0.497	0.497
MnO	0.262	0.320	0.347	0.350		0.706	0.945	0.130	0.031	0.130	0.348	0.005	0.289	0.187	0.185	0.266	0.182	0.692
MgO	0.044	0.175	0.073	0.629	0.706		0.000	0.215	0.861	0.507	0.107	0.328	0.667	0.476	0.760	0.158	0.595	0.724
CaO	0.138	0.151	0.130	0.595	0.945	0.000		0.251	0.841	0.591	0.123	0.407	0.499	0.454	1.000	0.451	0.839	0.987
K2O	0.854	0.059	0.000	0.415	0.130	0.215	0.251		0.069	0.013	0.001	0.170	0.328	0.291	0.662	0.485	0.728	0.108
Cu	0.154	0.184	0.218	0.906	0.031	0.861	0.841	0.069		0.305	0.147	0.065	0.781	0.146	0.055	0.378	0.863	0.073
Zn	0.403	0.209	0.025	0.350	0.130	0.507	0.591	0.013	0.305		0.043	0.140	0.979	0.771	0.754	0.799	0.067	0.781
Rb	0.368	0.020	0.002	1.000	0.348	0.107	0.123	0.001	0.147	0.043		0.554	0.663	0.597	0.443	0.858	0.999	0.484
Sr	0.126	1.000	0.432	0.234	0.005	0.328	0.407	0.170	0.065	0.140	0.554		0.747	0.235	0.524	0.720	0.165	0.323
Y	0.788	0.204	0.429	0.034	0.289	0.667	0.499	0.328	0.781	0.979	0.663	0.747		0.050	0.759	0.924	0.786	0.789
Zr	0.730	0.058	0.382	0.906	0.187	0.476	0.454	0.291	0.146	0.771	0.597	0.235	0.050		0.958	0.998	0.998	0.153
Nb	0.250	0.405	0.779	0.869	0.185	0.760	1.000	0.662	0.055	0.754	0.443	0.524	0.759	0.958		0.066	1.000	0.956
Ba	0.289	0.662	0.287	0.798	0.266	0.158	0.451	0.485	0.378	0.799	0.858	0.720	0.924	0.998	0.066		0.726	0.286
Pb	0.862	0.534	0.863	0.497	0.182	0.595	0.839	0.728	0.863	0.067	0.999	0.165	0.786	0.998	1.000	0.726		0.733
Th	0.216	0.418	0.218	0.497	0.692	0.724	0.987	0.108	0.073	0.781	0.484	0.323	0.789	0.153	0.956	0.286	0.733	

Table 12. Correlations [p (uncorr.)] for EDXRF data for samples from Naibor Soit Ndogo based on Kendall's Tau Monte Carlo simulations.

Naisiusiu																		
τ / p (uncorr.)	**SiO2**	**TiO2**	**Al2O3**	**Fe2O3**	**MnO**	**MgO**	**CaO**	**K2O**	**Cu**	**Zn**	**Rb**	**Sr**	**Y**	**Zr**	**Nb**	**Ba**	**Pb**	**Th**
SiO2		0.099	0.025	0.430	0.456	0.582	0.029	0.099	0.660	0.075	0.048	0.023	0.008	0.028	0.400	0.738	0.547	0.041
TiO2	-0.332		0.000	0.282	0.084	0.023	0.237	0.001	0.698	0.105	0.004	0.133	0.023	0.077	0.068	0.105	0.006	0.014
Al2O3	-0.451	0.796		0.177	0.076	0.078	0.104	0.002	0.912	0.119	0.001	0.023	0.002	0.011	0.045	0.119	0.071	0.005
Fe2O3	-0.158	0.216	0.271		0.077	0.396	0.013	0.865	0.193	0.097	0.955	0.003	0.011	0.020	0.790	0.864	0.822	0.030
MnO	-0.150	0.347	0.357	0.355		0.908	0.061	0.564	0.299	0.116	0.299	0.271	0.107	0.356	0.030	0.907	0.688	0.271
MgO	-0.111	0.456	0.354	0.171	0.023		0.056	0.068	0.406	0.131	0.293	0.148	0.135	0.005	0.068	0.911	0.011	0.014
CaO	-0.438	0.237	0.326	0.497	0.377	0.384		0.694	0.652	0.023	0.778	0.024	0.024	0.001	0.289	0.494	0.341	0.002
K2O	-0.332	0.689	0.619	-0.034	0.116	0.367	0.079		0.406	0.538	0.000	0.290	0.108	0.121	0.051	0.162	0.021	0.095
Cu	-0.088	-0.078	-0.022	0.261	-0.208	0.167	0.090	-0.167		0.083	0.618	0.058	0.472	0.166	0.118	0.162	0.441	0.578
Zn	-0.358	0.326	0.313	0.333	0.316	0.303	0.457	0.124	0.348		0.467	0.043	0.198	0.065	0.742	0.610	0.148	0.072
Rb	-0.398	0.578	0.685	0.011	0.208	0.211	0.057	0.844	-0.100	0.146		0.106	0.053	0.150	0.068	0.083	0.078	0.182
Sr	-0.456	0.302	0.456	0.594	0.221	0.291	0.455	0.212	0.380	0.407	0.324		0.004	0.001	0.844	0.368	0.347	0.022
Y	-0.530	0.456	0.619	0.512	0.324	0.300	0.452	0.322	0.144	0.258	0.389	0.581		0.007	0.152	0.240	0.271	0.003
Zr	-0.442	0.356	0.508	0.466	0.185	0.567	0.689	0.311	0.278	0.371	0.289	0.682	0.544		0.362	0.867	0.048	0.001
Nb	-0.169	0.366	0.403	0.054	0.436	0.366	0.213	0.392	-0.314	-0.066	0.366	0.039	0.288	0.183		0.693	0.746	0.326
Ba	-0.067	0.326	0.313	-0.034	0.023	0.022	-0.137	0.281	0.281	0.102	0.348	0.181	0.236	0.034	-0.079		0.045	0.736
Pb	-0.121	0.552	0.363	0.045	0.081	0.508	0.191	0.464	0.155	0.291	0.354	0.189	0.221	0.398	0.065	0.402		0.068
Th	-0.411	0.492	0.567	0.434	0.221	0.492	0.625	0.335	0.112	0.362	0.268	0.461	0.603	0.648	0.197	0.068	0.367	

Table 13. Correlations [τ / p (uncorr.] for EDXRF data for Naisiusiu based on Kendall's Tau coefficient.

Naisiusiu p Permutations	SiO2	TiO2	Al2O3	Fe2O3	MnO	MgO	CaO	K2O	Cu	Zn	Rb	Sr	Y	Zr	Nb	Ba	Pb	Th
SiO2		0.115	0.025	0.480	0.514	0.626	0.035	0.118	0.712	0.088	0.052	0.025	0.008	0.028	0.491	0.785	0.590	0.046
TiO2	0.115		0.000	0.316	0.105	0.025	0.247	0.000	0.743	0.128	0.003	0.136	0.026	0.079	0.110	0.120	0.006	0.017
Al2O3	0.025	0.000		0.204	0.104	0.091	0.125	0.002	0.956	0.137	0.000	0.025	0.001	0.013	0.075	0.139	0.080	0.006
Fe2O3	0.480	0.316	0.204		0.103	0.446	0.015	0.909	0.225	0.125	0.998	0.003	0.013	0.024	0.844	0.906	0.876	0.040
MnO	0.514	0.105	0.104	0.103		0.950	0.079	0.622	0.343	0.138	0.351	0.325	0.134	0.406	0.061	0.943	0.740	0.319
MgO	0.626	0.025	0.091	0.446	0.950		0.067	0.082	0.447	0.155	0.330	0.171	0.158	0.004	0.109	0.919	0.011	0.014
CaO	0.035	0.247	0.125	0.015	0.079	0.067		0.707	0.703	0.026	0.784	0.026	0.027	0.000	0.369	0.540	0.383	0.002
K2O	0.118	0.000	0.002	0.909	0.622	0.082	0.707		0.444	0.584	0.000	0.302	0.126	0.125	0.085	0.186	0.023	0.107
Cu	0.712	0.743	0.956	0.225	0.343	0.447	0.703	0.444		0.098	0.667	0.066	0.519	0.191	0.175	0.181	0.483	0.619
Zn	0.088	0.128	0.137	0.125	0.138	0.155	0.026	0.584	0.098		0.513	0.054	0.228	0.077	0.790	0.656	0.170	0.087
Rb	0.052	0.003	0.000	0.998	0.351	0.330	0.784	0.000	0.667	0.513		0.109	0.060	0.153	0.107	0.106	0.087	0.212
Sr	0.025	0.136	0.025	0.003	0.325	0.171	0.026	0.302	0.066	0.054	0.109		0.004	0.001	0.893	0.414	0.386	0.027
Y	0.008	0.026	0.001	0.013	0.134	0.158	0.027	0.126	0.519	0.228	0.060	0.004		0.007	0.215	0.273	0.300	0.002
Zr	0.028	0.079	0.013	0.024	0.406	0.004	0.000	0.125	0.191	0.077	0.153	0.001	0.007		0.447	0.912	0.050	0.001
Nb	0.491	0.110	0.075	0.844	0.061	0.109	0.369	0.085	0.175	0.790	0.107	0.893	0.215	0.447		0.759	0.814	0.405
Ba	0.785	0.120	0.139	0.906	0.943	0.919	0.540	0.186	0.181	0.656	0.106	0.414	0.273	0.912	0.759		0.052	0.786
Pb	0.590	0.006	0.080	0.876	0.740	0.011	0.383	0.023	0.483	0.170	0.087	0.386	0.300	0.050	0.814	0.052		0.085
Th	0.046	0.017	0.006	0.040	0.319	0.014	0.002	0.107	0.619	0.087	0.212	0.027	0.002	0.001	0.405	0.786	0.085	

Table 14. Correlations [p (uncorr.)] for EDXRF data for samples from Naisiusiu based on Kendall's Tau Monte Carlo simulations.

Oittii																		
τ / p (uncorr.)	SiO2	TiO2	Al2O3	Fe2O3	MnO	MgO	CaO	K2O	Cu	Zn	Rb	Sr	Y	Zr	Nb	Ba	Pb	Th
SiO2		0.142	0.142	0.796	0.327	0.624	0.380	0.142	0.142	0.770	0.142	0.624	0.327	0.142	0.050	1.000	0.327	0.624
TiO2	-0.600		0.014	0.796	0.050	0.624	0.143	0.014	0.624	0.143	0.014	0.142	0.327	0.142	0.050	0.327	0.050	0.142
Al2O3	-0.600	1.000		0.796	0.050	0.624	0.143	0.014	0.624	0.143	0.014	0.142	0.327	0.142	0.050	0.327	0.050	0.142
Fe2O3	-0.105	0.105	0.105		0.796	0.439	0.537	0.796	0.796	0.758	0.796	0.796	0.796	0.439	0.439	0.439	0.796	0.796
MnO	0.400	-0.800	-0.800	0.105		1.000	0.040	0.050	1.000	0.040	0.050	0.050	0.142	0.050	0.142	0.624	0.014	0.050
MgO	0.200	-0.200	-0.200	0.316	0.000		0.380	0.624	0.624	0.770	0.624	0.624	0.327	0.624	1.000	0.327	1.000	0.624
CaO	0.359	-0.598	-0.598	0.252	0.837	0.359		0.143	0.770	0.080	0.143	0.040	0.380	0.040	0.380	0.380	0.040	0.143
K2O	-0.600	1.000	1.000	0.105	-0.800	-0.200	-0.598		0.624	0.143	0.014	0.142	0.327	0.142	0.050	0.327	0.050	0.142
Cu	0.600	-0.200	-0.200	-0.105	0.000	0.200	-0.120	-0.200		0.380	0.624	0.624	1.000	0.624	0.327	1.000	1.000	0.624
Zn	-0.120	0.598	0.598	0.126	-0.837	0.120	-0.714	0.598	0.359		0.143	0.040	0.143	0.143	0.380	0.770	0.040	0.040
Rb	-0.600	1.000	1.000	0.105	-0.800	-0.200	-0.598	1.000	-0.200	0.598		0.142	0.327	0.142	0.050	0.327	0.050	0.142
Sr	-0.200	0.600	0.600	0.105	-0.800	-0.200	-0.837	0.600	0.200	0.837	0.600		0.327	0.142	0.327	0.327	0.050	0.142
Y	-0.400	0.400	0.400	0.105	-0.600	0.400	-0.359	0.400	0.000	0.598	0.400	0.400		0.327	0.142	0.624	0.142	0.050
Zr	-0.600	0.600	0.600	-0.316	-0.800	-0.200	-0.837	0.600	-0.200	0.598	0.600	0.600	0.400		0.327	1.000	0.050	0.142
Nb	-0.800	0.800	0.800	0.316	-0.600	0.000	-0.359	0.800	-0.400	0.359	0.800	0.400	0.600	0.400		0.624	0.142	0.327
Ba	0.000	-0.400	-0.400	-0.316	0.200	0.400	0.359	-0.400	0.000	-0.120	-0.400	-0.400	0.200	0.000	-0.200		0.624	1.000
Pb	-0.400	0.800	0.800	-0.105	-1.000	0.000	-0.837	0.800	0.000	0.837	0.800	0.800	0.600	0.800	0.600	-0.200		0.050
Th	-0.200	0.600	0.600	-0.105	-0.800	0.200	-0.598	0.600	0.200	0.837	0.600	0.600	0.800	0.600	0.400	0.000	0.800	

Table 15. Correlations [τ / p (uncorr.] for EDXRF data for Oittii based on Kendall's Tau coefficient.

Oittii																		
P permutations	**SiO2**	**TiO2**	**Al2O3**	**Fe2O3**	**MnO**	**MgO**	**CaO**	**K2O**	**Cu**	**Zn**	**Rb**	**Sr**	**Y**	**Zr**	**Nb**	**Ba**	**Pb**	**Th**
SiO2		0.232	0.240	1.000	0.490	0.823	0.613	0.231	0.236	1.000	0.231	0.821	0.488	0.234	0.084	1.000	0.484	0.821
TiO2	0.232		0.018	1.000	0.085	0.816	0.304	0.018	0.819	0.299	0.018	0.228	0.488	0.243	0.084	0.489	0.082	0.238
Al2O3	0.240	0.018		1.000	0.088	0.819	0.304	0.016	0.817	0.301	0.017	0.231	0.477	0.234	0.079	0.482	0.090	0.233
Fe2O3	1.000	1.000	1.000		1.000	0.631	0.749	1.000	1.000	0.903	1.000	1.000	1.000	0.632	0.634	0.635	1.000	1.000
MnO	0.490	0.085	0.088	1.000		1.000	0.104	0.088	1.000	0.092	0.082	0.083	0.231	0.086	0.232	0.814	0.017	0.083
MgO	0.823	0.816	0.819	0.631	1.000		0.594	0.812	0.825	1.000	0.819	0.820	0.493	0.821	1.000	0.492	1.000	0.815
CaO	0.613	0.304	0.304	0.749	0.104	0.594		0.301	1.000	0.291	0.289	0.099	0.600	0.104	0.594	0.603	0.098	0.309
K2O	0.231	0.018	0.016	1.000	0.088	0.812	0.301		0.818	0.296	0.014	0.240	0.479	0.232	0.085	0.480	0.081	0.225
Cu	0.236	0.819	0.817	1.000	1.000	0.825	1.000	0.818		0.598	0.827	0.816	1.000	0.812	0.478	1.000	1.000	0.818
Zn	1.000	0.299	0.301	0.903	0.092	1.000	0.291	0.296	0.598		0.295	0.096	0.298	0.301	0.599	1.000	0.104	0.097
Rb	0.231	0.018	0.017	1.000	0.082	0.819	0.289	0.014	0.827	0.295		0.229	0.487	0.237	0.093	0.492	0.082	0.244
Sr	0.821	0.228	0.231	1.000	0.083	0.820	0.099	0.240	0.816	0.096	0.229		0.480	0.242	0.489	0.476	0.080	0.234
Y	0.488	0.488	0.477	1.000	0.231	0.493	0.600	0.479	1.000	0.298	0.487	0.480		0.481	0.232	0.814	0.234	0.081
Zr	0.234	0.243	0.234	0.632	0.086	0.821	0.104	0.232	0.812	0.301	0.237	0.242	0.481		0.484	1.000	0.085	0.232
Nb	0.084	0.084	0.079	0.634	0.232	1.000	0.594	0.085	0.478	0.599	0.093	0.489	0.232	0.484		0.815	0.230	0.479
Ba	1.000	0.489	0.482	0.635	0.814	0.492	0.603	0.480	1.000	1.000	0.492	0.476	0.814	1.000	0.815		0.818	1.000
Pb	0.484	0.082	0.090	1.000	0.017	1.000	0.098	0.081	1.000	0.104	0.082	0.080	0.234	0.085	0.230	0.818		0.085
Th	0.821	0.238	0.233	1.000	0.083	0.815	0.309	0.225	0.818	0.097	0.244	0.234	0.081	0.232	0.479	1.000	0.085	

Table 16. Correlations [p (uncorr.)] for EDXRF data for samples from Oittii based on Kendall's Tau Monte Carlo simulations..

	Endonyo Osunyai	Naibor Soit Ndogo	Naibor Soit Kubwa	Naisiusiu	Oittii	Total
Endonyo Osunyai	4	0	0	0	0	4
Naibor Soit Ndogo	0	13	0	1	0	14
Naibor Soit Kubwa	0	0	9	0	0	9
Naisiusiu	0	0	0	10	0	10
Oittii	0	0	0	0	5	5
Total	4	13	9	11	5	42
% correctly classified			97.62%			

Table 17. Confusion matrix of DFA by outcrop classification.

	Endonyo Osunyai	Naibor Soit Ndogo	Naibor Soit Kubwa	Naisiusiu	Oittii	Total
Endonyo Osunyai	0	0	2	0	2	4
Naibor Soit Ndogo	0	11	0	3	0	14
Naibor Soit Kubwa	0	0	7	2	0	9
Naisiusiu	0	1	0	9	0	10
Oittii	2	0	0	0	3	5
Total	2	12	9	14	5	42
% correctly classified (Jackknife)			71.43%			

Table 18. Confusion matrix of DFA by outcrop classification using Jackknife method.

	G1	GR1	GR2	GR5	R3	R5	W2	W3	W4	Total
G1	1	0	0	0	0	0	0	0	0	1
GR1	0	4	0	0	1	0	0	0	0	5
GR2	0	1	6	0	0	0	0	0	0	7
GR5	0	0	0	1	0	0	0	0	0	1
R3	0	0	0	0	4	0	1	0	0	5
R5	0	0	0	0	0	2	0	0	0	2
W2	0	0	0	0	1	0	4	0	0	5
W3	1	0	0	0	0	0	1	11	0	13
W4	0	0	0	0	0	0	0	0	3	3
Total	2	5	6	1	6	2	6	11	3	42
% correctly classified						85.71%				

Table 13. Confusion matrix of DFA by RMG classification.

	G1	GR1	GR2	GR5	R3	R5	W2	W3	W4	Total

G1	0	0	0	0	0	0	1	0	0	1
GR1	0	3	0	0	1	0	1	0	0	5
GR2	0	1	3	3	0	0	0	0	0	7
GR5	0	1	0	0	0	0	0	0	0	1
R3	0	1	0	1	0	0	2	1	0	5
R5	0	0	0	0	0	2	0	0	0	2
W2	1	1	0	0	1	0	0	2	0	5
W3	1	1	0	0	0	0	2	8	1	13
W4	1	0	0	0	0	0	0	1	1	3
Total	3	8	3	4	2	2	6	12	2	42
% correctly classified (Jackknife)					40.48%					

Table 14. Confusion matrix of DFA by RMG classification using Jackknife method.